

**Recovery times of a spark gap with high pressure
gases as insulation suitable for repetitive applications**

By

C S REDDY BHOOMIREDDY

Enrolment No: ENGG01201104004

Bhabha Atomic Research Centre, Mumbai-400085 INDIA

A thesis submitted to the

Board of Studies in Engineering Sciences

In partial fulfillment of requirements

For the Degree of

DOCTOR OF PHILOSOPHY

of

HOMI BHABHA NATIONAL INSTITUTE

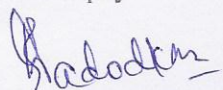


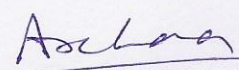
July-2016

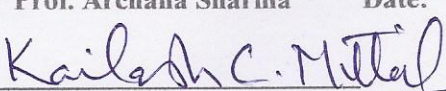
Homi Bhabha National Institute

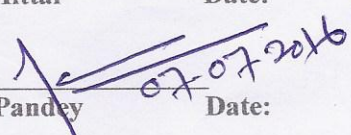
Recommendations of the Viva Voce Board

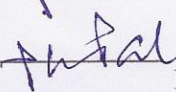
As members of the Viva Voce Board, we certify that we have read the dissertation prepared by C.S. Reddy Bhoomireddy, entitled "Recovery times of a spark gap with high pressure gases as insulation suitable for repetitive applications" and recommend that it may be accepted as fulfilling the dissertation requirement for the Degree of Doctor of Philosophy.

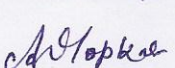

Chairman: Prof. D.N. Badodkar Date: 07.07.2016.

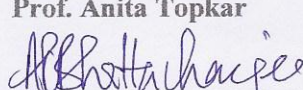

Guide/ Convener: Prof. Archana Sharma Date: 7/7/2016


Co-Guide: Prof. K.C. Mittal Date: 7/7/2016


External Examiner: Prof. R.K. Pandey Date: 07.07.2016


Member 1: Prof. P.K. Pal Date: 7.7.16


Member 2: Prof. Anita Topkar Date: 7/7/2016

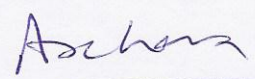

Member 2: Prof. A. Bhattacharjee Date: 7/7/2016

Final approval and acceptance of this dissertation is contingent upon the candidate's submission of the final copies of the dissertation to HBNI.

I hereby certify that I have read this dissertation prepared under my direction and recommend that it may be accepted as fulfilling the dissertation requirement.

Date: 7-7-2016

Place: Mumbai


Guide: Dr. Archana Sharma

STATEMENT BY AUTHOR

This dissertation has been submitted in partial fulfillment of requirements for an advanced degree at Homi Bhabha National Institute (HBNI) and is deposited in the Library to be made available to borrowers under rules of the HBNI.

Brief quotations from this dissertation are allowable without special permission, provided that accurate acknowledgement of source is made. Requests for permission for extended quotation from or reproduction of this manuscript in whole or in part may be granted by the Competent Authority of HBNI when in his or her judgment the proposed use of the material is in the interests of scholarship. In all other instances, however, permission must be obtained from the author.

B. Chandrab Sekhar Reddy

C S REDDY BHOOMIREDDY

DECLARATION

I, hereby declare that the investigation presented in the thesis has been carried out by me. The work is original and has not been submitted earlier as a whole or in part for a degree / diploma at this or any other Institution / University.

B. chandra Sekhara Reddy
C S REDDY BHOOMIREDDY

List of publications after registering for Ph.D.

International Journals

Published:

1. C.S.Reddy, Archana Sharma and K.C. Mittal, “*Experimental Investigations of Pulse Charged Spark Gap Recovery Times and Influencing Factors,*” *IEEE Transactions on Plasma Science*, Vol.44, Issue 3, pp. 331-337, 2016.
2. C.S.Reddy, A. S Patel, P. Naresh, Archana Sharma and K.C. Mittal, “*Experimental investigations of argon spark gap recovery times by developing a high voltage double pulse generator.*” *Review of Scientific Instruments* **85**, 064703 (2014); DOI: 10.1063/1.4883997. Published by the AIP Publishing LLC.
3. C.S.Reddy, Archana Sharma and K.C. Mittal, “*Recovery Analysis of Sparkgap by Anode Temperature Decay method for Different Materials.*” *International Journal of Applied Electromagnetics and Mechanics*, Vol47, pp 643-651, 2015. Published by IOP press.
4. C.S.Reddy, Archana Sharma and K.C. Mittal “*Recovery study of Argon spark gap after Breakdown.*” *IEEE Transactions on Plasma Science*. (Under minor review).

International Conferences

1. C.S.Reddy, A.K Tak, Archana Sharma and K.C. Mittal, “*Computational modeling of spark gap density recovery after breakdown*” *IEEE International Symposium On Discharges and Electrical Insulation in Vacuum (ISDEIV) -2014*.
2. C.S.Reddy, P. Naresh, Archana Sharma and K.C. Mittal, “*Voltage Recovery Characteristics of Spark gap using Repetitive Pulse Power System*” *IEEE International Power Modulator and High Voltage Conference (IPMHVC)*, USA, June-2014.

3. **C.S.Reddy**, P. Naresh, Archana Sharma and K.C. Mittal, “**Spark Gap Discharge Properties Measured by Optical Emission Spectroscopy**” *IEEE International Power Modulator and High Voltage Conference (IPMHVC)*, USA, June-2014.
4. **C.S.Reddy**, S.Mitra, S. B. Umbarkar, Archana Sharma and K.C.Mittal, “**Optimisation of Sequential Triggering Delay in a Coaxial Fast Erecting MARX Generator**” *IEEE Pulse power conference*, USA, June-2013.
5. **C.S.Reddy**, S. B. Umbarkar, Archana Sharma and K.C.Mittal, “**3D Particle in cell simulations of spark gap Discharge using Argon gas as dielectric medium**” *IEEE Pulse power conference*, USA, June-2013.
6. **C.S.Reddy**, S.V.Tewari, Archana Sharma, K.C.Mittal and D.P.Chakravarthy, “**Effect of anode temperature rise and decay on recovery times of sparkgaps**” *IEEE 4th Euro-Asian Pulsed Power Conference (EAPPC/BEAMS 2012)* Karlsruhe, Germany, October-2012.

Other Publications

7. S V Tewari, **C.S.Reddy**, Archana Sharma, K.C.Mittal “**Effect on electron drift velocity and ionization coefficient along a gas-solid interface**” *IEEE international conference on power, energy and control*, 174-176, FEBRUARY 2013.
8. S V Tewari, Amitava Roy, **C.S.Reddy**, Archana Sharma, K.C.Mittal “**Particle-in-cell simulations of discharge along angled insulators in compressed gases**” *International Conference on Pulsed Power and Plasma Science* , (2013).
9. S V Tewari, **C.S.Reddy**, R.Agarwal, P.C.Saroj, Archana Sharma, K.C.Mittal, D.P. Chakravarthy “**Development of a 300kV Compact Co-axial Marx Generator Based on PFN**” *IEEE 4th Euro-Asian Pulsed Power Conference (EAPPC/BEAMS)*, (2012)

Dedicated to

My Parents

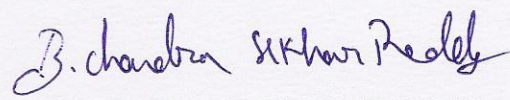
Shri. Krishna Reddy

Smt. Lakshmi

ACKNOWLEDGEMENTS

I express my deep gratitude to the following persons who have helped me in various ways.

- To my guides Dr. Archana Sharma, Head, Pulse Power Systems Section, Accelerator and Pulse Power Division, BARC, Mumbai and Dr. K. C. Mittal, Head, Accelerator and Pulse Power Division, BARC, (Retired on 31-05-2014), for stimulating discussions, providing facilities, cheerful help, valuable guidance through the entire period and correction of manuscript.
- To my doctoral committee, HBNI, Dr. D.N. Badodkar, Dr. P. K. Pal, Dr. A. Bhattacharjee and Dr. Anita Topkar for their valuable guidance during writing this thesis, putting me on the right track afterwards and also for meticulous suggestions & guidance to make this work complete and correction of manuscript.
- I would specially like to thank Dr. K.V. Nagesh, Accelerator and Pulse Power Division, BARC (Retired on 31-07-2011), Dr. M.S. Bhatia, Laser and Plasma Division, BARC (Retired on 31-11-2014), for simulating useful discussions and meticulous suggestions.
- I would like to thank Dr. N. M. Singh, VJTI, Mumbai, for providing the computer simulation facilities with ANSYS/Fluent software.
- Finally I express gratitude to my family for their heartfelt support without that I could not have done this work. In addition I express my gratitude to all persons who have not been listed here but helped to complete this work.


C S REDDY BHOOMIREDDY

CONTENTS

SYNOPSIS	11
LIST OF FIGURES	24
LIST OF TABLES	29
LIST OF SYMBOLS	30
LIST OF ABBREVIATIONS	33
CHAPTERS	
1.0 INTRODUCTION	
1.1 Introduction	35
1.2 Pulsed power system	36
1.3 Pulse Power Switches	40
1.3.1 Gas Switches	40
1.3.2 Solid state switches	43
1.3.3 Magnetic Switches	44
1.4 Two-pulse Method	45
1.5 Aim of the Work	49
1.6 Outline of the thesis	49
2.0 LITERATURE SURVEY	
2.1 Introduction	52
2.2 Fundamentals of a gas closing switch	53
2.3 Electrical breakdown in a gas gap under repetitive operation	54
2.4 Dielectric recovery properties	56
2.5 Gas Sparkgap recovery under static pressure condition	59

2.6 Gas Sparkgap recovery under Dynamic pressure condition (Purged Sparkgaps)	66
2.7 Low Pressure Sparkgaps	69
2.7.1 Pseudo Spark Switch	73
2.7.2 Crossed Field Switches	73
2.8 Vacuum Sparkgaps	74
2.9 Summary	76
3.0 DESIGN AND DEVELOPMENT OF DOUBLE PULSE GENERATOR	
3.1 Introduction	77
3.2 Design of double Pulse Generator	77
3.2.1. Design of pulse transformer	79
(a) Pulse Rise Region	81
(b) Pulse Top Region	82
(c) Pulse Tail Region	83
(d) Overshoot	85
(e) Rise time	86
3.2.2. Pulse transformer topologies	86
(a) Parallel Winding	86
(b) Cone Winding	87
(c) Foil winding	88
(d) Matrix Pulse Transformer	88
3.2.3 Transformer Core	90
3.2.4. IGBT triggering circuit	91
(a) Gate driver circuit	91

(b) Gate driver Power supply	93
(c) Optical pulse generator	93
3.3 Selection of IGBT	95
3.4. Diode	95
3.5 Spark gap chamber	96
3.6 Capacitor	96
3.7 Capacitor charging power supply (CCPS)	97
3.8 Summery	98
4.0 .EXPERIMENTAL RESULT AND DISCUSSION	
4.1 Introduction	99
4.2 Spark gap voltage recovery experimental procedure by Double pulse method	99
4.3 Effect of gas, gap distance and pressure variation on spark gap recovery	106
4.4 Experimental Investigations of Pulse Charged Spark Gap Recovery Times and Influencing Factors	111
4.4.1 Effect of electrode shape and size on spark gap recovery	112
4.4.2 Effect of pulse shape and size on spark gap recovery	116
4.4.3 Effect of discharge current on spark gap recovery	118
4.5 Summery	121
5.0 COMPUTATIONAL STUDY OF GAS DENSITY RECOVERY OF SPARK GAP	
5.1 Introduction	122
5.2 Simulation Method	123
5.3 Results and Analysis	126

5.4 Comparison of Neutral gas density recovery and Voltage Recovery	131
5.4.1 Explanation for faster gas density recovery time to voltage	
Recovery time of spark gap	131
5.4.2 Explanation of Voltage recovery curve pattern	134
5.5 Summery	136
6.0 RECOVERY ANALYSIS OF SPARK GAP BY ANODE TEMPERATURE DECAY	
METHOD	
6.1 Introduction	137
6.2 Theoretical Analysis	140
6.3 Spark gap temperature decay Model by FEM based simulations	147
6.4 Simulation Results and analysis	150
6.5. Summery	154
7.0 CONCLUSION AND FUTURE PERSPECTIVE	155
REFERENCES	159
ANNEXURE – I	170
ANNEXURE – II	184

SYNOPSIS

In the Pulsed power systems, the energy is accumulated over a relatively long period of time and release it into a load in a short time interval (also called energy compression) to obtain a transient huge power (GW) (voltage and currents in MV and MA respectively). This pulsed power technology has wide ranging applications in food processing, water treatment, medical treatment, research, industry, and defence applications etc., [1-3]. Many such applications require the pulsed power systems which can be operated in high voltage (kV), high current (kA), short duration (ns), high peak power ratings (MW) and high operating frequency (kHz). The switch used in the pulse power system plays an important and critical role in achieving the required performance.

“High pressure gas spark gap” switch can be the choice for such applications [4, 5]. This device exhibits many of the desired characteristics for pulsed power, including peak voltage and current handling capabilities. Spark gaps are triggerable with nanosecond jitter, have a large operating range, and give good time compression per switched stage. In addition they are rugged, lightweight, inexpensive, and relatively easy to use. On the negative side, they suffer from recovery problems at high repetition rates [6-8]. These limits the maximum PRF (pulse repetition frequency) of a pulsed power system to a few hundred Hz. Improvements in the voltage recovery time are possible by employing gas flow techniques which clear the remnants of the switching arc from the inter-electrode region during the inter-pulse period [9-11]. However, as the required PRF extends into the kHz regime, the gas flow requirements become expensive and tend to dictate the switch design and therefore considered undesirable approaches when designing inexpensive pulse generating systems. The study of voltage recovery rate of an un-blown gas spark gap, has received considerable attention in recent years due to the demands from the pulsed power field for the development of high repetitive pulsed power systems. The estimation of the recovery time is an important issue for the repetitive pulse power systems. The dielectric

Recovery data of spark gap plays a basic role, but it has been inadequately studied for the repetitive pulse charge conditions. Despite extensive research and theoretical studies, the understandings of the recovery process in a gas spark gap switch after the electrical breakdown, is far from complete. The present research problem has been taken up in order to develop a suitable high pressure gas sparkgap so that the single mode operating systems can be operated in repetitively pulsed mode. The area of research is focused on further understanding the recovery process of the dielectric strength of the spark gap with Argon and N₂ as gas mediums in Nanosecond time scales by developing a pulse transformer based double pulse generator capable of generating 40 kV peak pulses with rise time of 300 ns and 1.5 μ s FWHM and with a delay of 10 μ s - 1 s. Further, the study extended to find the effect of electrode materials (copper and stainless steel) on the recovery rate of spark gap switch, for developing repetitive pulsed power systems. Following chapters give brief introduction to work carried out in this thesis.

Chapter 1 is the introduction to the insulation aspects in high voltage pulse power systems and the application of pulse power system in industrial, defense and research areas. The phenomena of spark gap recovery in vacuum which is extensively reported in literature and the need to study the phenomena in compressed gas environment which forms the basis of this thesis is presented in this chapter. To understand the recovery process in an un-blown switch, the voltage recovery time has divided into three distinct phases. The phase one of the recovery is the de-ionization of the spark channel by recombination, de-excitation and attachment for about few 10 μ s [12]. The second phase is the cooling of the hot neutral gas to its ambient temperature in few milliseconds time [13]. The third and last phase of the voltage recovery is the ability of the spark gap switch to recover to a greater voltage than its DC breakdown voltage level. The measurement of voltage recovery of a gas spark gap in this study was found by using a well-known two pulse method [14, 15] shown in Figure.1.

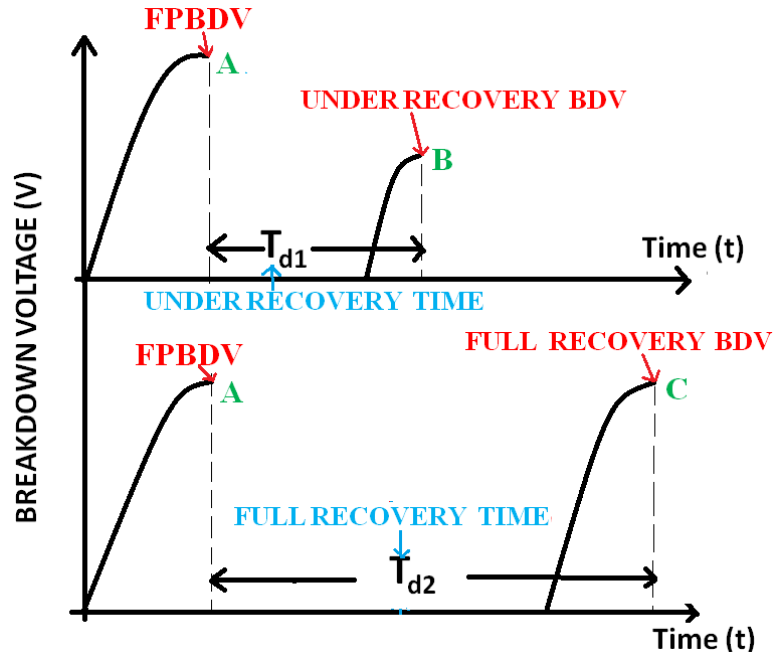


Figure 1. Voltage recovery time measurement by two pulse method

In this method, initially the first pulse is applied to the sparkgap. Next the second pulse (recovery pulse) is applied with a predefined time delay. This pulse can be same as the original pulse or of high voltage, low energy pulse. The amplitude of the second pulse shows the over-voltage recovery capability of the gas gap. The experiments have to be repeated a number of times with different time delays, to get complete data of the recovery time. The effect of heat dissipation capacity of the switch cannot be tested. The recording of breakdown voltages is very simple. This method has been widely used in recovery voltage / time measurements. The characterization of sparkgaps, types of measurements of recovery times and voltages are also presented in this chapter. Finally the aim of this work is also stated in this chapter.

Chapter 2 provides a review of the literature on spark gap recovery in gases and summarizes the different factors influencing the recovery rate of the spark gap. The mechanism in high pressure gases is discussed along with the different physical processes responsible for the delayed recovery of the spark gap switch. A few of the existing spark gap literature explaining physics of

the recovery process is also discussed. Based on this review, a high pressure gas sparkgap has been selected for the recovery study. The summary of the review and necessity of the present research are also presented in this chapter.

Chapter 3 gives the details of the experimental set up developed for present studies. A Pulse transformer based generator was designed and developed two conduct the recovery experiments by using two-pulse method. The pulse generator produces two identical pulses of having 40 kV amplitude and 300 ns rise time with an inter pulse period of 1 ms to more than 1sec. A matrix transformer topology is used to get fast rise times by reducing $L_i C_d$ product in the circuit [16]. The main components include a capacitor, an IGBT switch with effective triggering circuits, a spark gap chamber made with Perspex and a capacitor charging power supply as shown in figure 2.

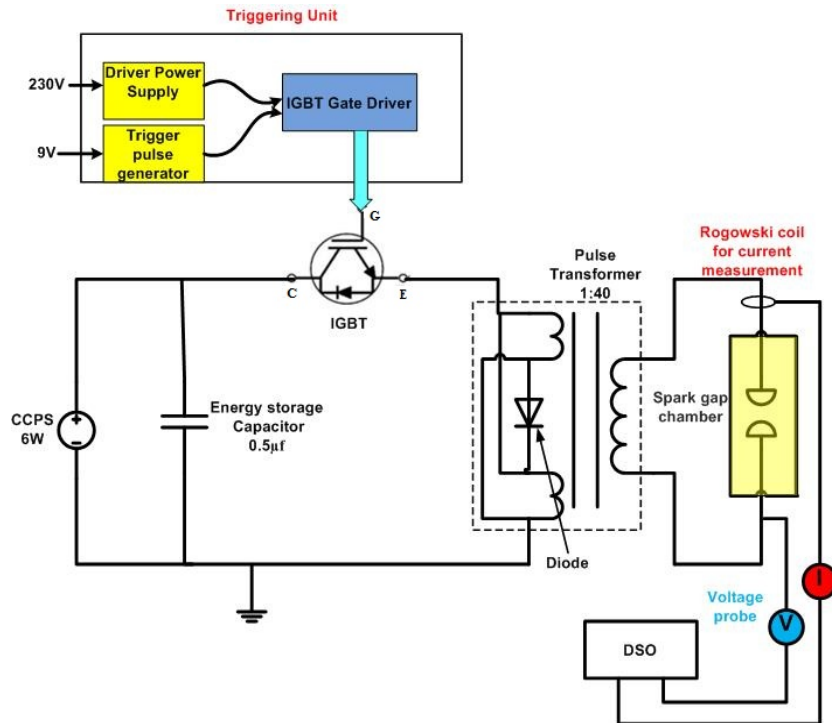


Figure 2. Experimental schematic of double-pulse generator with matrix transformer topology

The sparkgap chamber was fitted with 15 mm thick, Rogowsky profile type electrodes made by Stainless steel material with an inter electrode gap of 1 mm to 10 mm. The A two-pulse method is used to determine the voltage recovery times of gas spark gap switch with argon and nitrogen gasses [17]. The operating gas pressure range for the testing chamber is from 1 bar to 4 bars. First pulse is applied to the spark gap to over-volt the gap and initiates the breakdown (FPBDV) and second pulse is used to determine the recovery voltage of the gap (SPBDV)

Chapter 4 contains a detailed analysis on the spark gap voltage recovery results obtained by using a double pulse method. The effect of different parameters on the spark gap recovery rate was studied in detail and a better spark gap configuration has been suggested. The recovery data with effect to gas, gap distance, pressure, electrode shape and size, pulse rise time and also discharge current was obtained. Recovery Experiments has been conducted for 1 mm to 4 mm gap length between 0-4 bar pressure range for Argon and Nitrogen gases. The recovery time estimated for Argon and Nitrogen gases and a comparison have been made with the Sf_6 gas recovery time. The experiments show a significant effect of Pressure on the recovery of the spark gap. It is observed that time taken for complete recovery without gas flow techniques is more than 1s [18]. The percentage recovery voltage v/s time graphs show that the spark gap dielectric recovery is not linear and an intermediate plateau is observed in the recovery curves. This was observed by previous researcher Scott Macgregor [19] in high pressure gasses. It is attributed to the residual particles on the cathode to produce the initial electrons for the second breakdown. Recovery time of the spark gap decreases with increase in pressure and Shorter gaps in length are recovering faster than longer gaps. Also the factors which affect the recovery of spark gap switch for pulse charged operation like electrode size, pulse rise time and conduction current have been studied. The spark gap electrodes of 34 mm, 40 mm, 68 mm diameter and a point type were used in the study. The effect of rise time was studied by changing the charging capacitor to 100 nf, 500 nf and 1000 nf in the circuit. An increase in the output impedance resulted in a decrease in

the time taken for recovery of spark gap. Also, the switch recovery appears to be largely dependent of electrode shape and size compare to the pulse rise time [20].

Chapter 5 describes a two-dimensional axisymmetric computational model of the spark gap developed by using a CFD code ANSYS/Fluent to provide a better understanding of the dynamics of the recovery process. The understanding on recovery of temperature and density of the spark gap channel after breakdown provides a better knowledge for designing a high replate spark gap. For this purpose, we investigate the recovery of temperature and density of the spark gap channel after breakdown through the computational method. The spark gap voltage recovery time measured from the two-pulse generator experiment in chapter 4 is compared with the recovery of temperature and gas density inside the spark gap. This comparison shows the gas density in a 2 mm spark gap filled with argon gas recovers to 100% in 58ms, but the hold-off voltage of the spark gap after breakdown recovers about 45% of its original overvoltage breakdown voltage. This confirms that the voltage recovery of a spark gap is significantly slower compared to the gas density recovery. This mechanism for delayed recovery of the ability to be over-voltage was also observed by Xinjing Cai [21] for nitrogen gas. In his experiments, the nitrogen gas density recovery (100% recovery in 50 ms) was investigate by using Mach-Zehnder interferometry and the hold off voltage (21.4% in 50 ms) of a spark gap after breakdown by two pulse method. The processes governing the delay recovery of voltage was not fully clear, but we guess there may be long-lived particles that can continuously produce the electrons to quickly initiate the second breakdown [22]. For Argon, the long-lived metastable atom is famous for producing electrons [23]. These particles in the gap results in non-linear recovery curves which clearly has 3 time phases. First phase is the de-ionization of the arc channel by recombination, attachment and diffusion etc. This takes for the gap less than 1ms and R_{vb} (breakdown recovery voltage) recovers around 20%. Neutral gas density Recovery takes around 58 ms and it is due to energy decay of the gap by conduction, convection and radiation. At this point the voltage

recovers around 50% only. Later recovery attributes to over voltage capability of the spark gap. This 3rd recovery phase causes the long delay for the spark gap to recover to its full self-break down voltage level. Increasing the pressure also reduce the time required for 1 and 2 phases. We can improve the repetition rate by operating spark gap at reduced self breakdown voltage by triggering at lower break down voltage. (We can reduce the time required for the plateau). The possible operating frequencies that can be obtained by operating the spark gap at below self break down voltage level are also presented in this chapter.

Chapter 6 presents a method to estimate the effect of electrode temperature rise and decay on repetition rate of spark gap. The surface temperature variation of the anode during switching plays decisive role in recovery of spark gap. The breakdown in the gap is initiated by the breakdown of micro-projections on the cathode. The plasma produced acts as a source of electrons and results in breakdown of the gap due to gaseous discharge. In low current discharge, the anode is basically passive and acts as a collector of positive ions. In high current discharges, a fully developed anode spot is formed. This anode spot has a temperature near atmospheric boiling temperature of anode material and is a source of metal vapors and ions. The formation of anode spot is preceded by anode foot-point, which is luminous but cooler than anode spot [24], [25]. In present calculations it is assumed that anode foot-points can be formed as per [26], [27]. These have low temperatures compared to anode spots. Electrode surface evaporates due to discharge current in the gap depending upon the energy transferred to anode. The recovery process depends upon the metal vapor ejected from the electrode due to temperature rise of anode. The metal vapor decreases the pressure in the gap that reduces the breakdown voltage of the gap. In this chapter, a theoretical method has been proposed to estimate the effect of anode temperature rise and decay on repetition rate of spark gap. By using this method, the behavior of copper and stainless steel materials were studied for a current pulse of 30 kA. During the pulse period of 10 μ s, the temperature rise for SS is higher than Copper [28]. After current zero, the

anode temperature decays to the vaporization temperature of the material and determines the recovery time of the spark gap. The vaporization temperature for copper and stainless steel at atmospheric conditions are 2868 K and 3233 K respectively. The temperature decay is exponential for temperatures greater than 3273 K for Cu and 3773 K for SS. This temperature decay is also verified by a heat transient computational model developed in FEM based software. The spark gap chamber dimensions used in the simulations are length-160 mm, height-80 mm and depth-80 mm. Simulations have been carried out for different materials including Cu and SS. Some simulations are in good agreement with existing experimental data. The decay time for current pulses 5 kA, 10 kA, 15 kA, 20 kA, 25 kA and 30 kA are estimated. Similar experiments of measuring the decay of anode temperature after interruption of high current arcs was done by Edgar Dullini [29]. In his experiments, the anode temperature decays to 1600 K in 4 ms for a current pulse of 7 kA. This decay time is around 4.15 ms in our simulation results.

Chapter 7 presents the conclusions, findings and summarizes the future work. The following is the summary of the work reported in the thesis.

1. A pulse transformer based double pulse generator capable of generating 40 kV peak pulses with rise time of 300 ns and 1.5 μ s FWHM and with a delay of 1 ms - 1 s was developed. The voltage recovery study was carried out by employing double-pulse method without employing any gas flow technique.
2. Recovery Experiments has been conducted for 1 mm to 4 mm gap length between 0-4 bar pressure range for argon and nitrogen gases. The recovery time estimated for Argon and Nitrogen gases and a comparison have been made with the Sf_6 gas recovery time. Due to its electronegative nature Sf_6 has high percentage of voltage recovery than Argon followed by N_2 . Pressure has significant effect on the recovery of the spark gap. It was observed that time taken for complete recovery without gas flow techniques is

more than 1 s. An intermediate plateau was observed in the spark gap recovery curves. Recovery time decreases with increase in pressure and Shorter gaps in length are recovering faster than longer gaps.

3. The factors which affect the recovery of spark gap switch for pulse charged operation like electrode size, pulse rise time and conduction current have been studied. An increase in the output impedance resulted in a decrease in the time taken for recovery of spark gap. Also, the switch recovery appears to be largely dependent of electrode shape and size compare to the pulse rise time.
4. A two-dimensional axisymmetric computational model of spark gap recovery is presented to provide a better understanding of the dynamics of the recovery process. In this model, we investigate the internal changing parameters through the computational method, while the voltage recovery of spark gap was measured by two-pulse experiment. It was shown that the gas density in a 2 mm spark gap filled with argon gas recovers to 100% in 58ms, but the hold-off voltage of the spark gap after breakdown recovers about 45% of its original overvolted breakdown voltage. This shows the voltage recovery of a spark gap is significantly slower compared to the gas density recovery.
5. The repetition rate was improved by operating spark gap at reduced self breakdown voltage by triggering at lower break down voltage. The possible operating frequencies that can be obtained by operating the spark gap at below self break down voltage level are obtained.
6. A theoretical method has been proposed to estimate the effect of anode temperature rise and decay on repetition rate of spark gap. By using this method, the behavior of copper and stainless steel materials were studied for a current pulse of 30 kA. During

the pulse period of 10 μ s, the temperature rise for SS is higher than Copper. The temperature decay is exponential for temperatures greater than 3273 K for Cu and 3773 K for SS.

7. The temperature decay is also verified by a heat transient computational model developed in FEM based software. Simulations have been carried out for different materials including Cu and SS. Some simulations are in good agreement with existing experimental data. The decay time for current pulses 5 kA, 10 kA, 15 kA, 20 kA, 25 kA and 30 kA are estimated.

Further research is open for studying and analyzing different gas mixtures at higher pressure levels for understanding and minimizing the problem of recovery problems of spark gap. Finally some suggested future work is outlined

1. The recovery study in gas mixture can be studied in future and also data on D₂O gas recovery can be useful for achieving faster repetitive pulse power systems.
2. The use of streak camera to study the recovery phenomenon inside the spark gap with gas mixtures.

Present work has contributed to a better understanding of recovery in a spark gap used as a switch in high voltage pulse power systems. The study carried out in this thesis is useful in the development of reliable, efficient and high rep-rate spark gap switch for pulse power systems.

REFERENCES

- [1] H. Akiyama, T. sakugawa, and T. Namihira, "Industrial applications of pulsed power technology," IEEE Trans. Dielectr. Electr. Insul. 14(5), 1051–1064 (2007).
- [2] H. Bluhm, Pulsed Power Systems, 2006, Springer, ISBN-13 978-3—540-26137-7.

- [3] Paul.W.Smith, Transient electronics, pulsed circuit technology, wiley. 2002, ISBN 978-0-471-97773-5.
- [4] S. J. MacGregor,F. A. Tuema, S. M. Turnbull and O. Farish, “The operation of repetitive high pressure spark gap switches,” J. Appl. Phys.,vol. 26, p. 954-958, (1993).
- [5] H.Rahaman, J.W. Nam, Sang. H.Nam and K.Frank, “Investigation of a spark-Gap Discharge in a Regime of very high Repetition rate”, IEEE Transactions on Plasma Science, Vol. 38, No.10, (2010).
- [6] Anders Larsson, “Gas-Discharge closing switches and their time jitter”, IEEE Transactions on Plasma Science, Vol. 40, No.10, (2012).
- [7] Anders Larsson,D. Yap and Yong Wah Lim “Time jitter study of a corona-stabilized closing switch”, IEEE Transactions on Plasma Science, Vol. 40, No.10, (2012).
- [8] Yeong-jer chen,J. Dickens, J. Walter and M. Kristiansen “Jitter and recovery rate of a triggered spark gap with high pressure gas mixtures” IEEE pulsed power conference, pp. 244-249, (2009).
- [9] G. M. Molen, J. M. Kuhlman, S. H. Nam, and E. G. Ruf, ""A 250-kV Gas-flow spark gap,” proc. fifth IEEE Pulsed Power Conf., IEEE pub. No. 85C2121-2, pp. 473-476, Arlington, VA, June 1985.
- [10] “Flow technology for high PRF Rail gap switches,” Final Report to los Alamos scientific laboratory, by spectra technology (Formerly mathematical sciences northwest), Bellevue, WA, 1982.
- [11] M. S. Mazzola, G. M. Molen and J. M. Kuhlman, “Recovery of a Gas-blown spark gap with pre-ionization”, proc. eighteenth IEEE power modulator symposium, pp. 219-222, Hilton Head SC, 1988.
- [12] J.M. Meek and J. D Craggs, “Electrical Breakdown of Gases”, New York: Wiley, 1978, ch.8.
- [13] S.M Turnbull, S.J MacGregor, F.A.Tuema and O. Farish, “ A quantitative schlieren method for measurement of neutral gas density in high pressure gas switches”, *Meas. Sci. Technol.*, vol. 4, pp. 1154-1159, 1993.

- [14] Yin.Yi, liu jinliang, Zhong Huihuang and Feng Jiahuai, “Experimental study of the Recovery Times of Spark gap Switch with Different Gases”, *Plasma science and Technology*, vol.10, No.3, 2008.
- [15] Stuart Moran and Shelton Hairfield, “High pressure spark gap recovery after overvoltage breakdown,” proceedings of the 5th IEEE Pulsed Power Conference, Arlington, VA (IEEE, New York, 1985), p.473.
- [16] D. Bortis, G. Ortiz, J. W. Kolar and J. Biela “Design procedure for compact pulse transformers with rectangular pulse shape and fast rise times”, *IEEE Transactions on Dielectrics and Electrical Insulation*, Vol.18, No.4, (2011).
- [17] C.S.Reddy, A. S Patel, P. Naresh, Archana Sharma and K.C. Mittal, “Experimental investigations of argon spark gap recovery times by developing a high voltage double pulse generator.” *Review of Scientific Instruments*85, 064703 (2014).
- [18] C.S.Reddy, P. Naresh, Archana Sharma and K.C. Mittal, “Voltage Recovery Characteristics of Spark gap using Repetitive Pulse Power System” *IEEE International Power Modulator and High Voltage Conference (IPMHVC)*, USA, June-2014.
- [19] Scott J. Macgregor, Steven M. Turnbull, Fadhil A. Tuema, and Owen Farish, “Factors Affecting and Methods of Improving the pulse rep. freq .of pulse charged &DC charged high pressure gas switches”, *IEEE Trans. Plasma. Sci.*, Vol.25, NO.2, 1997.
- [20] C.S.Reddy, Archana Sharma and K.C. Mittal, “Experimental Investigations of Pulse Charged Spark Gap Recovery Times and Influencing Factors, ”*IEEE Transactions on Plasma Science*.(Under Review # TPS8263.R1).
- [21] Xinjing Cai, Xiaobing Zou, Xinxin Wang, Liming Wang, ZhichengGuan and Weihua Jiang, “Recovery of gas density in a nitrogen gap after breakdown”, *Applied physics letters*, 97, 101501, 2010.
- [22] A. Bogaerts and R. Gijbels, “Modelling of metastable argon atoms in a direct-current glow discharge” *Physical Review A*, Vol.52, No.5, Nov 1995.
- [23] M. M. Pejovic and G. S. Ristic, “Memory effects in argon, nitrogen, and hydrogen,” *IEEE Trans. Plasma Sci.*, vol. 30, no. 3, pp. 1315–1319, Jun. 2002.
- [24] H.C.Miller, “Vacuum Arcs Anode Phenomena”, *IEEE Trans. Plasma Science*, PS-11, 1983, pp-76-89.

- [25] H.C.Miller, "A review of Anode Phenomena in Vacuum Arcs", *IEEE Trans. Plasma Science*, PS-13, 1985, pp-242-252.
- [26] G.Gundersen, "Anode Spot formation in vacuum Arcs", Thesis, Norweg, Inst. Tech. Trondheim, Norway, 1971.
- [27] D.Klapas and R.Holmes, "Anode Spot Temperature in vacuum Arcs", Presented at XI Conf. Phen. Ion. Gases, 82, (Prague, Czechoslovakia) 1973.
- [28] C.S.Reddy, S.V.Tewari, Archana Sharma, K.C.Mittal and D.P.Chakravarthy, "Effect of anode temperature rise and decay on recovery times of sparkgaps" IEEE 4th Euro-Asian Pulsed Power Conference (EAPPC/BEAMS 2012) Karlsruhe, Germany, October-2012.
- [29] Edgar Dullni, Bernd Gellert, EkkehardSchade, "Electrical and Pyrometric Measurements of the Decay of the Anode Temperature after Interruption of High-Current Vacuum Arcs and Comparison with computations", *IEEE Trans. Plasma Science*, Vol.17, No.5, October 1989.

LIST OF FIGURES

Figure 1.1 A pulsed power system converts a low-power, long time input (a) into a high power short-time output (b).

Figure 1.2 Block diagram of a typical pulsed power system.

Figure 1.3 Voltage recovery phenomena explained by two pulse method.

Figure 2.1 Voltage and current versus time in a spark gap closing switch.

Figure 2.2 Illustration of pulsed charged and self-breakdown gas gap time scales.

Figure 2.3 Interferograms showing the recovery process of the gas density in a 2.7 mm gap at Atmospheric pressure. (a) $t < 0$, (b) $t = 266 \mu\text{s}$, (c) $t = 302 \mu\text{s}$, (d) $t = 504 \mu\text{s}$, (e) $t = 1 \text{ ms}$, (f) $t = 2 \text{ ms}$, (g) $t = 5 \text{ ms}$, (h) $t = 10 \text{ ms}$, (i) $t = 15 \text{ ms}$, (j) $t = 20 \text{ ms}$, (k) $t = 30 \text{ ms}$, and (l) $t = 50 \text{ ms}$.

Figure 2.4 Electric field distributions simulation in the spark gap switch.

Figure 2.5: (1) Geometries of electrodes. (a) Rod-plane gap. (b) Plane-parallel gap (c) Sphere gap.

(2) Convection heat loss model from hot gas sphere to ambient gas.

Figure 2.6: Typical cross section of gas-dynamic spark gap.

Figure 2.7: (1) Sequence of recovery process in low pressure sparkgaps

(2) Pulsed Paschen's characteristics

Figure 2.8 Two sources contribute to plasma injection. The initial source is formed by flashover of the trigger insulator, and the second source is formed by the electron impact heating of the anode. Both plasmas expand into the gap to form the conduction channel

Figure 3.1. Experimental schematic of double-pulse generator with matrix transformer topology

Figure. 3.2. Equivalent circuit for the consideration of optimum relationship among different elements of pulse transformer S indicates the switch location.

Figure. 3.3. Equivalent circuit for the computation of the rise of the pulse on a resistance load.

Figure. 3.4. Equivalent circuit for computation of pulse top.

Figure. 3.5. Equivalent circuit for computation of pulse tail.

Figure 3.6 Pulse Transformer Parallel winding arrangement description

Figure 3.7 Pulse Transformer Cone winding arrangement description

Figure 3.8 Pulse Transformer Foil winding arrangement description

Figure. 3.9. Matrix pulse transformer top view showing arrangement of winding.

Figure 3.10. (a) Block diagram of IGBT gate driver PCB. (b) IGBT gate driver PCB

Figure 3.11. Block diagram of gate driver power supply.

Figure 3.12. Gate driver power supply PCB.

Figure 3.13. Typical waveform of the trigger pulse given to the IGBT switch with 42 ms delay. The T_{p1} and T_{p2} are square pulse with amplitude of 15 v and 2 μ s pulse duration.

Figure 3.14. Perspex spark gap testing chamber with rogowsky profile electrode.

Figure. 4.1 Experimental setup

Figure. 4.2 Output voltage pulse of the pulse transformer, $T_r = 300$ ns, FWHM = 1.5 μ s.

Figure 4.3 Breakdown voltages histogram for 2 mm gap spacing with parallel Rogowsky profile electrodes.

Figure.4.4. Probability density of breakdown voltages for a 2mm gap spacing for parallel Rogowsky profile electrodes

Figure 4.5. Typical waveforms of single voltage pulse and discharge current

Figure 4.6. First pulse breakdown voltage as a function of gap pressure characteristics for Argon gas 0-2 bar, 2-4 mm gap distance

Figure 4.7 Typical waveform of the voltage across the gap in the experiment with two-pulse method. (a) Time delay between two pulse for argon gas, 4 mm gap, 0 bar, and 360 ms delay. (b) Breakdown and recovery voltages argon, 4 mm gap, 2 bars, 300 ms delay.

Figures 4.8 (a),(b), and (c) shows the percentage recovery as a function of the delay times for 2mm, 3mm and 4mm gap distances respectively for argon gas.

Figures 4.9 (a),(b), and (c) shows the percentage recovery as a function of the delay times for 1mm, 2mm and 3mm gap distances respectively for Nitrogen gas.

Figure 4.10. “% Voltage recovery” in 2mm spark gap at 2 bar pressure with Nitrogen, Argon and Sf_6 gas ambiances.

Figure.4.11. Different sized electrodes used for the spark gap recovery experiments.

(a) Thin needle used for the point-plane spark gap configuration (b) 34mm diameter (c) 40mm diameter and (d) 68mm diameter electrodes used for parallel-plane spark gap configuration

Figure.4.12. Rate of rise of voltage recovery for different electrode configuration with 2mm gap distance.

Figure.4.13. Rate of rise of voltage recovery for different electrode configuration with 3 mm gap distance.

Figure.4.14. Voltage recovery variation for 2mm and 5 mm spark gap distance with 68 mm diameter Parallel-Rogowsky electrode configuration.

Figure.4.15. Voltage pulses with different rise times due to capacitor variation in the pulse modulator.

Figure.4.16. Effect of pulse rise time on the Rate of rise of voltage recovery with 2mm gap distance.

Figure.4.17. Rate of rise of voltage recovery for variation in conduction current with 2 mm gap distance

Figure.4.18. Rate of rise of voltage recovery for variation in conduction current with 3 mm gap distance

Figure 4.19 The recovery characteristics of point-rogowsky profile with 2 mm gap for positive and negative polarity pulses.

Figure 5.1 Simulated geometry of spark gap at 20ms, 2mm and 1atm argon gas

Figure 5.2. Density and temperature variation for the simulation time for 2mm argon spark gap at 1atm pressure

Figure 5.3. Typical waveforms of voltage pulse and discharge current

Figure 5.4. Simulation contours showing the recovery process of the gas density and temperature in a 2mm gap at 1atm pressure, (a) gas density at $t=10\mu\text{s}$, (b) gas density at $t=150\mu\text{s}$, (c) gas density at $t=1\text{ms}$, (d) gas density at $t=50\text{ms}$, (e) Temperature at $t=10\mu\text{s}$, (f) Temperature at $t=150\mu\text{s}$, (g) Temperature at $t=1\text{ms}$, (h) Temperature at $t=50\text{ms}$.

Figure 5.5. Variation of Argon gas density along the spark channel length for $10\mu\text{s}$ to 100ms .

Figure 5.6. Variation of Argon gas density along the spark channel length for 1atm to 4atm pressure at 50ms simulation

Figure 5.7. Variation of argon gas density with time for 1atm to 4 atm pressures at 1mm distance along the spark gap

Figure 5.8 Neutral gas density recovery inside the gap

Figure 5.9 Voltage recovery of the gap

Figure 5.10 Voltage recovery curve explanation

Figure.6.1 Anode temperature rise for copper and stainless steel materials

Figure.6.2 Anode temperature Decay for copper and stainless steel materials

Figure.6.3. Simulated geometry of spark gap.

Figure. 6.4 Temperature decay curves for copper stainless steel, silver, tungsten and Graphite for 30 kA pulse.

Figure. 6.5 Temperature decay curves of copper for different current pulses.

Figure. 6.6 Temperature decay curves of stainless steel for different current pulses.

Figure. 6.7 Total temperature decay curves of stainless steel for different current pulses.

LIST OF TABLES

Table 1.1. A summary of various switch parameters for pulsed power applications

Table 2.1: primary interaction of electrons

Table 2.2: Secondary Interaction of electrons

Table 3.1. The parameters of the Pulse generator

Table 3.2. IGBT Gate drive requirements

Table 3.3. Power supply parameters for gate drive module

Table: 5.1 possible operating frequency of spark gap switch

Table 6.1. Temperature of Anode spots/Foot points.

Table 6.2. Thermal data for Cu and Stainless Steel materials

Table 6.3. Specific heat flux data for different current range

LIST OF SYMBOLS

E	Charge on electron	$1.6 \times 10^{-19} \text{ C}$
M	Permeability of free space	$4\pi \times 10^{-7} \text{ H m}^{-1}$
R	Resistance (ohms)	
L	Inductance (Henry)	
C	Capacitance (Farad)	
π		3.14285
H	Electric field	
B	Flux density	
J	Current density in amp/metre ²	
V_g	source voltage in volts	
R_g	source resistance in ohms	
L_e	effective shunt inductance in henrys	
R_e	effective shunt resistance in ohms	
C_c	mutual capacitance in farads	
L_l	leakage inductance in henrys	
C_d	distributed capacitance in farads	
R_l	load impedance in ohms	
I and V	current and voltage across load in amperes and volts	
A	Current in Amperes	
Z	Impedance in Ω	
W	Energy stored in capacitor	
ρ	Gas density	

u	gas velocity,
μ	Viscosity
g	gravity
H	total enthalpy
h_t	heat transfer coefficient
t	time in seconds
h	gap distance
r	radius of the spark.
t_t	Time Lag in seconds
t_d	Statistical time Lag
t_f	Formative Time lag
t_r	Rise Time
T	Temperature in K.
α	thermal diffusivity (cm^2 / s).
$\Delta\tau$	pulse time interval in sec.
c	specific heat.
τ	time since heat pulse is applied.
x	depth in the solid body.
S	Specific heat flux from arc to the surface
K	Thermal conductivity (W/m-K)
C_p	Heat capacity at constant pressure (J/kg-K)
h	Heat transfer co-efficient ($\text{W/m}^2\text{-K}$)
T_{ext}	External temperature (K)
ε	Surface emissivity

T_{amb}	Ambient temperature (K).
γ	Townsend's secondary ionization coefficient
P_a	Specific heat flux in watts /m ²
P_n	Neutral atom energy watts/cm ²
P_r	radiant energy density
J_a	Anode current density A/m ²
V_T	Electron thermal energy eV
ϕ	Work function of the electrode,
V_a	anode drop volts

LIST OF ABBREVIATIONS

BDV	Breakdown Voltage
BDVs	Breakdown Voltages
CFD	Computational Fluid Dynamic
DBV	Dynamic Breakdown Voltage
SBV	Static Breakdown Voltage or self breakdown voltage
FPBDV	First Pulse Breakdown Voltage or Main Pulse Breakdown Voltage
FEM	Finite element Method
SPBDV	Second Pulse Breakdown Voltage or recovery Pulse Breakdown Voltage
Max.	Maximum
Min.	Minimum
ms	milli-second
ns	nano-second
nf	nano farad
nh	nano henry
PBDV	Pulsed Breakdown Voltage
PFN	Pulse forming Network
PFL	Pulse forming line

PRF pulse repetition frequency

Pps pulses per second

PMMA Polymethylmethacrylate or Perspex or acrylic

RBDV Recovery Pulse Breakdown Voltage or Probe Pulse Breakdown voltage

TEMP Temperature

-Ve Negative Polarity,

+Ve Positive Polarity

CHAPTER 1

1.1 Introduction

Pulsed power is the term used to describe the technology of accumulating energy over a relatively long period of time and releasing it into a load in a short time interval (also called energy compression) to obtain a transient huge power. We can do a simple calculation to see the effect of energy compression. If we have one Joule of energy in the energy storage system and we release this energy within one nanosecond, we can achieve one Giga-Watt of instantaneous power (Figure 1.1). This unique characteristic of high peak-to-average power ratio makes pulsed-power techniques successful in applications such as accelerators, high power pulsed lasers, fusion research and electro-magnetic weapon research etc., which are not possible with other methods.

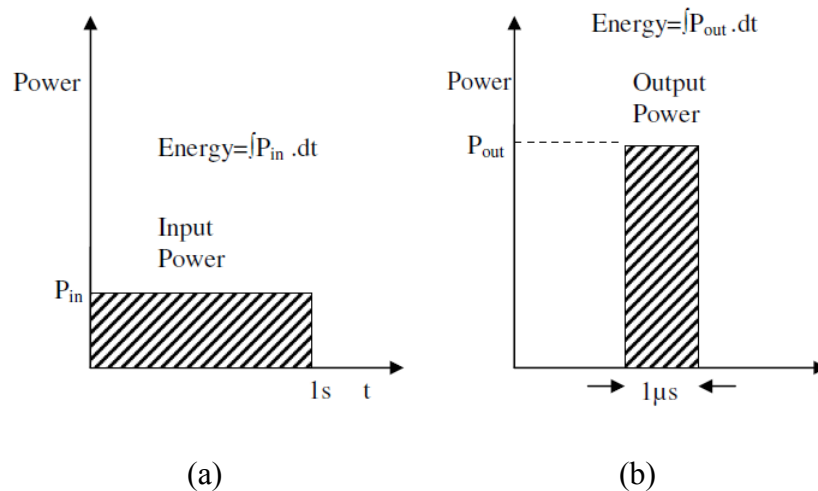


Figure 1.1 A pulsed power system converts a low-power, long time input (a) into a high-power, short-time output (b). [1]

Pulsed power was first developed during World War II for usage in Radar and afterwards, it has mainly been driven by military requirements, both for the advancement of pulsed-power-based weapons and for the evolution of new simulation and diagnostic tools. Considerable effort has

been undertaken to develop pulsed-power-based weapon systems such as electromagnetic mass launchers and beam weapons. Nowadays, pulsed power is widely spread into civil low energy compact systems like the ignition system in automobile [2, 3], pollution control [4, 5], food industry [6], bio-medical applications [7, 8] and others. The pulse power systems are classified as single shot systems and repetitive operating systems. The repetitive pulse power systems are the pumping source for gas lasers, as a driving source for plasma chemical reactors, microwave radiation curing of coatings, polymerizations and sludge disinfections etc. The switch used in pulsed power system, play a crucial role in deciding the total repetition rate of the system for a particular application.

1.2 Pulsed Power System

An overall scheme of a pulse power system consists of (i) a power source, (ii) primary energy storage system of capacitor banks at voltages of 10-100 kV, with charging times of a few ms to a few minutes, (iii) voltage multiplication / pulse compression to produce pulses of duration one micro-second to tens of micro-seconds, or even pulses of durations ranging from a few ns to less than a micro-second and (iv) the load impedance matching network. The typical structure of the pulsed power system is shown in figure 2.1.

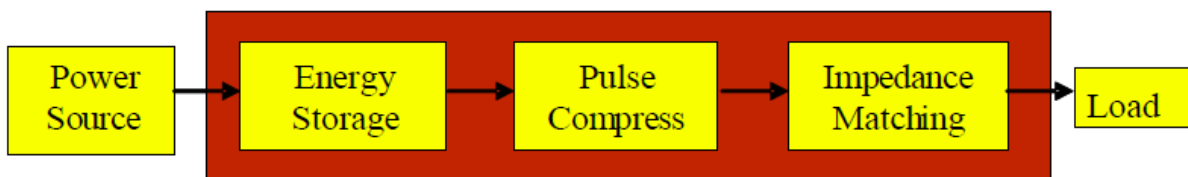


Figure.2.1 Block diagram of a typical pulsed power system

Once we turn on the power source, the energy is delivered to the energy storage components via the power charging circuit. The charging time for the energy storage is determined by the power

source and charging circuit. The primary / secondary switching devices employed in energy storage devices play an important role in transfer of stored energy and pulse compression.

There are two major methods for storing the electromagnetic energy: energy stored in an electric field (capacitive storage), and in a magnetic field (inductive storage). The simplified way to calculate the energy W stored in the capacitor can be written as $W = CV^2/2$, wherein C is the capacitance of the capacitor, and V is the voltage on the two electrodes of the capacitor. The maximum energy density stored in the capacitor is not only limited by the breakdown strength of the dielectric material, but is also limited by the capacitor package methods and the operation condition (such as working frequency, charging speed and voltage reversal). In another hand, inductive storage components are able to store the energy $W = LI^2/2$, wherein L is the inductance and I is the current flowing through the inductor.

The pulsed power switching is one of the main factors which not only determines the maximum energy transfer in the system, but also determines the speed of the energy transportation. Typically, the pulsed power switches are applied between the energy storage and PFN to transfer energy from relatively low power level to form higher power output. Based on the operation status, high power switches can be classified into two basic types: closing and opening switches. “Terms as ‘opening’ or ‘closing’ are used to describe which transitional state of the switch is controlled to achieve the desired circuit function.” In most cases, charge transportation through the previous medium requires maintaining the switch closure to construct the conduction path. In comparison, opening switches are not used as widely as closing switches. They are typically used in the inductive system. In addition, on the basis of the property of the medium that is employed between the switch electrodes, the pulsed power switches can be classified as gas switches, solid state switches and liquid switches. Although the specific terminology of the pulsed power switch

is sometimes different, the parameters that are used to evaluate the switch performances have much in common. The regular switch parameters are described below [9],

Hold-off Voltage:

It is the maximum voltage that can be provided between the electrodes of the switch without breakdown. It is also called stand-off voltage, self-breakdown voltage or blocking voltage sometimes. The units are volts (V) or kilovolts (kV). The value of the hold-off voltage is determined by the medium property between the electrodes and the dielectric strength of the insulating envelope outside the switch. In some special cases, the switch is charged up rapidly in pulse mode with voltage higher than the DC hold-off voltage, which is called over-voltage.

Peak Current:

The highest current conducting capability of the switch is called peak current. The usual units are amperes (A), or kilo amperes (kA). It is limited by the medium conducting property and the geometry of the electrodes. Especially in the gas switch, the hollow structure of the switch cathode improves the peak current.

Delay Time:

It is the time interval between the application of a trigger command and the initiation of switch conduction. The usual units are second (s), micro-second (μs) or nano-second (ns). This time interval is composed of processes which involve the generation of the initial charge carriers and the pre-breakdown phases to establish conducting channels between the electrodes. In addition, the inductance of the switch itself and the pulsed power system also increases the delay time of the switching.

Jitter Time:

The jitter time of a spark gap is the shot to shot variation in switching time and rise time characteristics. It depends upon the material of the electrode. Aluminum electrodes have been found to give less jitter compared to brass electrodes. Jitter reduces with gas flow compared to static gas. It plays a very important role in reliability of the switching operation when the switch is used for repetitive pulsed applications.

Recovery Times:

The recovery time is an important parameter of the spark gaps generally used in repetitive pulse power systems and circuit breakers. Full recovery (100%) means the spark gap has to recover to its original pre-breakdown status before the application of the next pulse. The recovery time mainly depends upon (i) the first pulse (or main pulse) breakdown voltage (FBDV), wave shapes, current magnitude and reversal, (ii) peak temperature and type of discharge, (iii) gas (iv) pressure and (v) gap distance. Special type of switches like photo-conductive switches and Saturable reactors can also be used for the pulse power applications. These switches are more suitable for repetitive pulsed applications due to absence of discharge. They have faster recovery time compared to spark gaps. However they have their own limitations like lower peak voltage, peak current capability, low current reversal ratings and poor capability to withstand surges.

Repetition Rate:

It is the rate at which the switch can be operated without degradation of characteristics. The usual units are Hertz (Hz) or kilohertz (kHz). The rate is limited by the switch recovery time and forward drop.

1.3 Pulse Power Switches:

In pulse generator design the switch is one of the most critical considerations. In particular, the main problem in developing high-voltage (10-100 kV) short pulse (1 ns - 100 ns) and high-repetition rate (up to 1 kHz) pulse generators is to choose a reliable and fast high-voltage switch [10]. A switch can be categorized by function, e.g. a closing or an opening switch, and by type, e.g. solid, liquid, gas, or plasma. Each switch has different limitations, including opening and closing times, maximum repetition rates, forward voltage drop, voltage hold-off strength, and peak current ratings. Typical characteristics for different switch types used for high voltage pulsed power applications are shown in **Table 1.1** [11], and the use of these switches is discussed in the following sections.

Table 1.1. A summary of various switch parameters for pulsed power applications [11].

Switch type	Hold-off voltage (kV)	Peak current (kA)	Forward drop (V)
Spark gap	100	10 to > 1000	20
Thyratron	125	20	150
Pseudo-spark gap	100	5-100	200
Thyristor	1 to 9	1 to 50	2
MOSFET	1	0.1	V_{DS}
IGBT	7	1	3

1.3.1 Gas Switches:

Gas switches are commonly used for high-voltage and high-power applications because they have very high hold-off voltages and current capabilities. The gas between the electrodes inside the switch acts as the insulator while the switch is off, so the breakdown voltage is determined

by the dielectric strength of the gas and the gap between the electrodes. The switch is typically electrically or optically triggered [12], which causes a portion of the gas to become ionized, producing a plasma. The plasma allows very fast switching times and the transport of very high currents, and the power dissipation is relatively low. The most common gas switches for pulsed power applications are spark gaps, thyratron, and pseudo-spark switch [13, 14].

Spark Gaps:

Spark gaps are a gas closing switch that are among the most commonly used switches in laboratory pulsed power experiments because they are simple, inexpensive, and have extremely high operating voltage and current [15]. Despite the fact that spark gaps have been used for over a century and many of these properties have been known for years, it has only been in the past few decades that the need for high peak power repetitive pulsed power systems has forced serious efforts to engineer systems compatible with these idiosyncrasies. A spark gap typically consists of two electrodes separated by a gas (or another insulating medium such as a vacuum, liquid, or solid). The switch is closed when the gap is significantly overvolted (self-breakdown), or by applying a trigger (electrical or optical) to a third electrode (breakdown by triggering mechanism) [16]. For high peak power pulsed power applications spark gaps are the normal choice for switches. This device exhibits many of the desired characteristics for pulsed power, including peak voltage and current handling capabilities which extend into the MV and MA ranges. They are triggerable with nanosecond jitter, have a large operating range, and give good time compression per switched stage. In addition they are rugged, lightweight, inexpensive, and relatively easy to use. On the negative side, they suffer from recovery problems at high repetition rates and have some instability (pre-firing) problems even in single shot applications. These limits the maximum PRF (pulse repetition frequency) to a few hundred Hz. The trend in repetitive

pulsed power is to higher peak power and higher repetition rate. Pushing spark gaps to higher repetition rates has long been a prime effort in the field. High peak power, single pulse systems historically have been spark gap switched but the sparks are formed in the device's insulating fluid, oil or water. Liquid spark gaps do not appear to be serious contenders for repetitive service because of the shock waves generated by sparks in liquids. Improvements in the voltage recovery time are possible by employing gas flow techniques which clear the remnants of the switching arc from the inter-electrode region during the inter-pulse period. However, as the required PRF extends into the kHz regime, the gas flow requirements become expensive and tend to dictate the switch design and therefore considered undesirable approaches when designing inexpensive pulse generating systems.

Thyratron:

A thyratron is a gas closing switch that can have hold-off voltages greater than 100 kV and can handle peak currents greater than 10 kA. Thyratron is a switch with a sufficiently long lifetime at a reasonable cost for high-power applications. The basic thyratron consists of an anode, cathode, baffle, control grid, and gas reservoir. The gas reservoir is filled with low-pressure (approximately 0.5 torr) hydrogen (H₂) or deuterium (D₂) [17, 18, 19], and the cathode is heated to emit electrons into the neutral plasma formed by the gas. An electrical pulse is applied to the grid to cause the switch to close by ionizing the fill gas. Compared to the spark gap, the thyratron has a much longer lifetime (billions of shots), however, a major disadvantage of this switch is the hot cathode, which adds significant overhead to the pulse generator design.

Pseudo-spark switch:

A pseudo-spark switch is a gas closing switch similar to a thyratron in that a plasma is formed in a gas that is around 0.5 torr, but the pseudo-spark differs from the thyratron in that it uses a cold

(hollow) cathode. A heater is still used [20], but it is used to control the gas pressure in the reservoir, not to heat the cathode. The limitation in the peak current capability for both the thyatron and the pseudo-spark switch is in the cathode, and the pseudo-spark was designed with the goal of increasing the peak current capability of the thyatron. In the pseudo-spark switch, a hollow cathode discharge is formed, which results in the self-heating of a thin cathode surface layer due to the field and the plasma. The cathode layer reaches extremely high emission through both field emission and thermionic emission [21]. Peak currents can be greater than 100 kA. The pseudo-spark switch used in this work is capable of switching 30 kA, with a rise time of 8 kA/ns. Similar to the thyatron, a major disadvantage of the pseudo-spark is the overhead associated with heating, as well as the size of the switch itself. However, because of special properties of the pseudo-spark discharge, which can prevent arcing at very high current densities, these switches have lifetimes comparable to Thyatron [22].

1.3.2 Solid state switches

Solid state switches are attractive because they eliminate the overhead (e.g. heating) associated with a gas switch, reduce size and weight, and increase reliability and lifetime. The drawback of solid state switches is lower hold-off voltages and peak current capacities compared to gas switches, which place strict requirements on the rest of the system to compensate for those limitations. The most common solid state switches for pulsed power applications are Thyristors, MOSFETs, and IGBTs. A detailed review on power semiconductor switches was given in [23].

Undergoing research efforts in solid-state switches are focusing on two directions: 1) to push performance limit of silicon-based power switches by adapting advanced materials and device processing techniques, this direction is mainly driven by the semiconductor industry; 2) to develop devices based on advanced semiconductor materials with the higher carrier mobility and

wider band gap than Silicon. For more than a decade, GaAs has been considered as an attractive candidate to develop power switches for its optoelectronic properties and very high electron mobility [24 to 27]. The latter, the carrier mobility, suggests that this is a great solution for pulsed power – fast rise. However, due to possible scattering through intrinsic defects (EL₂) or electron-electron collisions, the electron velocity of GaAs saturates as a function of applied electric field, which results in a high forward drop and limits switching performance [28]. Recently, SiC and GaN have attracted interests for their wide band gaps (> 2 eV), resulting in higher hold-off voltages. Significant progress in SiC power devices has been reported by [29, 30] including the fabrication of UMOSFETs with breakdown voltages of 1400V (10μm drift region) and 5050V (100μm drift region).

1.3.3 Magnetic Switches:

Magnetic switches are based on the nonlinear relation between the magnetic field H applied to a core made from amorphous metals (i.e., metallic glass) and the resulting flux density B . The inductance of a winding around the magnetic core depends on the current passing through the winding and can change very quickly. Magnetic switches can operate in the 10 ns range with a repetition frequency in the kHz range with no moving parts and no discharge. A disadvantage of using magnetic switches for high-power applications is that they have an efficiency of 50–70% so the core requires cooling because the saturation flux density is temperature dependent [31]. The basic operating principle of magnetic switching is that sufficient current is driven through the winding on a magnetic core so that the applied field H produces a flux density B in the core in excess of the core's saturation flux, causing the inductance in the winding to change from a relatively high value to a very low value. The change in μ can be greater than three orders of magnitude, e.g. from around 1000 to around 2.

Magnetic switches are excellent for pulsed power applications because they have a very long lifetime and are very reliable compared to gas switches, they can be operated at high repetition rates (>1 kHz), and they can allow pulse rise times comparable to gas switches. Their biggest disadvantage is that they must be cooled in high-power applications, and that core reset must be monitored carefully to ensure pulse consistency.

So, at present, the spark gap switch is still not replaceable when a compact pulsed power system is required to generate high voltage (> 10 kV) and high current (> 1 kA) with fast rising (sub-nanosecond) electric pulses for pulse power applications. The primary limitation lies in lifetime and repeatability. Other shortcomings with spark gaps are related to strong electrode erosion, insulator degradation, high arc inductance, and costly triggering [32]. Operating gas spark gaps at high pressure can reduce the switching time and obtain the stable switching performance. Small liquid spark gap switches, typically using water as breakdown medium because of its high dielectric constant, have been developed [33, 34]. In order to reduce the water recovery time, hence to increase the repetition rate, post breakdown phenomena and dielectric recovery have been studied [35]. The main disadvantage is the water contamination and shock waves generated by sparks in liquids [36]. Thus a water circulation system is required at this time.

1.4 Two-pulse Method:

The recovery time is an important parameter of the sparkgaps generally used in repetitive pulse power systems and circuit breakers. Full recovery (100%) means the sparkgap has to recover to its original pre-breakdown status before the application of the next pulse. The recovery time mainly depends upon, the first pulse (or main pulse) breakdown voltage (FBDV), wave shapes, current magnitude and reversal, peak temperature and type of discharge, gas mediums and (iv) gas pressure.

There are a number of ways by which the recovery time of a sparkgap can be measured. The most important ones are (i) repetitive pulsing method [37 to 41], ii) two pulse method [42 to 45] and (iii) three pulse method [46]. In these methods the first pulse should be the normal discharge pulse. The second (recovery pulse, RPBDV) and subsequent pulses can be same as the first pulse or a probing pulse. These pulses may be electrical in nature like $1.2\mu\text{s}/50\mu\text{s}$ impulse. Here the recovery time is directly measured. The other recovery time measuring methods are (a) microwave interferometer [47], (b) laser Schliren techniques and (c) spectroscopic method (48). These are used to study the recovery process in a discharge, by measurement of the charge particle density or neutral particle density. Even though they can be used in principle for measurement of recovery time, these methods are not preferred.

(i) In repetitive pulsing method, normally same type of pulses are applied repeatedly and the breakdown voltages are measured. This method gives full information on recovery time with rated current and heat dissipation capability of the sparkgap. Another alternative is to apply recovery pulses like $1.2\mu\text{s}/50\mu\text{s}$ impulse to record the breakdown voltages till the full recovery of the gap. The recovery pulses are selected such that they do not affect the discharge conditions during recovery process in the gap. The heat dissipation capacity of the sparkgap cannot be tested by this method. This method is suitable in case of circuit breakers where large currents have to be handled and normally they do not have to withstand high voltages except while breaking the gap. The recording of breakdown voltages is somewhat complicated. Advantages of this method is that complete recovery data can be obtained in one discharge.

(ii) In two pulse method, initially the first pulse is applied to the sparkgap. Next the recovery pulse is applied with a delay. This pulse can be same as the original pulse or of high voltage, low energy pulse similar to $1.2\mu\text{s} / 50\mu\text{s}$ impulse (probe pulse). The experiments have to be repeated

a number of times to get complete data of the recovery time. The effect of heat dissipation capacity of the switch cannot be tested. The recording of breakdown voltages is very simple. This method has been widely used in recovery voltage / time measurements.

(iii) The three pulse method is a slight variation of the two pulse method. This method is generally used while using the same type of pulses for second and third pulses for recovery time measurements. However the low energy pulses can also be used for recovery time measurement. The third pulse is used for confirmation of the second pulse breakdown voltage. The first pulse is applied to the sparkgap followed by two recovery pulses applied in sequence with same delay between them. The effect of heat dissipation capacity of the switch cannot be tested by this method. This method has not been widely used in recovery time measurements due to additional requirement of power supply. The experiments have to be repeated to get complete data of the recovery time.

We choose the two pulse method over other methods in this work for obtaining voltage recovery time of the spark gap. An experimental setup was made based on the matrix transformer topology to produce two voltage pulses of 40 kV amplitude, 300 ns rise time, with controlled delay between the pulses.

There are 3 recovery phenomenon's that can be observed in the repetitive operations of a spark gap namely,

1. Under recovery
2. Full recovery
3. Over recovery (at low pressures)

These phenomenon can be explained by two similar voltage pulses which over volts the spark gap. The measurement is as follows: first a fast rising voltage pulse applied to spark gap

which breakdown at point A, represents first pulse Breakdown voltage (FPBDV). Now a similar second pulse is applied after some time delay, which breakdown the spark gap at a voltage known as second pulse Breakdown voltage (SPBDV). If the second pulse breakdown voltage (SPBDV) at lower voltage level compared to first pulse breakdown voltage (FPBDV), then it is called under recovery. Similarly, if SPBDV is equal to FPBDV, it shows full recovery. And if SPBDV is higher than FPBDV, it represents an over recovery in the spark gap. This 3rd phenomena (over recovery) was observed in only at low pressure experiments [49, 50]. For over-recovery of the gap, the recovery pulse voltage should be higher than the first pulse voltage. The under-recovery, full and under recovery times and voltages are shown in the figure 1.3.

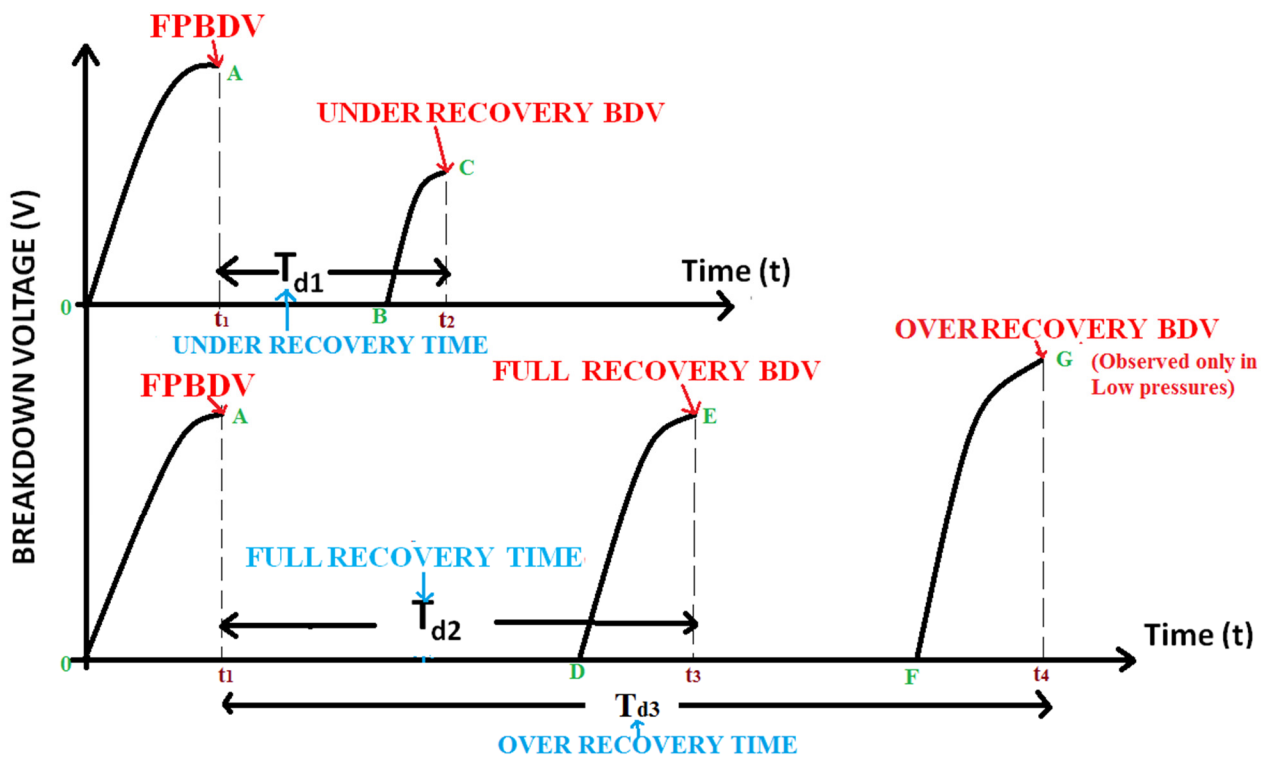


Figure 1.3 Voltage recovery phenomena explained by by two pulse method.

The under-recovery time (T_{d1}) is from point t_1 to point t_2 and the full recovery time (T_{d2}) is from point t_1 to point t_3 and the over recovery time (T_{d3}) is from point t_1 to t_4 . The under-recovery

voltage is from point B to point C and the full recovery voltage is from point D to point E and over recovery voltage is from point F to point G.

1.4. Aim of the Work

A few pulse power systems have been developed at Bhabha Atomic Research Centre, Mumbai for wide ranging applications, which are presently working in single shot mode. The various applications require systems to operate in the range of a few Hz to 10 kHz. Some systems operate in the burst mode involving high repetition frequency for a short period. These bursts may be single or repetitive in nature. The sparkgap is the most important and complicated component in the repetitive pulse power system and plays an important role in deciding the ultimate performance. The sparkgaps for repetitive pulsed applications should have a short rise-time, low jitter and fast recovery rate. The aim of this work is to develop and study sparkgap system having a peak voltage of 40 kV and a rise time of 300 ns and a pulse width of 1.5 μ s. Also to study the effect different operating parameters like pressure, type of gas, gap distance, pulse rise time, the electrode shape and size, which are useful for designing a suitable spark gap for repetitive applications. The sparkgaps suitable for the above applications could be in the configurations of high pressure gas devices.

1.5 Outline of the thesis

The thesis highlights the study on the recovery of spark gap with Argon and Nitrogen gases as insulating medium at high pressure range. The study further involves the use of different Electrode shapes and sizes, discharge currents, pulse rise times and also gap distance and its impact on the recovery rate of the spark gap switch.

The thesis has been organized as follows:

Chapter 1 is the introduction to the insulation aspects in high voltage pulse power systems, application of pulse power system in industrial, defense and research areas, types of switches used in pulse power applications, the phenomena of spark gap recovery and the method used in the study. Also, the need to study the phenomena of spark gap switch recovery in compressed gas environment which forms the basis of this thesis.

Chapter 2 provides a review of the literature on spark gap recovery in gases and summarizes the different factors influencing the recovery rate of the spark gap. The mechanism in high pressure gases is discussed along with the different physical processes responsible for the delayed recovery of the spark gap switch. A few of the existing spark gap literature explaining physics of the recovery process and effect of operating parameters is also discussed.

Chapter 3 gives detailed design and development of the double pulse generator, which produces two identical pulses of having 40 kV amplitude and 300 ns rise time. A matrix pulse transformer was used to give fast rise times for the voltage pulses and selection procedure for the components used in the experimental setup was given. The main components include a capacitor, an IGBT switch with effective triggering circuits, a spark gap chamber made with Perspex and a capacitor charging power supply.

Chapter 4 contains a detailed analysis on the spark gap voltage recovery results obtained by using a two pulse method. The effect of different parameters on the spark gap recovery rate was studied in detail and a better spark gap configuration has been suggested. The recovery data with effect to gas, gap distance, pressure, electrode shape and size, pulse rise time and also discharge current was obtained.

Chapter 5 describes a two-dimensional axisymmetric computational model of the spark gap developed by using a CFD code ANSYS/Fluent to provide a better understanding of the dynamics of the recovery process. In this work, we investigate the recovery of temperature and density of the spark gap channel after breakdown through the computational method. The mechanism for the delayed recovery of breakdown voltage compared to gas density was discussed. Based on the observations, the possible operating frequencies that can be obtained by triggering the spark gap at below self-break down voltage level was also suggested.

Chapter 6 presents a method to estimate the effect of anode temperature rise and decay on repetition rate of spark gap. By using this method, the behavior of copper and stainless steel materials for a range of specific heat flux densities corresponding to different current pulses were studied. This temperature decay is also verified by a heat transient computational model developed in FEM based software. Simulations have been carried out for different materials including Cu and SS.

Chapter 7 presents the summary and future scope of work in this area.

Chapter 2

Literature Survey

2.1 Introduction:

The continuous development of high peak power applications has resulted in an increasing demand for the development of reliable high power switches capable of operating at pulse repetition frequencies (PRFs) of 1 kHz and above. One of the most widely employed devices for high peak power switching is the high pressure gas spark gap switch [51]. Advantages of this device include, simplicity, robustness, a wide range of voltage and Current handling capabilities (up to MV and MA levels) as well as excellent switching characteristics such as high dV/dt (up to 10^{15} Vs^{-1}) and low jitter (few ns) [52,53]. The major disadvantage of the spark gap is the time taken after switching for the hold-off voltage to recover. This limits the maximum PRF to a few hundred Hz. This problem severely limits the application of these switches in repetitive systems. Improvements in the voltage recovery time are possible by employing gas flow techniques which clear the remnants of the switching arc from the inter-electrode region during the inter-pulse period. However, as the required PRF extends into the kHz regime, the gas flow requirements become expensive and tend to dictate the switch design.

This chapter discusses some of the findings of an extensive and ongoing investigation into the repetitive operation of spark gap switches. Also, the existing spark gap literature explaining physics of the recovery process and effect of operating parameters like insulating medium type, pressure, electrodes shape and size, mode of operation and conduction current upon the voltage recovery characteristics are discussed.

2.2 Fundamentals of a gas closing switch:

Ionization processes in the inter-electrode space and the secondary electron emissions from the cathode cause rapid increase of the current. This rapid transformation of current produces a non-self-sustaining discharge to some form of self-sustaining discharge. This phenomenon is known as electrical breakdown. Electrical breakdown in a gas is a rapid sequence of irreversible events, which quickly lead to a transition of the gas from its 'normal' insulating state (conductivity $\sim 10^{-14} \Omega^{-1} \text{m}^{-1}$) to high conducting state (e.g., over 14 orders of magnitude larger for the transition to an arc discharge). Gas filled spark gaps employ high or atmospheric pressure gases such as air, nitrogen, hydrogen and Sf_6 . The voltage standoff capabilities of the switch are determined by the breakdown characteristics of the dielectric and the field emission characteristics of the separated electrodes. For high pressure gas switches, breakdown of the bulk dielectric medium is usually close to but before the field emission from electrodes becomes a problem. One of the desirable operating characteristics such as voltage & current relationship pertinent to a closing switch is shown in Figure 2.1.

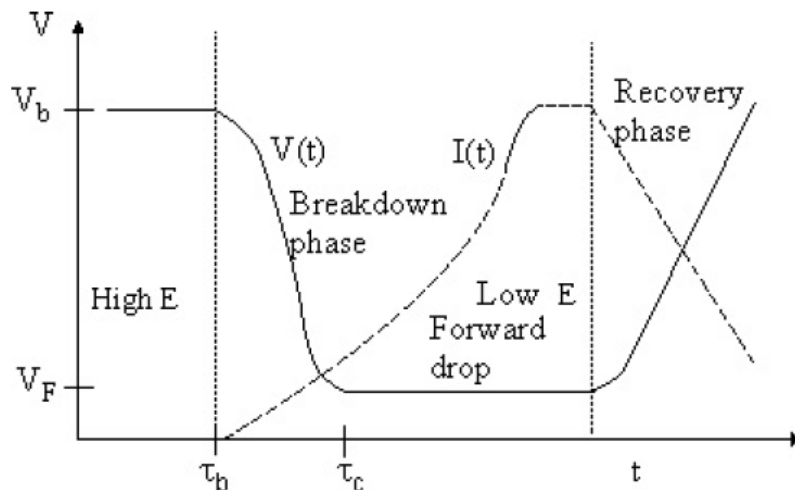


Figure 2.1 Voltage and current versus time in a spark gap closing switch [54].

The efficient operation of the closing switch requires a gaseous medium with a large breakdown strength V_b , extremely small forward voltage drop or low conduction voltage V_F , and a short formative time lag or turn-on time ($\tau_f = \tau_c - \tau_b$). The switch is initially opened (non-conducting) at time $\tau < \tau_b$. At this stage, the voltage V_b applied between the electrodes of the spark gap is high in the ambient temperature T . When the switch closes (start conducting) at time $\tau = \tau_b$ the voltage $v(t)$ drops and the current $i(t)$ increases. This is referred to be as the breakdown phase or turn-on time or closure phase. The voltage V_F across the two electrodes during the conducting stage is much lower than V_b depending on the degree of ionization. The gas temperature is very high during this stage. It is highly desirable that such switches should close quickly and with a minimum energy loss.

2.3 Electrical breakdown in a gas gap under repetitive operation

The self-breakdown characteristics of a gas gap are dependent upon many parameters, including the duration, which the gap has been exposed to the applied voltage. The important time intervals associated with the pulsed charged spark gap are illustrated in Figure 2.2:

- 1) The time required to raise the gap voltage to the self-breakdown voltage V_{sb} is the charging time τ_c .
- 2) The time lapse between the self-breakdown voltage V_{sb} and the application of the voltage V_{ov} for the appearance of a suitably located initiatory electron in the electrically stressed system is known as the statistical delay time τ_{sd} .
- 3) The time interval after the statistical delay time to the onset of breakdown is related to streamer formation τ_{sf} .

4) The time required for the gap closure through heating of the electrons is the column heating time τ_{ch} .

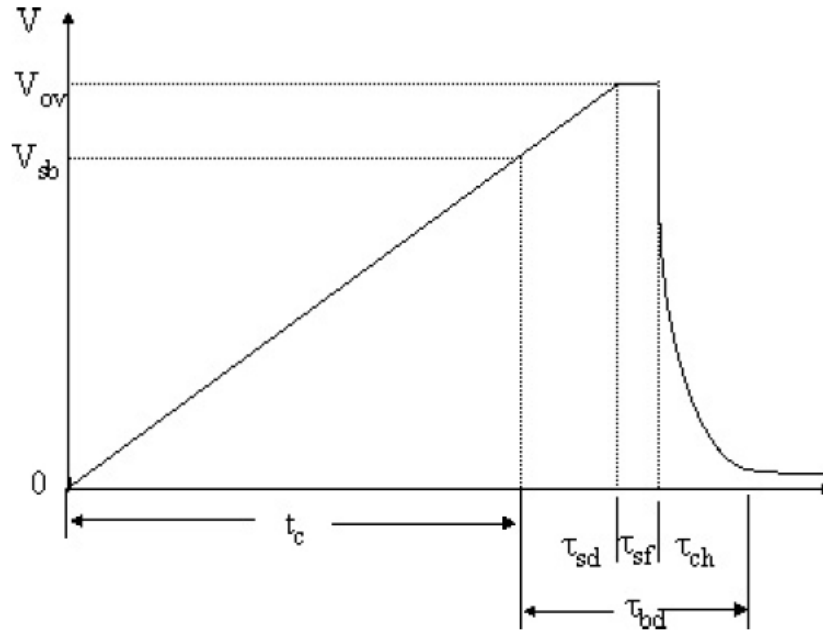


Figure 2.2 Illustration of pulsed charged and self-breakdown gas gap time scales [55].

When the pulses are applied at a higher repetition rate, the ionization produced due to first pulse is to be cleared before the application of next pulse. So, the recovery time generally refers to the time for the recovery of dielectric properties of the plasma gap so that the voltage can be reapplied to it at some rate (dV/dt). The corresponding re-breakdown voltage is referred to be the recovery voltage. The recovery voltage of spark gaps that are operated at the high PRR has typically been below the DC hold off voltage. Most plasma gaps require the concept of recombination and attachment of electrons in the recovery processes. The recovery processes are functions of the plasma kinetic characteristics of the conducting medium; i.e., charge density, mobility temperature, recombination, attachment and other cross sections, mean free paths, externally applied fields, etc. Only after a finite delay, the recovery phase will progress to a point that a certain voltage can be withstood. This leads to the recovery characteristics that limit the

PRR of the switch operation. If a certain rate of reapplication of voltage is exceeded, then there is a high probability that a conducting state will be reestablished.

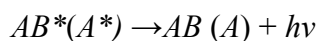
In many cases, recombination and attachment may occur rapidly but the gas is then left in a highly heated state. Therefore, low gas density regions may persist. It means the mean free path of stray charges is much higher and sudden reapplication of voltage may initiate an avalanche. Thus, the gas should not only be deionized but also be cooled and homogenized to allow full voltage recovery. This is the primary reason why gas flow is employed in many situations. Some switches may require little or no flow if the electrode gap geometry or operating conditions result in sufficient cooling and reduced energy deposition. At very high pressures, the recovery processes are such that the recovery time may decrease significantly because, in part, of intense cooling of the arc plasma.

2.4. Dielectric recovery properties

Many physical processes affect the dielectric properties of gases. These involve electrons, positive and negative ions, excited and unexcited atoms and molecules, and photon interactions with the gas and with the electrodes. The principle physical processes associated with the gas are listed in Appendix: Table 2.1 and Table 2.2. The majority of these processes affect the dielectric behavior of the gas directly or indirectly by their effect on the number density and energy of the free electrons, which are present in the electrically stressed system.

Principle physical process [56]: $AB (A^*)$ represents an unexcited and $AB^*(A^*)$ an excited molecule (atom); the double arrow indicated that the reaction can produce a multiplicity of products.

Photon interactions may follow interactions viz.



For the parent negative ion AB^- to be formed, the excess energy of the metastable AB^{*-} ion must be removed in collision with other molecules (a much less likely way is radioactive stabilization of AB^{*-}).

Table 2.1: primary interaction of electrons

Representation	Description
$e + AB \rightarrow AB + e$	Elastic electron scattering (direct)
$e + AB \rightarrow AB^* + e$	Inelastic electron scattering (direct)
$e + AB \Rightarrow A + B + e$	Dissociation by electron impact
$\Rightarrow A + B^* + e$	Dissociation excitation by electron impact
$e + AB \Rightarrow A^+ + B^- + e$	Ion pair formation
$(a) e + AB \rightarrow AB^{*-} + e$	Elastic (inelastic) electron scattering
$\rightarrow AB (AB)^* + e$	
$(b) \Rightarrow A + B^-$	Dissociative electron attachment
$(c) \rightarrow AB^- + \text{energy}$	Parent negative ion formation
$a) e + AB \rightarrow AB^{++} + 2e$	Ionization by electron impact
$b) \Rightarrow A + B^+ + 2e$	Dissociative ionization by electron impact
$c) \Rightarrow A^* + B^+ + 2e$	Dissociative ionization with fragment excitation

Principle physical process [56]: AB^* (A, B) represents an unexcited and AB^* (A^*, B^*) an excited species while $AB^{(*)}$ ($A^{(*)}, B^{(*)}$) represent species in either an excited or an unexcited state; the double arrow indicates that the reaction can produce a multiplicity of products.

Table 2.2: Secondary Interaction of electrons

Representation	Description
<p>Photon–Molecule Interaction</p> $h\nu + AB \rightarrow AB^*$ $h\nu + AB \rightarrow AB^+ + e$ $\Rightarrow A + B^+ + e$ $h\nu + AB \rightarrow A + B^{(*)}$ $h\nu + AB^-(B^-) \rightarrow AB(B) + e$ $\Rightarrow A^- + B$	<p>Photo absorption</p> <p>Photoionization</p> <p>Dissociative photoionization</p> <p>Photo dissociation with(*)/without excitation of the fragment (*)</p> <p>Photo detachment</p> <p>Negative ion photo dissociation</p>
<p>Ion–Molecule (Atom) Interaction</p> $AB^-(A^-) + C \rightarrow AB(A) + C$ $AB^-(A^-) + C \rightarrow AB(A) + C + e$ $AB^-(A^-) + C \rightarrow ABC(AC) + e$ $AB^- + n C \rightarrow AB^- C_n, n \geq 1$ $AB^+ + n C \rightarrow AB^+ C_n, n \geq 1$ $AB^-(A^-) + CD(C) \Rightarrow \text{products}$ $AB^+(A^+) + CD(C) \Rightarrow \text{products}$	<p>Ion conversion (charge transfer)</p> <p>Collision detachment</p> <p>Associative detachment</p> <p>Cluster formation involving negative ions</p> <p>Cluster formation involving positive ions</p> <p>Negative ion–molecule (atom) reactions</p> <p>Positive ion–molecule (atom) reactions</p>
<p>Electron–Ion and Negative Ion–Positive ion, Recombination reaction</p> $e + B^+(A^+) \rightarrow AB^{(*)}(A^{(*)})$ $\Rightarrow A + B^{(*)}$	<p>Electron–positive ion recombination with(*)/without excitation</p> <p>Dissociative recombination with(*)/without excited fragment (s)</p>

$\rightarrow AB (A) + h\nu$ $A^- + e \rightarrow A + 2e$ $A^- + B^+ \rightarrow AB^{(*)}$	Radioactive recombination Detachment by electron impact Negative ion–positive ion recombination with (*)/ without excitation
Interactions Involving Excited and Neutral Species $AB^*(A^*) + C \rightarrow AB (A) + C^+ + e$ $A^* + B \rightarrow AB + e$ $AB^*(A^*) + e(\epsilon) \rightarrow AB (A) + e(\epsilon')$ $AB(A) + C \Rightarrow products$	Penning ionization Associative ionization $\epsilon' > \epsilon$ Super elastic collision Chemical reaction involving neutral species

2.5 Gas Sparkgap recovery under static pressure condition:

Gas filled sparkgaps employ gases at atmospheric or high pressures. Commonly used gases are nitrogen, air, Sf_6 and argon. High pressure spark gaps are the most versatile switches available for the design of repetitive pulsed power system. These gas spark gaps conduct current through a hot, diffuse, partially ionized Plasma channel. The parameters of the channel depend upon the circuit driving the spark. They combine good trigger ability with the largest operating voltage and dI/dt available from any switch. On the negative side, high pressure spark gap switches, which tend to be rather simple to use in single shot applications or in repetitive service at low energy per pulse, can develop a variety of "quirks" in high average power repetitive service. The most common problem is a collapse of the triggering range. Normally for any switch at any fixed pressure, there is a voltage below which the switch will not trigger acceptably and a voltage above which the switch will self-fire. Generally the switch operates better near the self- firing Voltage in the sense that it is easier to trigger there and closes with minimal time dispersion

(jitter). Unfortunately, when operated even as low as 70% of the nominal self-firing voltage there seems to be a finite probability of un-triggered switch closure, at least in high current operation (~100 kA). This is equally true for repetitive or single shot service; however, as a result of repetitive operation the self-firing voltage is reduced without their necessarily being a corresponding reduction in the minimum triggering Voltage. A few of this type of sparkgaps used in repetitive pulse power systems are described below.

Moran et. al [46, 57, 58] describe a high repetition rate hydrogen sparkgap operating at pressures up to 7MPa and 0.1mm to 10mm gap. In a triggeratron mode, a recovery time of 100 μ s has been obtained. Faster recovery times have been reported when the sparkgap was operated well below the self BDV. Recovery times lower by an order of magnitude can be obtained by operating the sparkgap below fifty percent of self BDV. A two-pulse system was used for these studies. The recovery times were found to be independent of the energy transferred. The recovery times of hydrogen were slower at low pressures by an order of magnitude compared to argon, but an order of magnitude faster at very high pressures. The recovery of a mixture of hydrogen and argon falls between the curves for separate gases. Experiments of fast recovery of hydrogen gas switch were also conducted on a 600 kV, 10 μ s, 5 pulse, and 10 kHz burst mode pulse power system.

The recovery and break down study of a small nitrogen gaps of 0.8 mm to 3.7 mm distance, was done using two pulse method by Xinjing Cai [60, 61]. He found that the breakdown voltage of the gap changes from shot to shot even with the same experimental conditions and obeys Gaussian distribution. The over-volted factor is reduced with an increasing pressure. With a 2.7-mm gap the over-volted factors are 4.53 for 0.1 MPa pressure and 1.74 for 0.4 MPa.

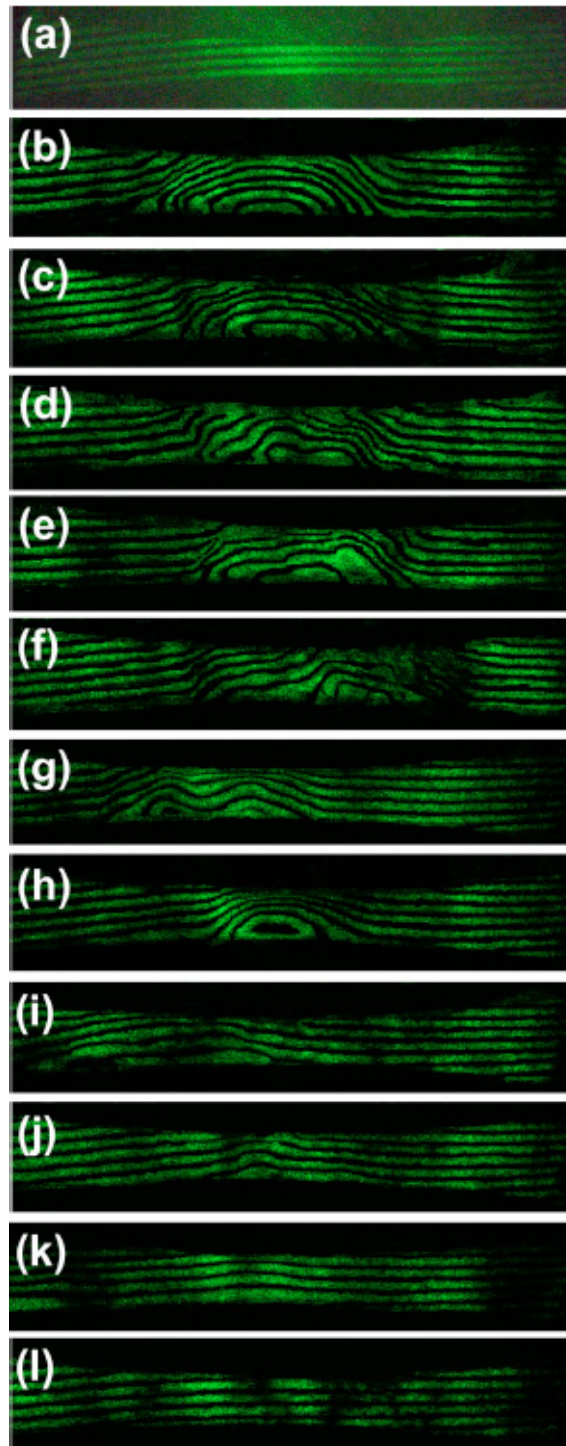


Figure 2.3 Interferograms showing the recovery process of the gas density in a 2.7 mm gap at atmospheric pressure. (a) $t < 0$, (b) $t = 266 \mu\text{s}$, (c) $t = 302 \mu\text{s}$, (d) $t = 504 \mu\text{s}$, (e) $t = 1 \text{ ms}$, (f) $t = 2 \text{ ms}$, (g) $t = 5 \text{ ms}$, (h) $t = 10 \text{ ms}$, (i) $t = 15 \text{ ms}$, (j) $t = 20 \text{ ms}$, (k) $t = 30 \text{ ms}$, and (l) $t = 50 \text{ ms}$. [60].

And also his experiments shows that the over-volted breakdown voltage depends individually on the gap spacing d and the gas pressure p , rather than on the product of Pd . The second spark generally does not follow the path of the first spark. And also the recovery of the gas density and the hold-off voltage of a spark gap after breakdown were investigated with Mach–Zehnder interferometry and compared with two pulse experiments. The interferograms of gas density recovery process is shown in Fig.2.3. It was shown that the gas density in a 2.7 mm gap filled with atmospheric nitrogen almost fully recovers at $t=50$ ms but the breakdown voltage of the gap only recovers to its static hold-off voltage, about 21.4% of its original overvolted breakdown voltage.

A number of Tesla-transformer type accelerators from 500 keV to 5MeV has reported by Abramyan et. al., [58]. These transformers are of helical wound type, and contain the accelerating tube at the center. These transformers are Sf_6 / N_2 insulated. ELITA-1.5 (1.5MeV, 100A), ELITA-3 (3MeV, 20/40A) are Tesla-transformer type accelerators. The pulse width can be varied from 50ns to 10ms at 1 to 100 pulses per second (pps), with a triode electron gun. The average beam power is 20 kW with a maximum energy/pulse of 1kJ. RIUS-5 is a 5MeV, 30kA, 40ns pulse duration system with repetition rate of one pulse in 2-5 minutes, operates with a mixture of Sf_6 and N_2 gases (static filling) over-volted secondary sparkgap.

The experimental study [62, 63] of the voltage recovery characteristics of spark gap switch with H_2 , N_2 and Sf_6 gases under the breakdown voltage of 450 kV (the vacuum diode voltage is about 200 kV), and current 30 kA. His experiments show that hydrogen has the best recovery characteristic. At a pulse interval of 8.8ms, recovery percentages of both gas breakdown voltage and vacuum diode voltage exceed 95%. For Sf_6 , N_2 with the interval of 25ms and 50ms, 90% voltage recovery percentages are obtained. The experiments also prove that the repetitive rate of

high power accelerator with pulse forming line is mainly restricted by the gas switch repetitive rate. He also analyzed theoretically the electric field stress of the switch under high pressure. The electric field distribution of the spark gap switch is shown in Fig. 2.4. The results of simulation show that electric field distribution between electrodes of the switch is the strongest, and the field distribution along axis is better uniform. It is favorable to the breakdown and improving performance of the spark gas switch. The pressure of hydrogen gas in the switch was hydrostatically tested up to 30atm. Such a switch was employed on high power pulse modulator with water dielectric PFL (Pulse Forming Line). At the switch breakdown voltage of 520 kV and the pressure of hydrogen 12atm, a 230 kV, 31 kA and 60ns during time electron beam is obtained at the field-emission diode. The results show that the rise times of diode voltage is reduced obviously when hydrogen is used as the dielectric of spark gap switch.

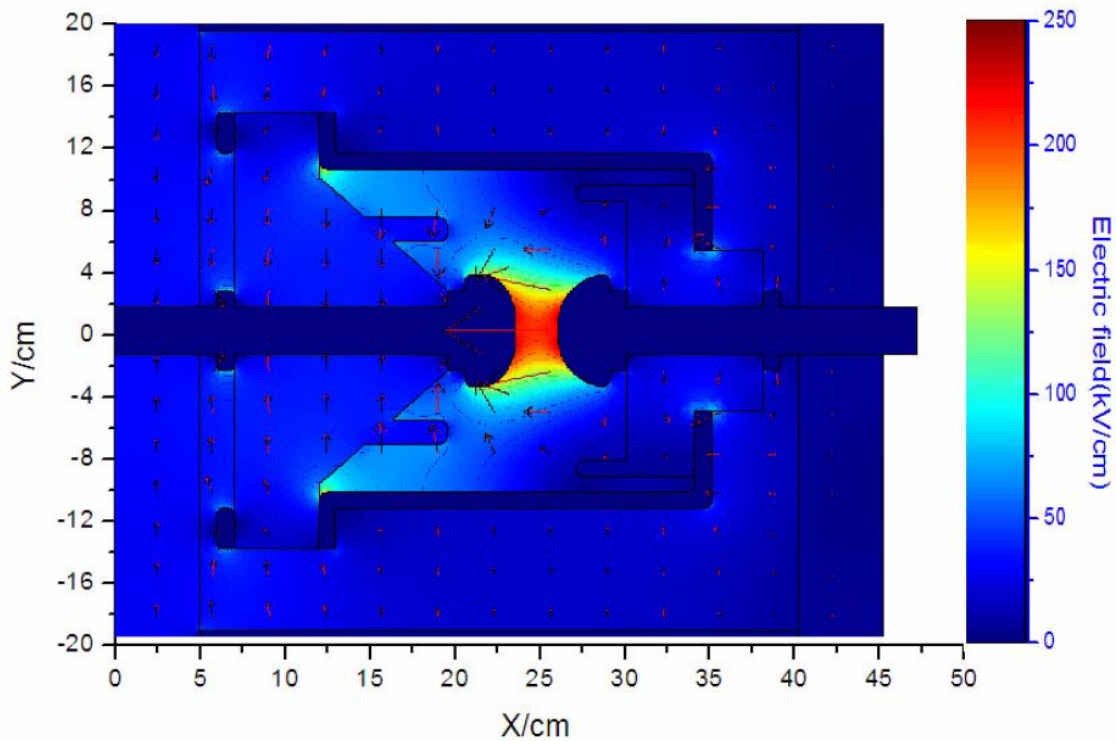


Figure 2.4 Electric field distributions simulation in the spark gap switch. [63]

It has been demonstrated [64, 65] that the free voltage recovery process (no gas flow) which occurs in a spark gap following breakdown can be divided into three distinct phases.

The first phase of the free voltage recovery process is the deionization of the arc channel following voltage breakdown. Deionization occurs through processes including recombination, de-excitation and attachment [66]. The degree of ionization existing in the arc channel is assumed to approach the background level relatively quickly after the current ceases to flow (a few $10ps$).

The second phase in the recovery process is the cooling of the hot, electronically neutral gas left in the region of the former arc channel. During conduction, the gas in the arc column is heated to several thousand Kelvin which results in a severe drop in the local value of the gas density. If the second voltage pulse is re-applied to the switch too quickly following the initial pulse, the gap can break down at a much lower voltage. Full voltage recovery to the initial breakdown voltage of the electrode gap only occurs when the gas is given time to cool to the ambient temperature. This normally takes a few ms [67] to occur and is thought to limit the PRF to several hundred Hz. Under continuous repetitive operation, electrode heating can also significantly affect the gas temperature, which in turn limits the PRF even further.

The third phase of the voltage recovery process is the recovery of the ability of the switch to be pulse charged to a level greater than the dc breakdown level. In some switching applications, the pulse charged breakdown voltage may be up to three times the dc breakdown voltage in order to improve switching characteristics (voltage collapse time, jitter). It is therefore important in pulsed power applications requiring faster rise times and higher voltages. The recovery of the pulse charged breakdown voltage may be delayed by as long as several hundred ms and has been attributed to the existence of residual ions in the gap.

Fiorentino et al. [68] reported a high repetition rate electron beam generator using resonant transformer at 300 keV, 20 ns, 20 kA, and 25 pps for laser pumping. The primary gas sparkgap having a low stray inductance of 10 nH was triggered by a 50 kV, 100 ns, 20 ns rise-time pulse. The secondary gas sparkgap has been operated with gas mixtures of $N_2 - Sf_6$ for 600 kV, triggered by a spiral wound double wire line with impedance of 300Ω . The system has been operated with static gas pressures at low repetition rates of one Hz and up to 25 Hz, 290 kV with gas purging, for a few seconds.

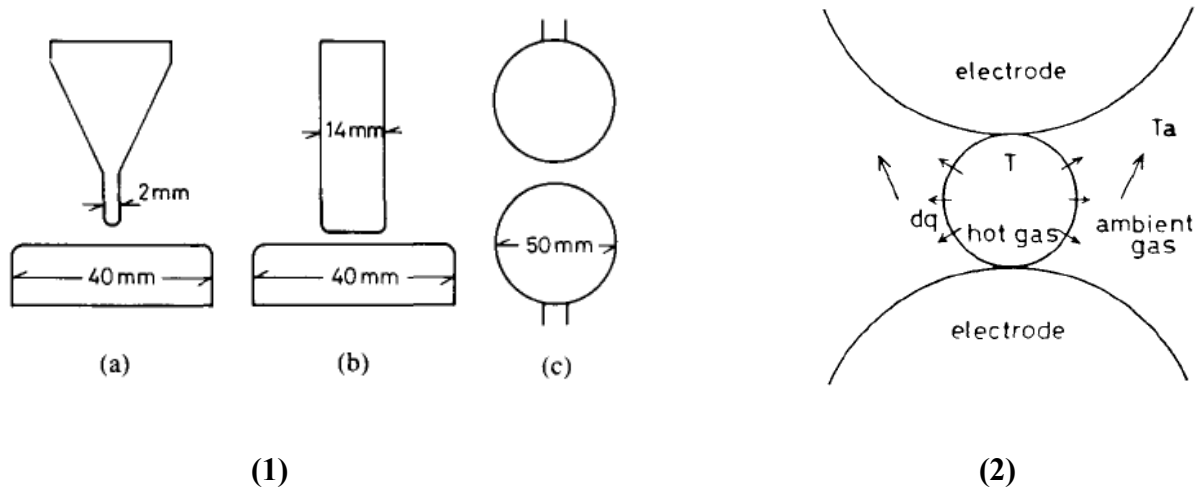


Figure 2.5:

(1) Geometries of electrodes. (a) Rod-plane gap. (b) Plane-parallel gap (c) Sphere gap. [44]

(2) Convection heat loss model from hot gas sphere to ambient gas. [69]

Tsuruta et al., [44, 69] describe the voltage recovery characteristics of small air-gaps between 0.3 to 0.9 mm gap spacing, 50 μ s to 100 ms delay time and 40 to 200 A for copper, aluminum and stainless steel, rod / sphere gap electrodes. The electrode arrangement is as shown in fig 2.5 (1). His experiments also shows, the shorter gaps recovered faster than longer gaps. The authors proposed a gas temperature decay model according to which the air-gap recovery depends upon

the heat flow from the arc. The convection heat loss model from hot gas sphere to ambient gas is as shown in fig 2.5 (2). The recovery of long air-gaps, for gap greater than 8mm, depends on radial heat flow and for medium gap lengths on the total heat flow from the sparkgap. The temperature decay model includes the properties of (a) geometry of the gaps, (b) arc temperature, (c) Physical properties of the gas like, thermal conductivity, density, specific heat and kinematic viscosity. There is a reasonable agreement between calculated and experimental recovery times.

2.6 Gas Sparkgap recovery under Dynamic pressure condition (Purged Sparkgaps):

The purging gas flow pattern generally takes one of two forms namely straight (axial) or vortex (rotary). In essence, straight line flow follows the shortest path from the gas source to the exhaust port (center of the electrodes). In vortex flow the gas velocity has a large azimuthal component. The argument for vortex flow is that a given element of gas sweeps over the entire electrode area and is available for cooling wherever the spark may occur. The countering argument at rates below 100 Hz is that the heat disperses itself via conduction in the time between pulses so that the gas flow needs to cool the entire surface at all times. Gas flow is needed over the entire electrode, independent of the current spark location. The speed of flow becomes the relevant parameter together with the presence or absence of dead air spaces that are not cooled.

Gas purged sparkgaps employ generally high pressure air, N_2 or mixtures of N_2 and 5 to 8% of Sf_6 gases. The gases are either purged out as in case of air or re-circulated under high velocities, in case of other gases, through the arc which removes the plasma and ionic debris before occurrence of the next pulse. The required velocity of purging increases with the repetition rate linearly. The purging rate should increase in proportion to the product of the voltage and the

active switch electrode area because this product determines the STP volume of heated gas times the density. The factor F is given by

$$F = \frac{\text{gas flow (SCFM)}}{\text{Voltage (kv)} * \text{electrode area (cm}^2\text{)} * \text{rep rate (Hz)}}$$

It is important to realize that having an appropriate value for F does not guarantee success in a repetitive spark gap. Any gaps with even higher F values have been failures. Nevertheless, it is noteworthy that a variety of workers with different geometries and with switching parameters covering a wide range have a remarkably consistent value of F in their final design.

The recovery of these Purged sparkgaps is limited by gas de-ionization and subsequent cooling by the gas circulation. A few kHz repetition rate is the practical limit with high pressure sparkgaps due to high blow power requirements, which varies as the cube of the velocity. A few of the repetitive pulsed power systems having this type of sparkgaps are described below.

Sandia Laboratories, USA [70], as a part of development of fusion research program, developed repetitive pulsed power systems based on Tesla-transformers (1.5 MV, 10pps, 30ns and 350 kV, 100pps, 30ns,) and Marx generators (1 MV, 10 kJ, 10-100Hz). The primary switch has been operated at 30% of self BDV, for stable operation over a wide range. The high voltage self-triggered sparkgap switches 35 kA, 30ns up to 100pps with 1MPA pressure and 3 to 6cms gap length. Minimum required gas flow rate as a function of maximum repetition rate data has been reported. An air flow of about 56.6m³/hour is required for operation at 80pps, 550 kV, 14 kA. Cylindrical annular plant and flat button three electrode switches have also been developed for various applications. A repetitive pulsed Marx generator has been developed with ratings of 1MV, 10J, 10 to 100pps. A new low inductance sparkgap named half switch has also been

developed for discharging capacitor banks of positive and negative polarities. Ramrus et. al. [38, 39] report the 100 kV, 10 kA, 10mC/shot, 100 pps, burst mode sparkgap. This gap has been tested up to 100 kV, 250Hz, 0.25C, 5 kA with flow rates of 59.5 m³/hour of dry air. The breakdown probability data with respect to pressure of the gas have been reported for negative and positive polarities having velocities of 2.5 and 5m/s. The estimated jitter works out to be 12% in about 100 shots. The Cross section of gas-dynamic spark gap used in his experiments is shown in figure 2.6.

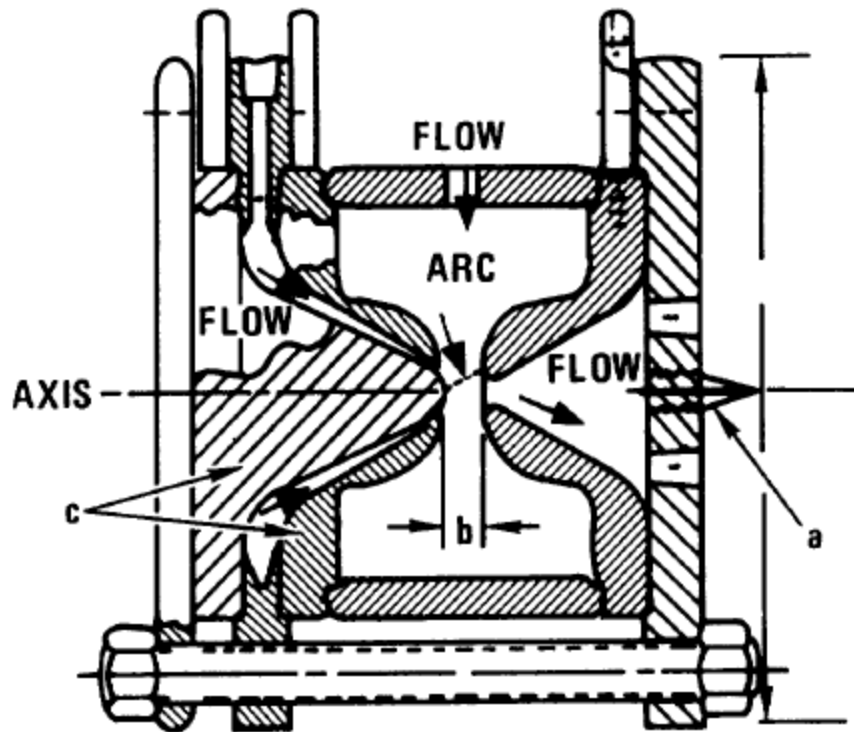


Figure 2.6: Typical cross section of gas-dynamic spark gap. [39]

A 20 kHz repetition rate miniature triggered, continuously purged, nitrogen gas sparkgap in the pressure range of 101.3kPa to 346.6kPa is reported by Rose et. al., [40, 71]. The electrode damage, jitter and BDV of the switch have been reported for electrodes of brass and aluminum. Watson et al., [72, 73] reports a high voltage pulse generator with a triggered sparkgap and a

pulse forming network for CS₂ laser cavity load. This pulse generator produces a 300J, 700ns, 100ns rise-time, 1 to 50pps, ± 100 ns jitter pulse when charged to 116 kV. The system has been insulated by nitrogen gas at 310.3kPa (purged). The performance of two electrode and three electrode sparkgaps have been compared and the conclusions are reported. The loss increases with arc length and non-uniformity of the gap. The jitter has been slightly higher in air compared to nitrogen, due to inferior trigger mode.

2.7 Low Pressure Sparkgaps

The low pressure sparkgaps can be operated over a wide range of working voltages and can switch large currents. They have long life, high pulse to pulse repeatability and can be operated at high repetition rates. Their construction is relatively simple. These sparkgaps normally operate on the left hand portion of the Paschen's minimum. Some types of low pressure sparkgaps are (i) simple low pressure sparkgaps, (ii) low pressure pseudo spark sparkgaps and (iii) low pressure crossed field tubes. A few repetitive pulse power systems using these types of sparkgaps are described below.

K.V Nagsh et al., [49, 50] observed the Over Recovery phenomena in low pressure spark gaps. He conducted experiments in the time interval of 300 μ s to 50ms and observed the influence of gap spacing (2.5 and 10 mm), and pulse voltages of 45 kV rising in 2.5 μ s for positive and negative polarities at a pressure range of 1.3 to 34.7 Pa. The gases used in the experiments are hydrogen, argon, and deuterium. A two-pulse system, capable of generating two pulses rising to 45 kV each in 2.5 μ s and separated by a variable delay of 100 μ s to 50ms, has been used to study the recovery characteristics. It has been observed that the breakdown voltage under the second pulse is higher than the breakdown voltage under the first pulse along the left-hand side of Paschen's characteristics and this has been defined as over recovery (>100% recovery) in these

studies. The over recovery was found to be up to 120% and is dependent on the gas pressure {<23 Pa for argon, <12.1 Pa for H₂, <4.5 Pa, -ve polarity, and <14.3 Pa, +ve polarity for D₂ gases}, discharge current magnitude (>1 kA), and its reversal. This over recovery in low pressure sparkgaps is due to pressure reduction in the gap after the first pulse discharge. The sequence of recovery process is shown in figure 2.7. The recovery times are independent of gas pressure for negative polarity. It increases with pressure for positive polarity and also with increase in molecular weight of the gas in the gap.

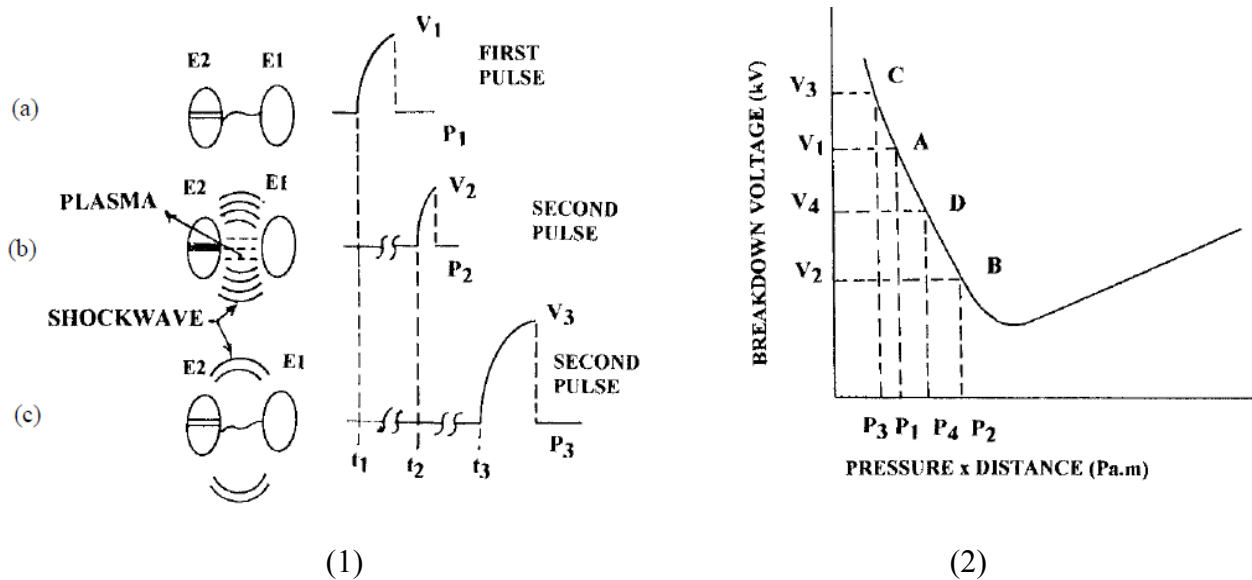


Figure 2.7

(1) Sequence of recovery process in low pressure sparkgaps [49]

(2) Pulsed Paschen's characteristics [49]

The Over recovery phenomena in low pressure spark gaps is explained as follows. The first pulse is applied to the electrode E₁ at a time t₁ with a pressure in the gap P₁ as shown in Fig. 2.7(1-a). The gap breaks down at a voltage V₁ (point A) and produces plasma and shockwaves in the gap as shown in Fig. 2.7(1-b). The possible ways the breakdowns of second and subsequent pulses are affected can be explained as follows. The first pulse breakdown increases temperature and

pressure in the discharge column of the gap. The temperature and pressure in the gap starts reducing due to diffusion of plasma to the walls, resulting in recovery of the gap. The pressure in the gap reduces to P_2 at a time t_2 (point B). If the second pulse is applied at this instant, the gap breaks down at a voltage $V_2 < V_1$ as shown in Fig. 2.7-(2) (point B). This shows that the gap has not recovered to its pre-breakdown status (under recovery). It can be seen from Fig. 2.7-(2) that increase in pressure results in reduction of the breakdown voltage and vice-versa. If the second pulse is applied at a later instant t_3 , at which time if the pressure P_3 is equal to P_1 , it will breakdown at a voltage V_3 . It is called full recovery if V_3 is equal to V_1 . It is presumed that all ionizations in the gap have been neutralized by this time. Alternatively if the pressure P_3 is less than P_1 (point C), it will breakdown at a voltage as shown in Fig. 2.7 (1-c) and Fig. 2.7-(2), which is called over recovery. This over recovery is possible only in case of low pressure sparkgaps where the pressure can reduce below nominal operating pressure under large discharge currents. The interval from A to B and to C is called over-recovery time and the corresponding breakdown voltages are over-recovery voltages. Dufouret. al. [74] Report a sealed off low pressure, quenching high voltage sparkgap capable of switching voltages up to 25 kV. This sparkgap operates at a repetition rates of a few kHz having recovery times of a few microseconds. The recombination of positive ions and their diffusion to the walls are mainly responsible for fast recovery times of the sparkgap. The recovery time of the gap can be reduced by proper gas pressure and additives like Sf_6 . Reduction of spacing to the wall, results in faster diffusion of positive ions and faster gap recovery. Filling in the gap with a porous material reduces the mean free path of ions and distance to the walls. A long capillary glass tube filled with sand (1-30 mesh) has been used in this switch for higher static BDV. Two metallic electrodes are attached to the glass tube by two rubber sleeves for connections. Sparkgap has

been triggered by a coil (surrounding the capillary tube) which develops a 30 kV pulse. The sparkgap having an internal diameter of 2mm and 500mm in length, can switch 15 kV pulses with a recovery time of 4ms. Glass-wool filling density of 200kg/m³ in 7mm internal diameter tube, 100 kV/m length are required for operations of voltages higher than 15 kV. The resistance of the sparkgaps are high when compare to normal gas sparkgaps (~110Ω). Cooling of sparkgaps is required at high repetition rates. Lauer et. al. (75 -77) presented the design of a low pressure sparkgap to replace the existing high pressure gas sparkgap currently being used in Experimental Test Accelerator (ETA) / Advanced Test Accelerator (ATA). The parameters of the sparkgap are 250 kV, 10.8Ω, 50ns pulse. The pressure in this sparkgap is maximum at the centre and reduces towards the insulator surfaces. This sparkgap operates near Paschen's minimum where the critical pd is almost independent of applied voltage. The flow of gas is controlled by pulsed piezo-electric gas valve. This pressure remains constant for about 1ms during which a burst of pulses are applied. The sparkgap can be triggered with a maximum of 12 trigger pulses on cathode. Rate of rise of current increases proportional to molecular weight of the gas, for constant gap and charging voltage. The rise times are longer for charging voltages greater than 100 kV and gap lengths greater than 10mm, due to very low pressure region under slow charging mode. The pressure in the gap can be increased to three times for constant gap spacing with faster charging mode. This leads to three times faster rate of rise of current in the gap. The stainless steel electrodes suffered large damages in localized regions and deposition of a layer of tungsten (0.75mm) results in less damage. Large 0.25m diameter electrodes suffered less damage. Recovery times of 0.1 to 0.2 ms have been obtained for slow charging modes (8 to 20 ms charging time) with 50 to 100 kV charging voltage for nitrogen gas. The recovery time

has increased to several milliseconds due to negative polarity voltage applied to the gap by the reset pulses of saturating magnetic cores, under fast charging modes.

2.7.1 Pseudo Spark Switch

Claudius Kozlik et. al [78] report a triggered low pressure pseudo spark based high power switch rated 40 kV, 25 kA, 40J, 8×10^{11} A/s and 95% current reversal. The pre-ionization is provided by a 0.1-0.3mA glow discharge. The low current gas discharge trigger pulse rated 2 to 3kV, 1ms has unlimited trigger life time and can be operated up to 1 kHz. The trigger electrode has been protected from main discharge by a cylindrical metal cage. The positive auxiliary voltage of a few hundred volts prevents misfiring and pre-firing of the switch. The delay time of the switch is 250ns with a jitter time of 4ns. The short circuit current rating is 32 kA with 95% current reversal. The rate of rise of current varies from 3.5×10^{11} A/s to 8.4×10^{11} A/s depending upon voltage and pressure. This switch has been operated for about 5×10^6 discharges at 50 Hz, 20 kV, 10J, 15 kA.

2.7.2 Crossed Field Switches

Low pressure crossed field switches operate at the far left of Paschen's minimum region (≈ 3.9 Pa). The field emission and vacuum breakdown phenomena limit the maximum stand-off voltage in this switch. The maximum gap length is limited to less than one mean free path so that the glow discharge cannot be self-sustained. Application of magnetic field makes the electrons spiral around the magnetic field lines, thereby increasing the probability of ionization collisions and results in glow discharge between electrodes. Removal of magnetic field results in de-ionization of plasma and recovery of the switch. This switch can be used in either the glow discharge mode or in the arc mode. The arc mode has the advantages of simple trigger requirements, and probability of arc spot occurring at different locations on

cathode and anode. This enables the device to operate at high average powers and at high repetition rates with less localized heating. Harvey (79) describes the characteristics of a crossed field closing switch, rated 40 kV, 20 kA, 125Hz, 1ms rise time and 10ms pulse width. The details of (a) inductive, and gas clean-up effects, (b) grid and anode ignition characteristics, (c) grid response, (d) current rise-time with magnetic field triggering, (e) hollow cathode mode and (f) anode and grid pulling have been discussed in detail.

2.8 Vacuum Sparkgaps

Vacuum sparkgaps used for repetitively pulsed operation are relatively simple, require minimum support systems and has high electric field hold-off capability, of the order of 10MV/m. These have good trigger capability down to fairly low voltages. They have faster recovery and capable of high repetition rates. The disadvantages of vacuum switches are slow closure times of more than 100ns, longer trigger delay times, large jitter, high power dissipation, inconsistent recovery performance and decreased rate of recovery with large rate of fall of current. Sampayanet. al. (43) reported the recovery properties of a 90 kV, 15 kA multiple site triggered vacuum spark gap (1.32 kPa). The authors have reviewed the past work in the field of low pressure sparkgap and presents the results of vacuum sparkgap recovery studies in the areas of high current, short duration pulses of less than 5 μ s having large current fall rates. Trigger configurations of (i) capacitive coupled plasma source and (ii) resistively coupled plasma source have been investigated. A recovery rate of 75V/ μ s with a current fall of 4000A/ μ s has been obtained, with a fibre glass substrate. The mean value of the recovery voltage is 46 kV. Results of ceramic substrate plasma source show a sharper degradation of full recovery rate of 120V/ μ s having a current fall rate of 7000 A/ μ s.

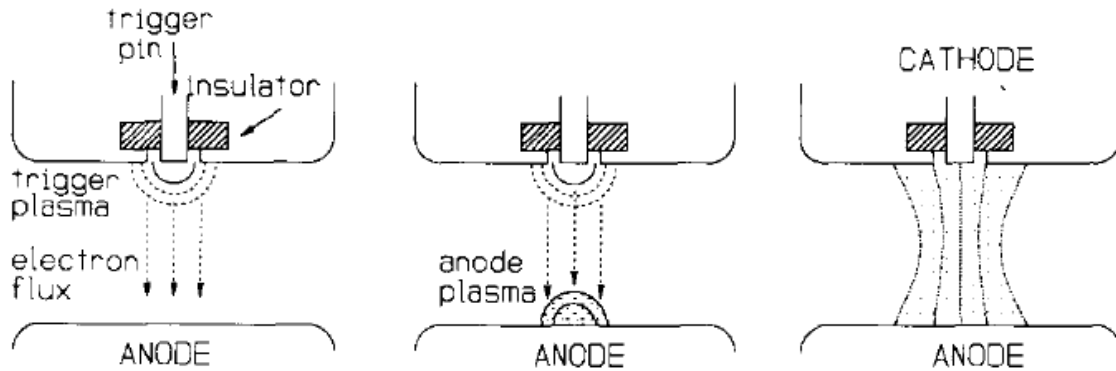


Figure 2.8 Two sources contribute to plasma injection. The initial source is formed by flashover of the trigger insulator, and the second source is formed by the electron impact heating of the anode. Both plasmas expand into the gap to form the conduction channel. [80]

Dougalet. al. [80] report a low loss high repetition rate vacuum sparkgap. This trigatron sparkgap operates in series with a saturable inductor at a high repetition rate. The authors devised a method by which the poor turn-on and high power dissipation characteristics of vacuum sparkgap has been modified to fast turn on, low power dissipation and low electrode erosion sparkgap. This has been accomplished by the addition of a suitable saturable inductor in series with the sparkgap. This is called magnetically delayed vacuum switch. The mechanism contribute to conduction of plasma due to the triggering is shown in figure 2.8. The saturable magnetic core delays the onset of significant current conduction till sufficiently dense ionized vapours have been developed in the inter electrode gap, to carry the current with low losses. This vacuum switch operates at a pressure of 5×10^{-3} Pa with aluminium planar profile electrodes, 50mm diameter and 3 to 5mm gap. This is triggered by a kryotron tube connected to 25Ω , 200ns pulse forming line, and charged to 5 kV. This inductor of 300nH, has been designed for a voltage hold-off of 45 kV with 100ns hold-off interval. This can switch voltages from 20 kV to 0V smoothly, with forward conduction drop of less than 200V, peak power dissipation of

less than 65mJ and 4ns jitter. This has been operated up to 10 kHz repetition rate in burst mode up to 200 pulses.

2.9 Summary

This chapter reviews the work carried out in the field of gas switches in pulsed power technology mainly under pulse voltages in High pressure gas, low pressure gas and also vacuum environment and the factors influencing their dielectric strength recovery with an emphasis on studies related to pulse voltages. The understanding of the mechanism of recovery of gas medium in a high pressure spark gap and the development of a fast recovery spark gap is a step forward in the design of repetitive pulse power systems.

CHAPTER 3

DESIGN AND DEVELOPMENT of DOUBLE PULSE GENERATOR

3.1 Introduction

In order to design the sparkgap switch for repetitive pulse power system, as discussed in previous chapter, it is proposed to develop an experimental facility to study the voltage recovery times of high pressure sparkgaps. The Two-pulse method was used for the measurement of voltage recovery time of the spark gap. A Pulse transformer with matrix topology was made to generate Two Voltage pulses with predefined delay, which are going to over-volt the spark gap. An IGBT triggering circuit was developed to generate trigger signal with controllable delay time. The details of design and development of the experimental setup to study the recovery characteristics of the sparkgap are described in this chapter.

3.2 Design of Double Pulse Generator

In this study, a two pulse method was adopted to study the voltage recovery time of the spark gap. So, a double pulse generator is developed to generate two identical fast rising pulses with a predefined delay between them, which over volts the spark gap switch. The generator made with series pulse transformer topology to achieve the high output voltage keeping input voltage low. In order to achieve the fast rise time of the generated pulse, the Pulse Transformer was developed with Matrix configuration. To keep current in the switches to minimum, primary windings of Pulse Transformer will be split on both legs of the core and will be excited separately. An Insulated Gate Bipolar Transistor (IGBT) was used as the fast switch between the

pulse transformer and testing spark gap chamber. The parameters of the pulse generator are summarized in Table.3.1. The Experimental schematic of generator is shown in Fig.3.1.

TABLE 3.I. The parameters of the Pulse generator

Input DC Voltage	1 kV
Output Pulse Voltage	40 kV
Rise time	300 ns
Pulse Width	1.5 μ s

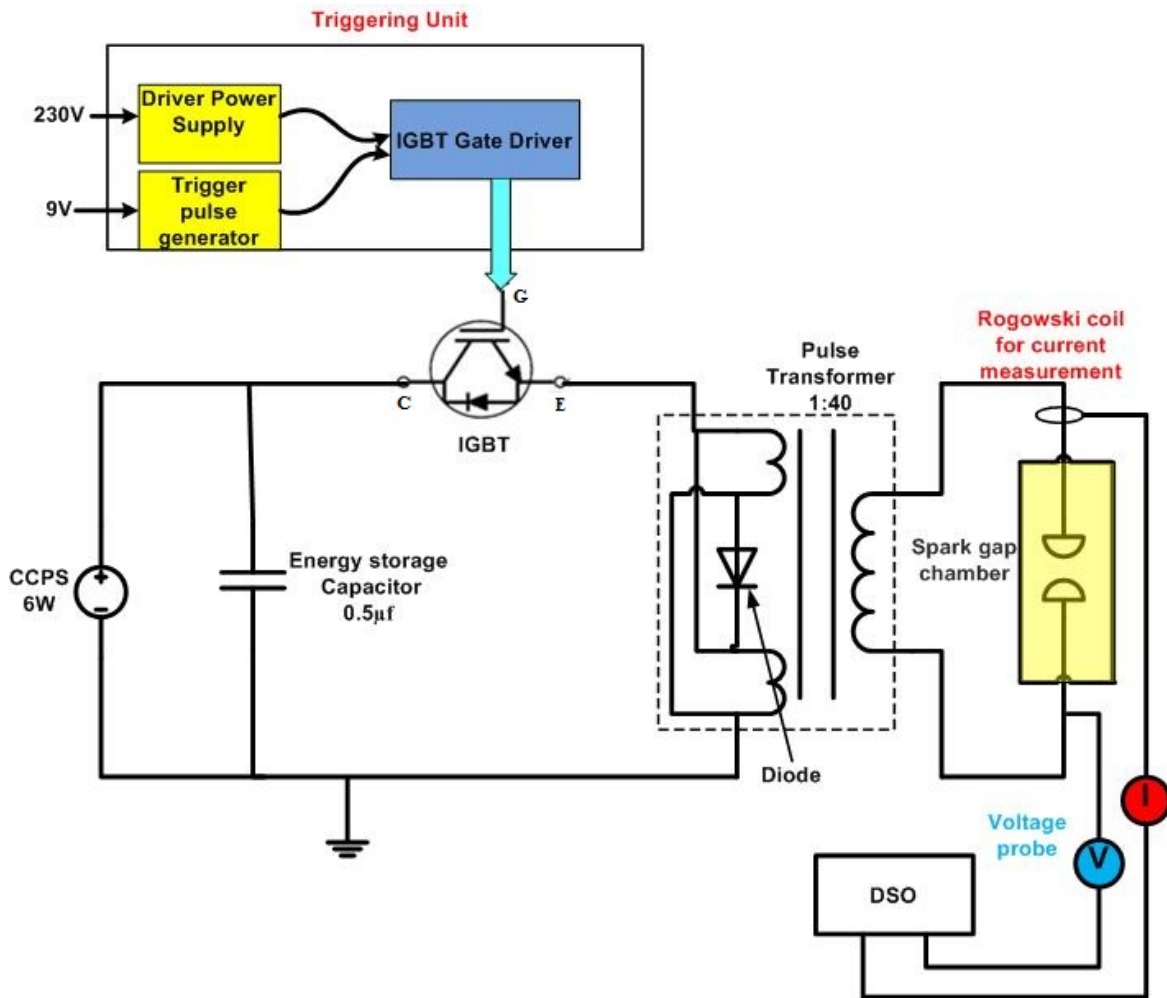


Figure 3.1 Experimental schematic of double-pulse generator with matrix transformer topology

A capacitor charging power supply of rating 6w is used to charge (0-1000V) the 0.5 μ F capacitor which is connected to a pulse transformer through an IGBT switch. This switch will turn on by a triggering circuit which will generate two pulses sequentially to discharge the stored energy of capacitor into the pulse transformer primary. The spark gap testing chamber is connected to the secondary of the pulse transformer. This test cell (spark gap) consists of two Rogowsky profile electrodes, placed in a Perspex container filled with gas insulating medium. The diameter of the electrodes used in the study was 38mm and made by stainless steel material. The gap between two electrodes is set at 2 mm and operates in self-breakdown mode. The output voltage of the pulse generator is around 40 kV peak voltage (for 1kV charging) with rise time of 300ns and pulse width of 1.5 μ s. A 100 kV North-star high voltage measurement probe is used to measure the voltage and all the observations recorded below have been measured with Agilent technologies Digital Oscilloscope 350 MHz with sampling frequency of 2.5 Giga Samples per second.

The components for the recovery study experiment were designed or selected as per the requirement of Pulse Generator. Below sections describe the selection of the each component.

3.2.1 Design of Pulse Transformer

The main component in our experimental setup is the pulse transformer, which couples a source of pulses of electrical energy to a load. The achievable rise and fall times of the pulses are mainly determined by the parasitic capacitances and inductances in the power circuit, which consists of capacitor bank, switches, interconnections, and the load. Due to the insulation requirements, the same minimal distances are required in the design. Furthermore, the voltage drop of the pulse top is relatively independent of the pulse generator type, since it is determined mainly by the amount of stored energy and/or by an existing droop compensation.

However, pulse generators based on pulse transformers offer an additional degree of freedom – the turn’s ratio – which enables the adoption of the primary voltage on the available switch technologies. A second advantage of the transformer based pulse generators is the reduction of the switching losses and the over voltage at turn-off, due to the parasitic capacitance of the pulse transformer and the load. Additionally, this effect could also result in faster turn-off times.

The pulse transformer is one of the key components of pulse generators, which mainly defines the achievable rise time T_r and overshoot ΔV_{max} of the output voltage pulse. In these pulse generators, performance of pulse transformer plays important role in pulse shaping hence it is important to consider the relationship between different elements [81]. The equivalent circuit of pulse generator, pulse transformer along with load is as shown Figure 3.2.

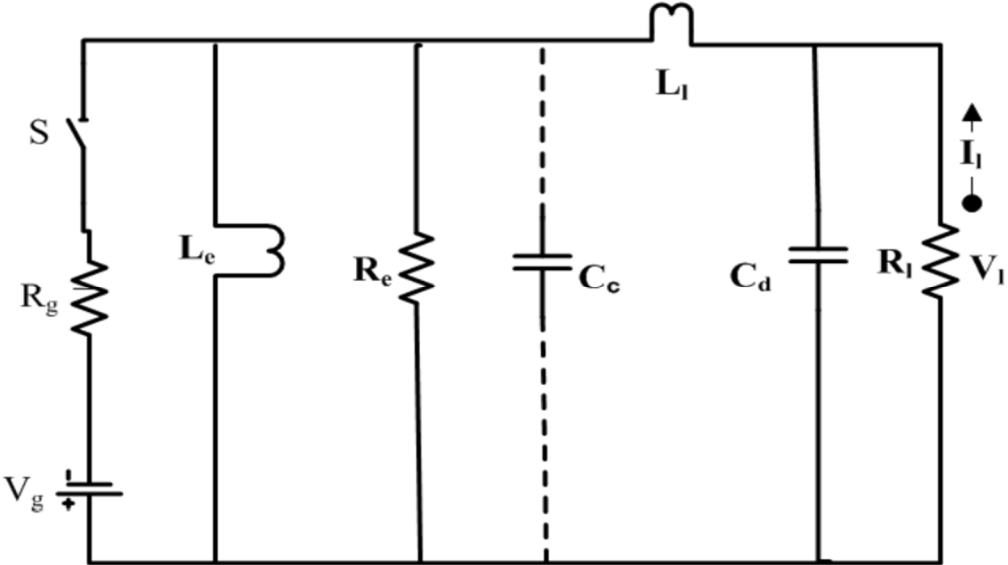


Figure. 3.2. Equivalent circuit for the consideration of optimum relationship among different elements of pulse transformer S indicates the switch location.

Here V_g is the source voltage, R_g is the source resistance, L_e is the effective shunt inductance, R_e is the effective shunt resistance, C_c is the mutual capacitance between low voltage winding and

high voltage winding, L_l is the leakage inductance, C_d is the distributed capacitance, R_l is the load impedance (resistance), and I_l and V_l are current and voltage across load.

Different portions of the pulse i.e., Rise, top and Fall or pulse tail regions, as shown below, can be treated separately as different set of circuit elements come into play in these three regions. These three regions are presented below along with the equivalent applicable circuit [82].

(a) Pulse Rise Region

Figure .3.3 presents the equivalent circuit of the pulse rise region. Effect of R_e is considered to be negligible compared to R_l , and due to a very fast rise time, effect of L_e is also negligible. Initial energy in L_e , L_l , and C is assumed to be zero.

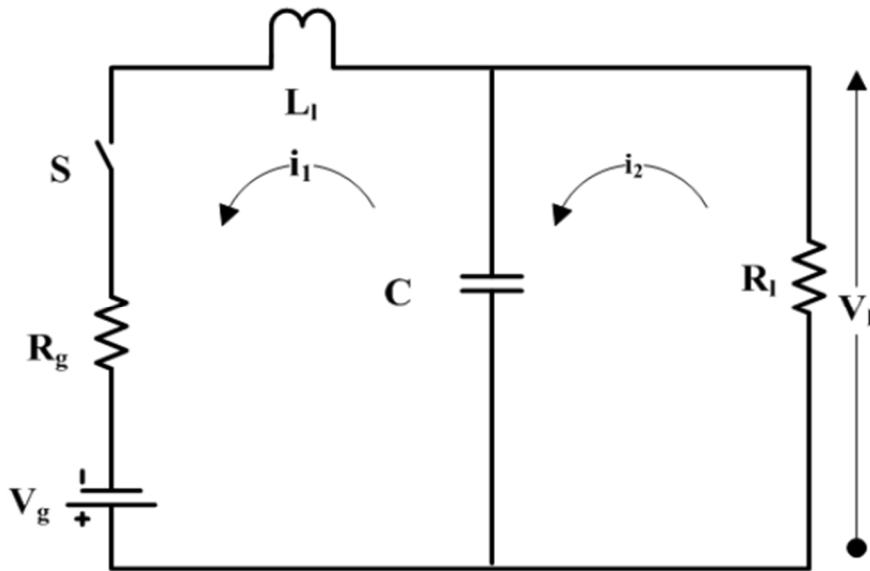


Figure 3.3. Equivalent circuit for the computation of the rise of the pulse on a resistance load.

Using Kirchoff current law, for the loop of current i_1 , we can write

$$L_l \frac{di_1}{dt} + i_1 * R_g + \frac{1}{C} \int i_1 dt - \frac{1}{C} \int i_2 dt = V_g \tag{3.1}$$

Taking Laplace transform and solving for i_1 , we get

$$I_1(s) \left[\frac{1}{s \cdot C} + s \cdot L_l + R_g \right] - \frac{1}{s \cdot C} I_2(s) = \frac{V_g}{s} \quad (3.2)$$

For the current loop i_2 ,

$$i_2 \cdot R_l + \int i_2 dt - \frac{1}{C} \int i_1 dt = 0 \quad (3.3)$$

Taking Laplace transform and simplifying for i_2 , we get

$$I_1(s) = I_2(s) \cdot (s \cdot C \cdot R_l + 1) \quad (3.4)$$

Replacing equation (2) in equation (1) for finding current in load resistor, we get

$$I_2(s) = \frac{V_g \cdot C}{R_l \cdot C^2 \cdot L_l} \left[\frac{1}{\left(s + \frac{1}{R_l \cdot C}\right) \left(s^2 + s \frac{R_g}{L_l} + \frac{1}{C \cdot L_l}\right) - \frac{1}{R_l \cdot C^2 \cdot L_l}} \right] \quad (3.5)$$

For finding voltage across R_l we multiply this expression by V_g and taking inverse Laplace transform,

$$V_{l(t)} = \frac{V_g \cdot R_l}{(R_l + R_g)} \left[1 - e^{-a \cdot t} \left\{ \cosh kt + \frac{a}{k} \sinh kt \right\} \right] \quad (3.6)$$

$$\text{Where } \left\{ \begin{array}{l} 2a = \frac{R_g}{L_l} + \frac{1}{R_l C} \\ b = \frac{1}{C L_l} \left(1 + \frac{R_g}{R_l} \right) \\ k^2 = a^2 - b \\ \sigma = \frac{a}{\sqrt{b}} = \frac{C R_g R_l + L_l}{2 \sqrt{R_l L_l C (R_g + R_l)}} \end{array} \right.$$

(b) Pulse Top Region

The beginning of the top of the pulse is influenced by L_l and C . The droop in the pulse is present due to $R_g > 0$, since the current builds up in L_p (L_p is the representation of the core inductance and resistance effects). The effects of L_l and C are relatively unimportant as far as this droop is

concerned, the equivalent circuit shown in Figure 3.4. may be used in the computation of this droop. The initial current in L_p is assumed to be zero and t is reckoned from the beginning of the top of the pulse. We will then get the expression of voltage droop as below

$$V_{l(t)} = \frac{V_g * R_l}{(R_l + R_g)} e^{-\frac{1}{L_p} \frac{R_l * R_g}{(R_l + R_g)} t} \quad (3.7)$$

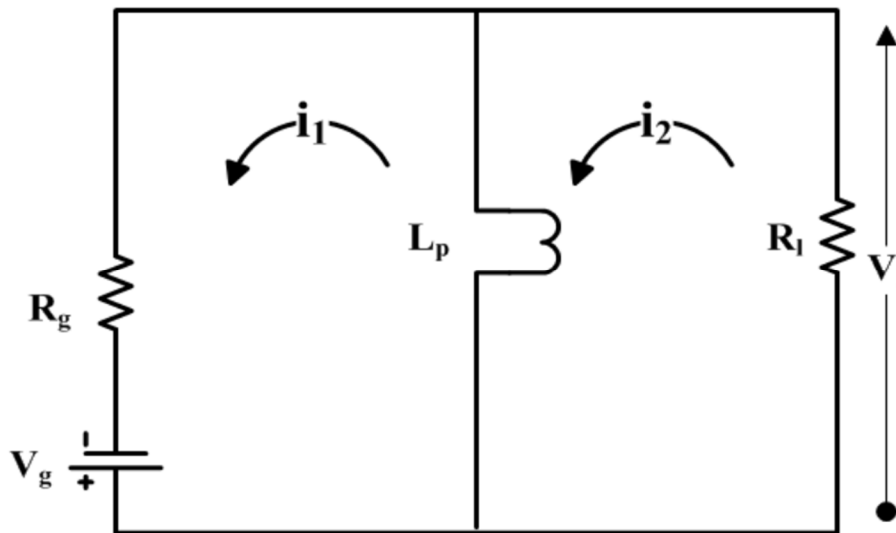


Figure 3.4. Equivalent circuit for computation of pulse top.

The drooping in the current pulse is higher for relatively small current loads like magnetron than a higher resistance load R_l . The current oscillations produced due to the voltage fluctuations are much higher in small resistance loads.

(c) Pulse Tail Region

There is a characteristic back-swing on the tail of the pulse produced by the pulse transformer since the flux density must return to the same remanent point before beginning of each pulse. The interval of time taken between two pulses is taken large enough so that the voltage becomes zero. Thus whenever a pulse transformer is used, there is always a general voltage backswing

whose area is equal to that of the pulse itself, but whose shape is determined by the values of R_e , C , L_e and R_l . If R_l is disconnected shortly after the pulse there are oscillations of a higher frequency superimposed upon general backswing because of the energy stored in L_l . The shape of the general backswing may be calculated by assuming that the constant voltage generator V_g is disconnected from the circuit at the time after the pulse.

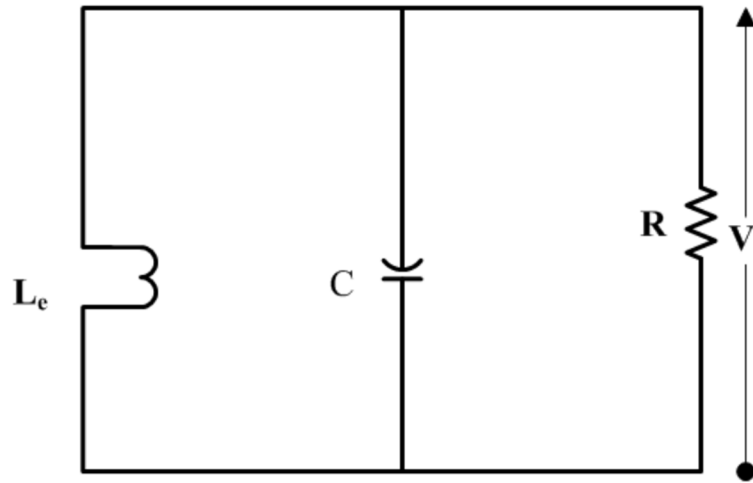


Figure 3.5. Equivalent circuit for computation of pulse tail.

The circuit shown in Figure 3.5 approximates the equivalent circuit, which is a parallel RLC circuit. To a good approximation, the initial current in L_e is $(V_l \cdot t_2) / L_e$ and the initial voltage on C is V_l . Then if $t = 0$ at the time of start of backswing, voltage pulse for a non oscillatory condition can be written as

$$e(t) = V_l * e^{-a*t} \left\{ \cosh kt + \frac{\frac{t_2}{L_e C} + a}{k} \sinh kt \right\} \quad (3.8)$$

and for the oscillatory condition $e(t) = V_l * e^{-a*t} \left\{ \cosh \omega t + \frac{\frac{t_2}{L_e C} + a}{\omega} \sinh \omega t \right\}$ (3.9)

$$a = \frac{1}{RC}$$

$$\text{where } \omega = \sqrt{\frac{1}{L_e C} + \left(\frac{1}{2RC}\right)^2}$$

$$k = j\omega$$

For an ideal pulse transformer, once the primary switch is opened the secondary pulse should immediately end. This does not happen. The pulse transformer tries to dissipate the energy stored in L_m and in the parasitic capacitive and inductive components. The inductance will induce voltages as their magnetic fields collapse. The capacitor charge will drain, but not instantaneously. The capacitances may temporarily supply current to the inductances. As a result, there is a sloped decline of the secondary output voltage after the primary switch is opened. This sloped decline is referred to as the “trailing edge”. Some combinations of capacitance and inductance could produce spurious oscillations.

(d) Overshoot

Considering the equation of damping co-efficient σ , it is dependent on L_l and C i.e., on pulse transformer’s mechanical dimensions and on the load impedance R_l . For a given load impedance and σ , ratio of L_l and C is fixed by

$$2R_l\sigma = \sqrt{\frac{L_l}{C}} \quad (3.10)$$

(e) Rise Time

In addition to the overshoot, the rise time T_r of the output voltage can be derived from above equation and it is found to be proportional to the product of L_1 and C .

$$T = \frac{\sqrt{b}}{2\pi} t$$
$$T_r = 2\pi T_{10\%-90\%} \sqrt{L_1 C} \quad (3.11)$$

3.2.2 Pulse transformer topologies

In order to fulfill the requirements for the maximum overshoot and the maximum rise time, both a given ratio of L_1 to C and a maximum product of L_1 and C have to be guaranteed. In general the pulse generator connected to the transformer's primary as well as the load connected to the secondary winding have a certain inductance L_{gen} and capacitance C_{load} , which also have to be considered. The ratio of L_1 and C can be varied by the mechanical dimensions of the transformer i.e., the distances the heights and the lengths of the windings. The product of L_1 and C however is defined by the transformer topology and can be assumed to be approximately constant [81]. Therefore the transformer topology resulting in the smallest $L_1 * C$ product has to be selected.

Different topologies of transformer available are as given below.

(a) Parallel Winding

It has simple construction and hence is most widely used topology in which the primary and secondary windings are wound on two parallel bobbins as shown below. The distance between the primary and secondary winding is constant throughout the winding height. The leakage

inductance is mainly defined by the volume and the magnetic fields strength between the bobbins. The arrangement of parallel winding is depicted in Fig.3.6.

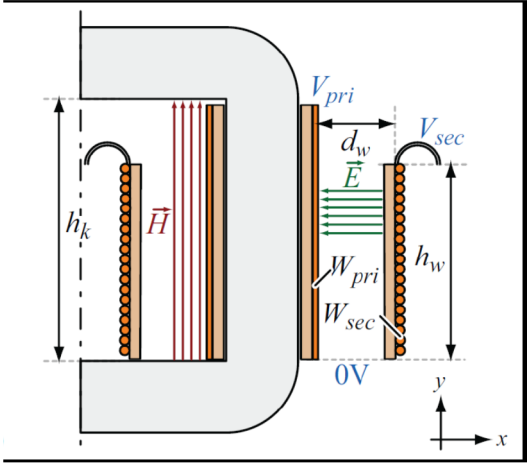


Figure 3.6 Pulse Transformer Parallel winding arrangement descriptions

(b) Cone Winding

In this winding type, the distance between the primary and secondary is not constant and is linearly increasing with height of the winding as shown below.

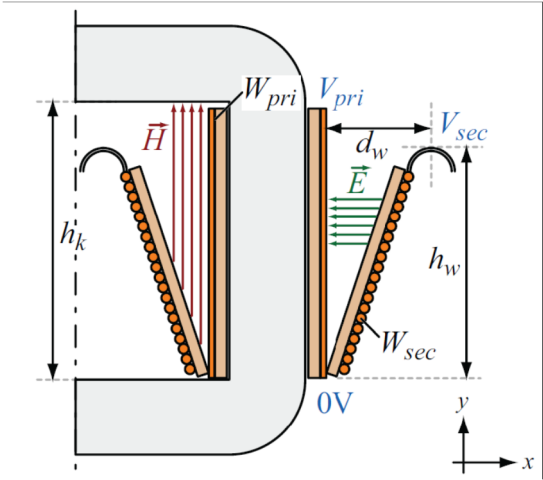


Figure 3.7 Pulse Transformer Cone winding arrangement descriptions

Compared to the parallel winding, the volume between windings and also the leakage inductance can be reduced by a factor of two. The arrangement of cone winding is depicted in Fig.3.7.

(c) Foil Winding

In this winding type, secondary winding is in the shape of foil, wound with thin lamination between successive turns. Height of winding reduces successively with each turn to maintain safe distance from the core and to avoid breakdown due to the high voltage at extreme edge of the winding and the grounded core. The arrangement of foil winding is depicted in Fig.3.8.

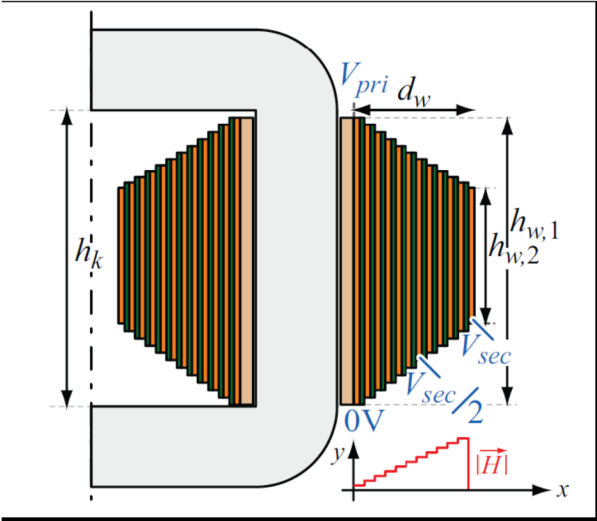


Figure 3.8 Pulse Transformer Foil winding arrangement descriptions

(d) Matrix Pulse Transformer

In order to achieve high voltage on secondary of pulse transformer, while keeping the primary voltage and current to suit the available switch capacity, multiple transformers can be used in series. However this also introduces additional Leakage inductance and distributed capacitance, thereby increasing the rise time of pulse on the secondary. To overcome the slow rise time of the

pulse, transformer topology with multiple primary windings and single secondary winding is used. This type of Pulse transformer is referred as Matrix Pulse Transformer.

Hence, instead of connecting the secondaries in series, both secondaries can be combined to one secondary which encloses both cores, whereas some volume between the primary and secondary winding is saved. The saved volume directly results in a reduced leakage inductance and distributed capacitance compared to the series connection of the standard transformers. For this transformer configuration the conversion ratio between the primary and secondary voltage is not only defined by the turns ratio n but also by the ratio of enclosed core areas A_{pri} and A_{sec} [83].

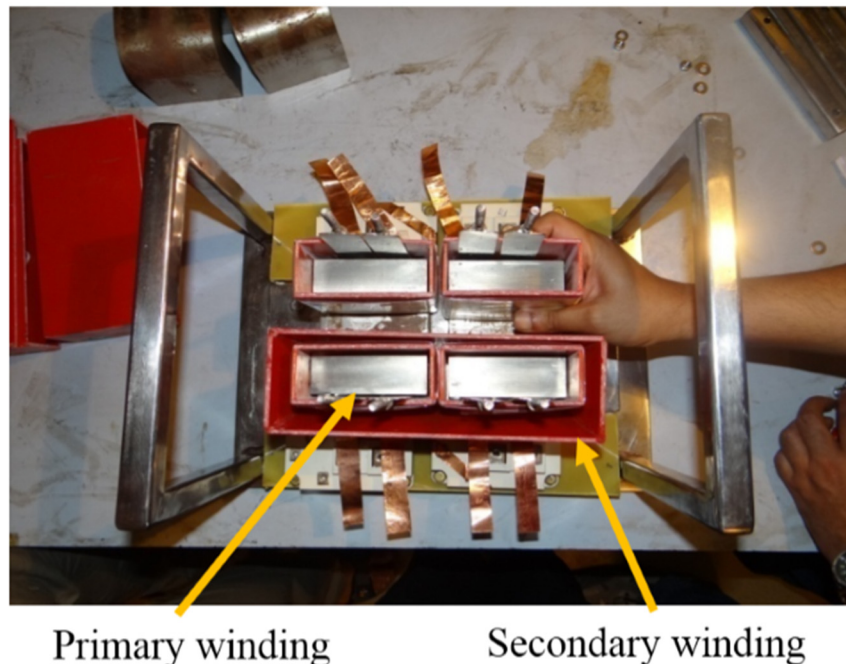


Figure 3.9 Top view of the Matrix pulse transformer showing winding arrangement.

Since T_r is proportional to the winding length, the reduction of T_r can directly be calculated by the winding length's reduction. This design will also limit the current in individual primary circuit and therefore in the switch. The pulse may repeat at regular or irregular interval of time, the inter-pulse period being long relative to the pulse duration, with this type of operation, the

power delivered to a load has a high ratio of peak power to average power. The top view of the pulse transformer is shown in fig. 3.9. The transformer must have a low value of leakage inductance and distributed capacitance which have effect in the pulse rise time, overshoot and backswing. Since the leakage inductance depends on the number of turns, to keep the primary inductance low, transformer with only one turn primary was designed.

3.2.3. Transformer Core

In order to avail the advantage of Amorphous core, two AMCC 1000 core will be used which have high saturation flux density of 1.56 T. It also has high value of permeability and very low core loss as suggested by the B-H curve. For safe operation, ΔB value up to 2.5T can be planned. In this region, value of permeability μ_r is minimum 1000 as obtained from the B-H curve. Two mm thick fiber optic lamination sheet will be used as the bobbin for the windings, which can withstand high voltages. This will provide insulation to primary winding from core and also inter-winding insulation. The thickness of insulation has to be kept optimum to utilize the insulating properties without increasing the distributed capacitance. In the entire transformer, all the exposed wires / strips will have to be covered from the HV insulation tape.

For Matrix Transformer, it can be written

$$\frac{V_{out}}{V_{in}} = \frac{N_{sec}}{N_{pri}} \times \frac{A_{sec}}{A_{pri}} \quad (3.12)$$

$$\frac{40000}{1000} = \frac{N_{sec}}{1} \times \frac{2 \times 23 \times 10^{-4}}{23 \times 10^{-4}}$$

$$N_{sec} = 20 \text{ turns}$$

Hence 20 turns secondary will be required to achieve the required voltage level. The secondary will encompass two primary windings. The effective turn's ratio of the transformer will be 1: 40.

3.2.4. IGBT Triggering Circuit

In order to generate the two pulses at the output of the pulse transformer, the IGBT switch should be triggered with a millisecond delay. The triggering circuit in our experiment was designed for a delay of 10 μ s to more than 1s. This circuit consists of 3 major parts viz., gate driver circuit, gate driver power supply circuit and an optical pulse generator.

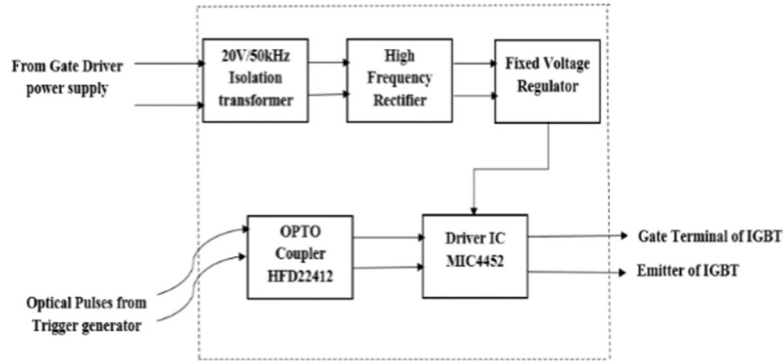
(a) Gate driver Circuit

The IGBT's are connected to 1000 V DC. Therefore it is necessary to provide a floating gate signal to the IGBT. To turn on the IGBT, the Gate drive requirements for most of the IGBT's are given in Table.3.2.

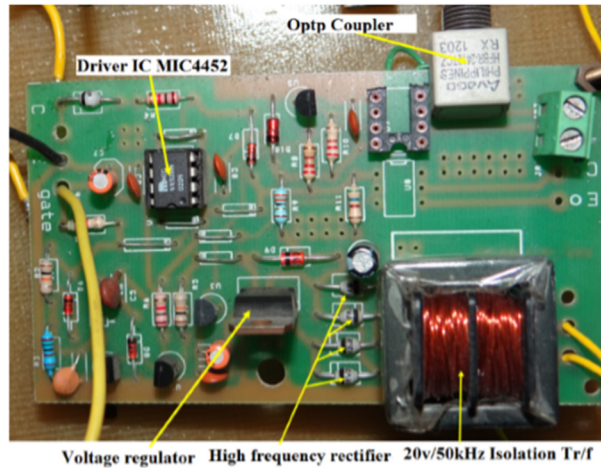
TABLE 3.2. IGBT Gate drive requirements

Output voltage	15V
Supply	15V
Gate charge (for most of IGBT's)	308nC
Gate current	0.04A
Current used	0.075 A
Transistor Current	0.01 A
MIC4452 Current	3mA
Total current	max 150mA

From the above specifications the Gate driver is designed and depicted in Figure 3.10. The gate driver module requires 20V/50kHz power input from the gate driver supply which is rectified by using a high frequency rectifier. This rectified signal will be given to the driver IC MIC4452 through a voltage regulator. The required triggering signal across the IGBT gate and emitter terminals will be applied by this driver IC. The power supply requirement for gate drive module is given in Table.3.3.



(a)



(b)

Figure 3.10 (a) Block diagram of IGBT gate driver PCB. (b) IGBT gate driver PCB.

TABLE 3.3. Power supply parameters for gate drive module

Supply frequency	50 kHz
Duty cycle of power supply	0.8
Off time	2 μ s
Minimum voltage drop across regulator	2.7V
Power dissipation allowed	2W
Max V drop allowed	5.7V
Charge to be supplied during 2 μ s	0.7 μ C
Rectifier drop	1.4V
Minimum input voltage	20V

(b) Gate driver Power supply

The high frequency power supply for Gate drive is designed based on the requirements of gate driver mentioned. Here the power supply is i.e. 230v ac is converted to 15Vdc with the help of bridge rectifier, filter & the associated circuitry of LM317. The 15V DC taken from LM317 is to be converted to 15Vac/50kHz. For this we are using push pull inverter concept. This push pull action is done by IC SG3525 & the MOSFET. The output transformer steps up the voltage from 15V/50kHz to 20V/50kHz. The block diagram of gate driver power supply is shown in Fig. 3.11, and the PCB realization is shown in Figure 3.12.

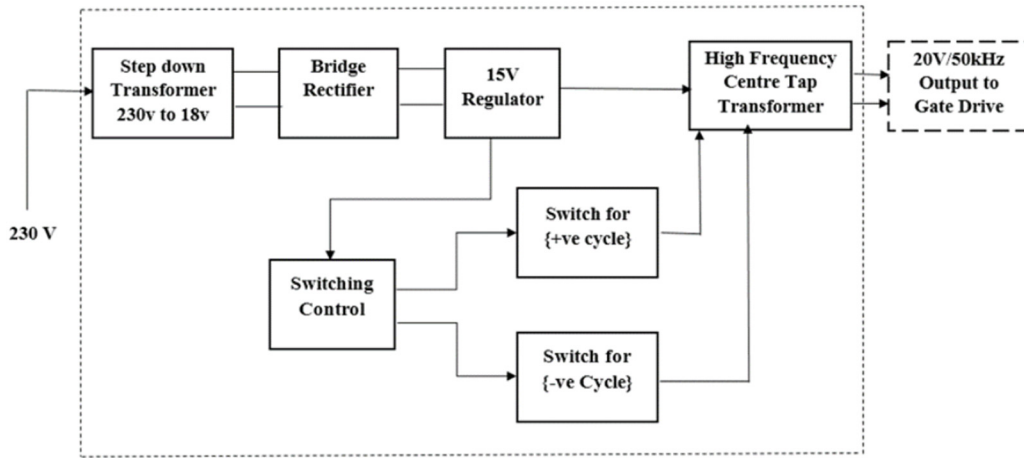


Figure 3.11 Block diagram of gate driver power supply.

(c) Optical pulse generator

From Figure 3.10, the Triggering pulse for IGBT gate is generated by IC MIC4452. An optical signals with the required delay is generated by using a separate embedded program and is fed to IC MIC4452. An example program for 10 ms delay is given in Annexure-1. The coupling will be done by an OPTO-coupler HFD22412. The Fig.3.13 shows typical triggering pulses applied

across the IGBT. These rectangular pulses have 15v amplitude and 2 μ s pulse duration which are good enough to turn on the IGBT.

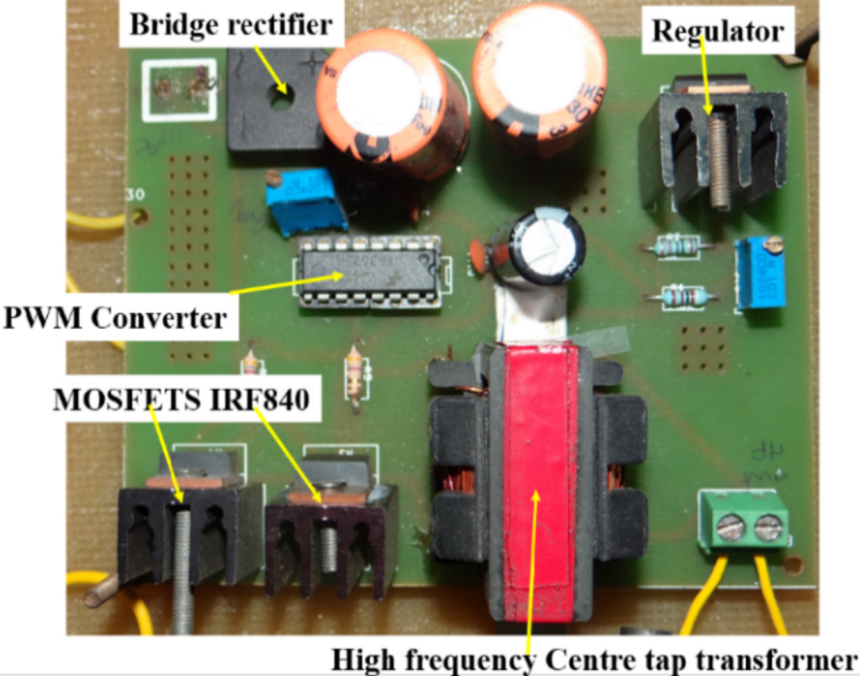


Figure 3.12 Gate driver power supply PCB.

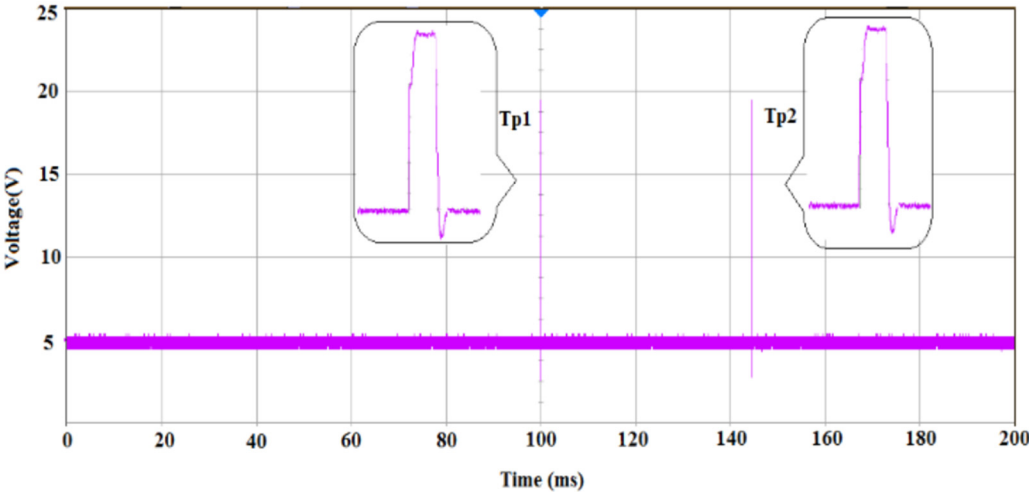


Figure 3.13 Typical waveform of the trigger pulse given to the IGBT switch with 42 ms delay. The T_{p1} and T_{p2} are square pulse with amplitude of 15 v and 2 μ s pulse duration.

3.3 Selection of IGBT

The commonly used fast high power semiconductor device is the inverter grade thyristor which is available with voltage rating > 1 KV at KA average currents. Due to the requirement of current reversal through the device to commutate off, most high voltage pulsed power applications have limited the use of thyristors as replacements for other closing switches. IGBT is a three-terminal device that combines the high input impedance and gate characteristics of a MOSFET for fast switching capability and the low saturation voltage of a bipolar transistor to handle high current values. In our experiment the required IGBT should be able to withstand the max voltage and current while maintaining the rise time of pulse as 300 nS. IGBT make 'Eupec' model no SKM 600 GA 12 T4 SEMIKRON is used in the experiment, which is of higher current rating than the desired value and is hence selected. It also meets the rise time requirement for the pulse generator and can switch currents up to 100 A within 200 ns.

3.4 Diode

Diode is used in the circuit to protect IGBT in case one of the driver does not turn it on and rest of the IGBTs turn on thereby inducing voltage in the secondary circuit which in turn induces the reverse voltage across IGBT. If the diode is used, the reverse voltage appears across it and the switch does not have to withstand any reverse thereby ensuring the protection of IGBT.

In the transformer under consideration, if one of the IGBT does not turn on, then the inverse voltage across primary winding is 1000 V. Hence diode with the following rating is desired:

Peak Inverse Voltage rating : 1000 V

Pulse Current rating : 80A

3.5 Spark Gap Chamber

The test cell consists of two stainless steel electrodes of rogowsky profile placed in a Perspex™ container filled with argon gas at different pressures (0-5 bar). The gap between two electrodes is varied from 2mm to 4 mm. The spark gap chamber is shown in Figure 3.14. The output pulse is having 300 ns rise time and a full width half maximum of 1.5 μ s.

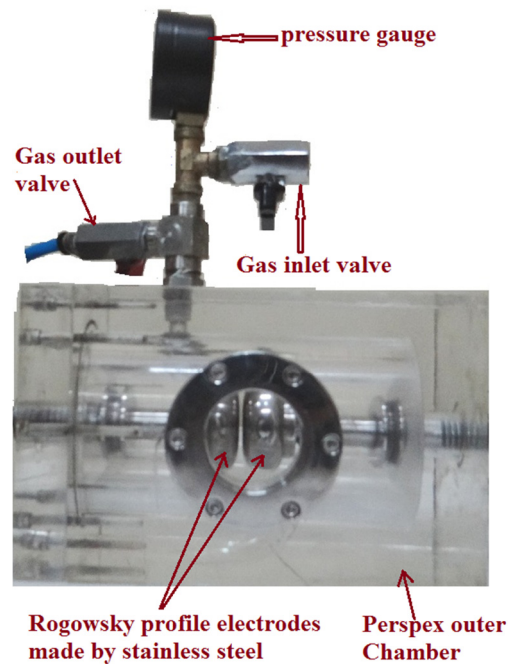


Figure 3.14 Perspex spark gap testing chamber with rogowsky profile electrode.

3.6 Capacitor

Energy Storage Capacitors, provide a convenient method of storing electrical energy, which can be released, as required, for a very short duration of time, under controlled conditions. The capacitor is designed to suit the waveform and duty cycle to which it will be subjected in service and the life it is expected to give. The life expectancy of an Energy Storage Capacitor is a function of the electrical stress, the voltage reversal and the repetition rate of discharges. To

obtain maximum peak current, the Self-Inductance Value of the capacitor should be low. The minimum capacitor value is calculated as per the parameters of the generator as follows:

$$\text{Capacitor Energy} = \frac{1}{2} * C * V^2 \quad (3.13)$$

$$\text{Energy required per shot} = V * I * t = 40 \text{ KV} * 1 \text{ A} * 1.5 \mu\text{S} = 0.06 \text{ Joules}$$

Voltage drop of 15% was assumed per pulse from charging voltage of 1000V i.e., $V_2 = 0.85 * V_1$

$$\text{Hence, } 0.06 = \frac{1}{2} * C * (V_1^2 - V_2^2)$$

$$C = 0.432 \mu\text{F} \approx 0.5 \mu\text{F}.$$

3.7 Capacitor Charging Power supply (CCPS)

CCPS is used to charge capacitors in a very short duration with constant current in order to generate repetitive pulses. The time taken for charging capacitors also decides the achievable frequency of operation of Pulse generator. CCPS should be capable of charging the capacitor during the pulse gap. The pulse repetition rate is 100 hence after every 1/100 sec, i.e., 10mS, new pulse is generated. The pulse width is 1.5 μ S and hence it can be safely considered that capacitor needs to be charged every 10 mS to 1000 volts, starting from the remaining voltage of capacitor, after every pulse. The energy to be supplied by the CCPS in 10 mS is 0.06 J, i.e. the energy lost by capacitor in each pulse. Hence the rating of CCPS of our experiment should be $0.06/10e-3 \approx 6\text{W}$.

3.8. Summery

A pulse transformer based double pulse generator capable of generating 40 kV peak pulses with rise time of 300 ns and 1.5 μ s FWHM and with a delay of 10ms – 1s was developed. A matrix transformer topology is used to get fast rise times by reducing L_i , Cd product in the circuit. To keep current in the switches to minimum, primary windings of Pulse Transformer will be split on both legs of the core and will be excited separately. IGBT will be used as the fast switch. This double pulse generator was used for the spark gap recovery experiments by two pulse method which are presented in chapter 4. The operating procedure and design of different components used in the experimental study is also described in this chapter.

CHAPTER 4

EXPERIMENTAL RESULTS AND DISCUSSION

4.1 Introduction

In order to conduct experiments to study the voltage recovery times of a spark gap on the basis of (i) Breakdown voltage (BDV) (ii) Gas insulating mediums, (iii) Gas pressure, (iv) Output current, (v) Pulse shape and (v) Electrode size and shape, an experimental facility was developed and the design procedure of the setup was explained in the previous chapter. In this chapter, the voltage recovery times of spark gap with noble gas (Argon) and a diatomic gas (Nitrogen) were obtained with different gap distance (1 mm to 4 mm) and gas pressure range (1 atm to 4 atm). The results are also compared with the electro negative gas, Sf_6 to estimate the recovery time. Also, an attempt has been made to see the effect of electrode shape, size, and pulse rise time, gap resistance on the recovery time of spark gap. The complete experimental procedure to conduct the study was also elaborated in the below sections.

4.2 Spark gap voltage recovery experimental procedure by double pulse method

A double pulse generator based on the series pulse transformer topology was designed in order to use the benefits of pulse transformer to achieve the high output voltage keeping input voltage low. For this transformer configuration the conversion ratio between the primary and secondary voltage is defined not only by the turn's ratio but also by the ratio of enclosed core areas. It can generate two 40 kV voltage pulses with delay of 1ms to more than 1s in between. The experimental setup of the pulse generator is shown in Figure.4.1. An energy storage Capacitor of 0.5 μF was charged by a capacitor charging power supply of rating 6w (0-1000 V) and discharge into a pulse transformer through an IGBT switch. This switch will turn on by a separate triggering circuit which will generate two optical pulses sequentially to discharge the stored energy of capacitor into the pulse transformer primary. The two voltage

pulses with predefined delay will be applied to the spark gap testing chamber which is connected across the secondary of the pulse transformer.

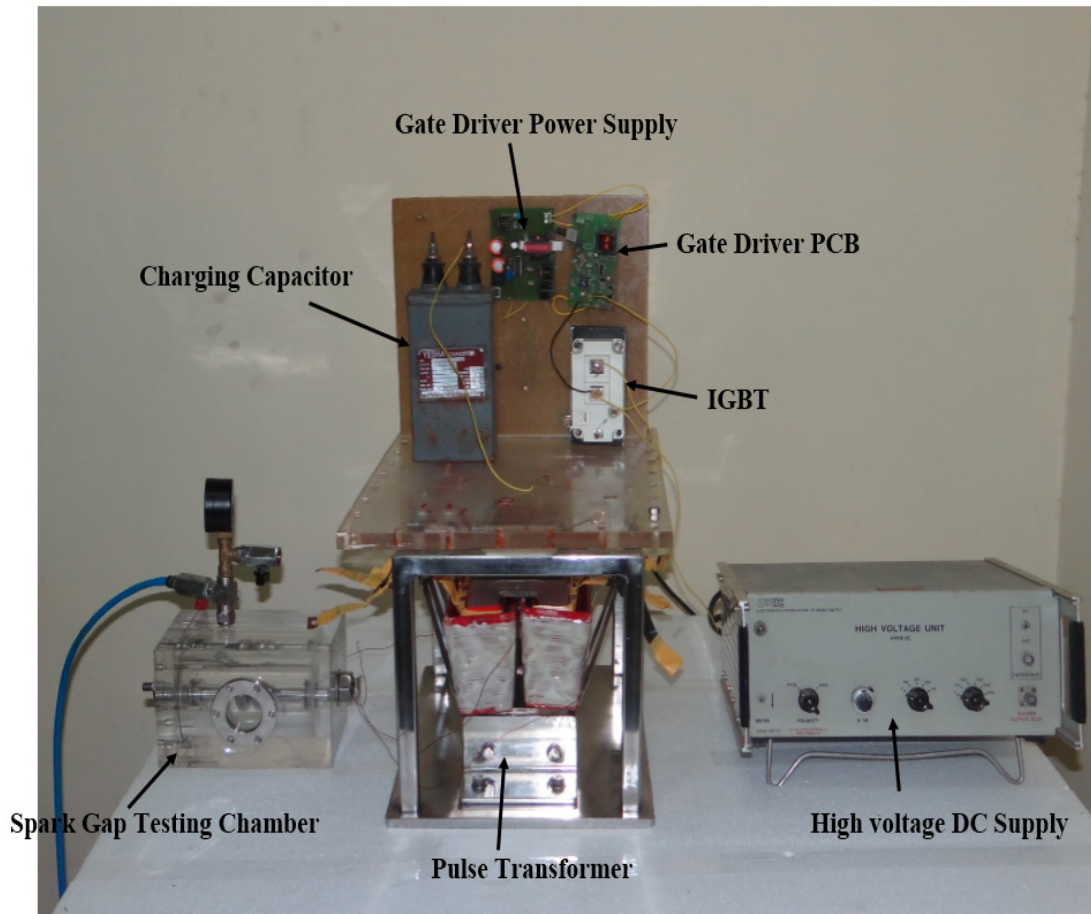


Figure.4.1 Experimental setup

This test cell consists of two stainless steel electrodes of rogowsky profile placed in a Perspex container. The gap between two electrodes can be varied from 1 mm to 5mm operates in self-breakdown mode. The output voltage of the pulse generator is around 40 kV peak voltage (for 1kv charging) with rise time of 300ns and pulse width of 1.5us. Figure.4.2 shows the voltage pulse obtained. A 100kv North-star high voltage measurement probe is used to measure the voltage and an indigenously developed rogowsky coil was used to measure the current. The voltage to current ratio of the rogowsky coil is 2 V/kA. All

observations recorded below have been measured with Agilent technologies DSO7034A, Digital Oscilloscope 350 MHz with sampling frequency of 2.5 Giga-cycle per second.

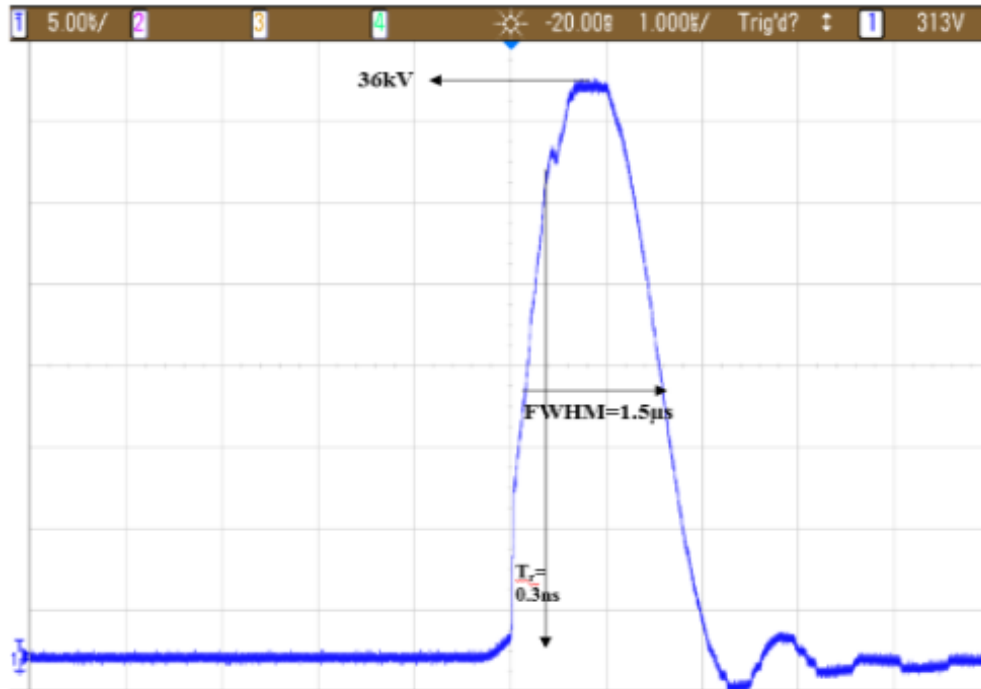


Figure.4.2 Output voltage pulse of the pulse transformer, $T_r = 300$ ns, $FWHM = 1.5$ μ s.

Before conducting the double-pulse experiment, the breakdown characteristics of the spark gap was studied with single pulse method i.e., only one pulse voltage was applied to the spark gap. The tests were performed with 2 mm air gap at atmospheric pressure. The breakdown voltage is 16 kV.

The statistical behaviour of the spark gap was studied by performing 100 breakdown shots under the same experimental conditions. It was observed that the spark gap breakdown voltage changes from shot to shot even under same experimental conditions (2 mm gap spacing, air gap at atmospheric pressure, same applied voltage and same electrode configurations). Figure 4.3 shows the histogram of 100 breakdown voltage of 2 mm spark gap at atmospheric air with rogowsky profile shaped electrodes.

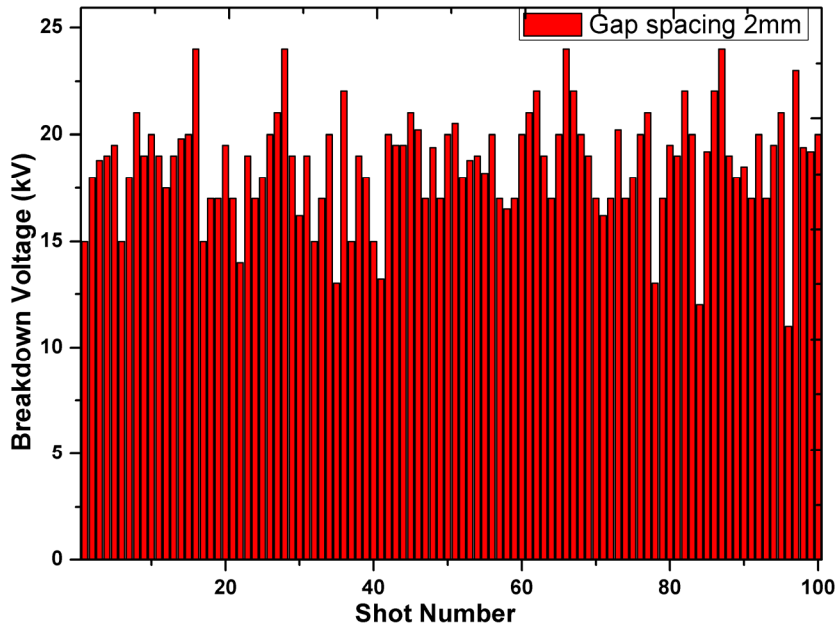


Figure. 4.3 Breakdown voltages histogram for 2 mm gap spacing with parallel rogowsky profile electrodes.

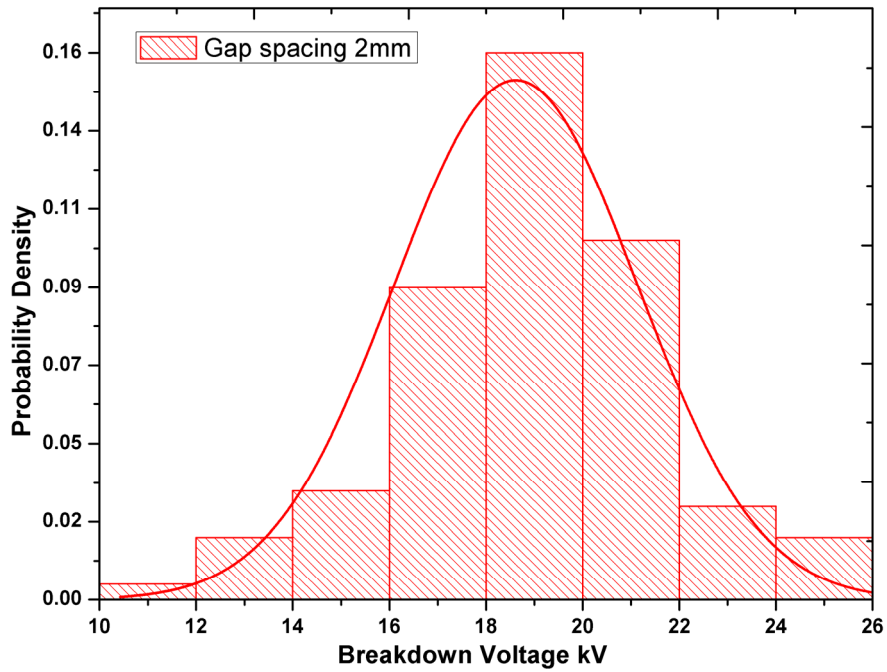


Figure.4.4. Probability density of breakdown voltages for a 2mm gap spacing for parallel rogowsky profile electrodes

In the statistical experiment, the 100 shots were divided into 10 groups of 10 shots. After 10 shots for each group, the spark gap chamber was cleaned for any remnants and a time interval of 1 minute used between the shots, which are long enough for the gap to entirely recover from the previous breakdown. The 100 columns represent the 100 breakdown events and the height of each column shows the breakdown voltage for each shot. The lower breakdown voltage is 11.2 kV and highest is of 24 kV. The averaged breakdown voltage is 17.2 kV. The probability density of the breakdown voltage was plotted in figure 4.4. We tried to fit the probability density distribution to some known distribution functions and found that it is best fitted to a Gaussian distribution with normalised standard deviation of 2.5%. Figure 4.5 shows the typical waveforms of voltage pulse and discharge current pulse of the spark gap. It was found that the discharge current was almost same for both 2 mm and 3 mm gap space when the charging voltage was kept same, which means that the impedance of the discharge circuit is way higher compared to impedance of the spark gap.

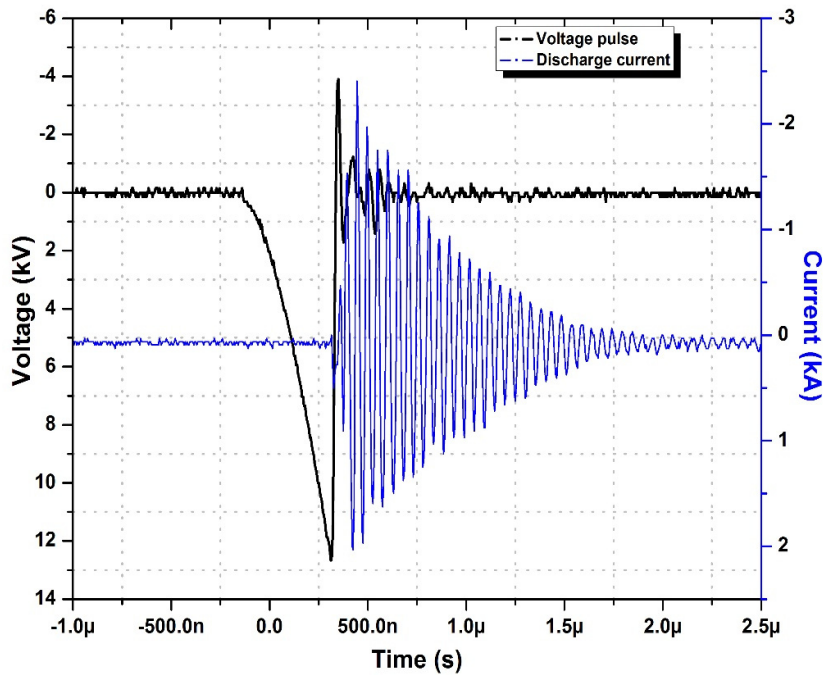


Figure 4.5. Typical waveforms of single voltage pulse and discharge current

Also, the break down voltage of the single pulse as a function of the gap pressure for 0-2 bar pressure with 2mm to 4mm spark gap distances was measured and depicted in figure 4.6. The results indicate that breakdown voltage and the pressure relation follows the paschen's curve in the high pressure region.

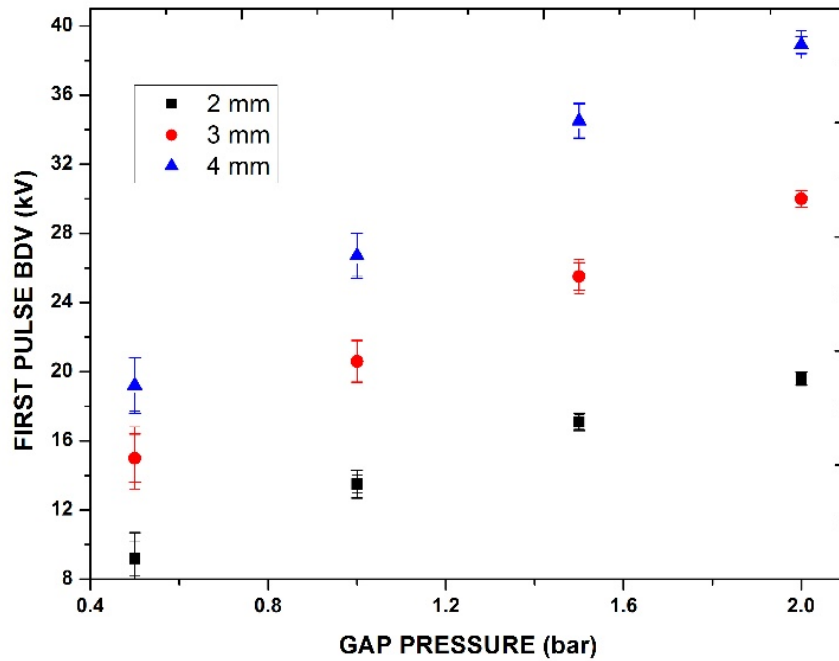
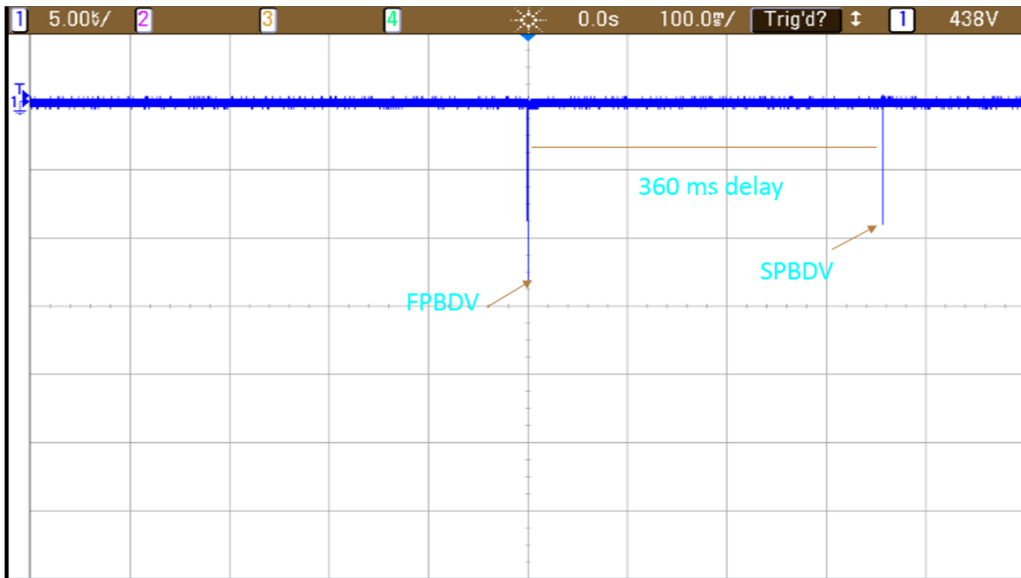


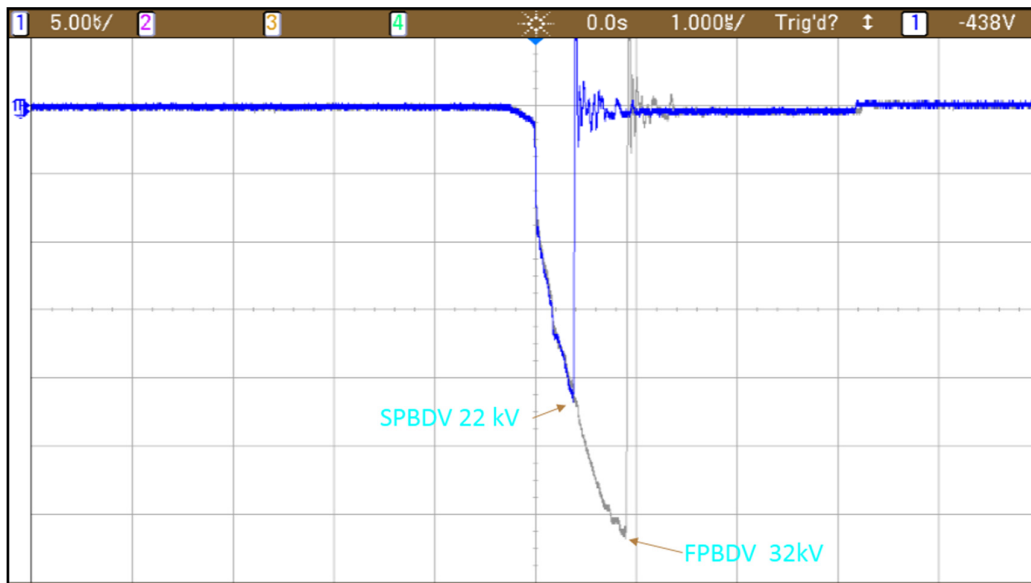
Figure 4.6 first pulse breakdown voltage as a function of gap pressure characteristics for Argon gas 0-2 bar, 2-4 mm gap distance

Now, the voltage recovery times were measured by a commonly used double pulse technique. In two pulse method, initially the first pulse is applied to the sparkgap. The breakdown voltage is measured as FPBDV (First pulse breakdown voltage), Next the recovery pulse is applied with a delay. This pulse is same as the original pulse. The breakdown voltage for second pulse also measured (SPBDV). The percentage of spark gap recovery is decided by the SPBDV. The experiments have to be repeated a number of times

to get complete data of the recovery time. The recording of breakdown voltages is also very simple. This method has been widely used in recovery voltage / time measurements.



(a)



(b)

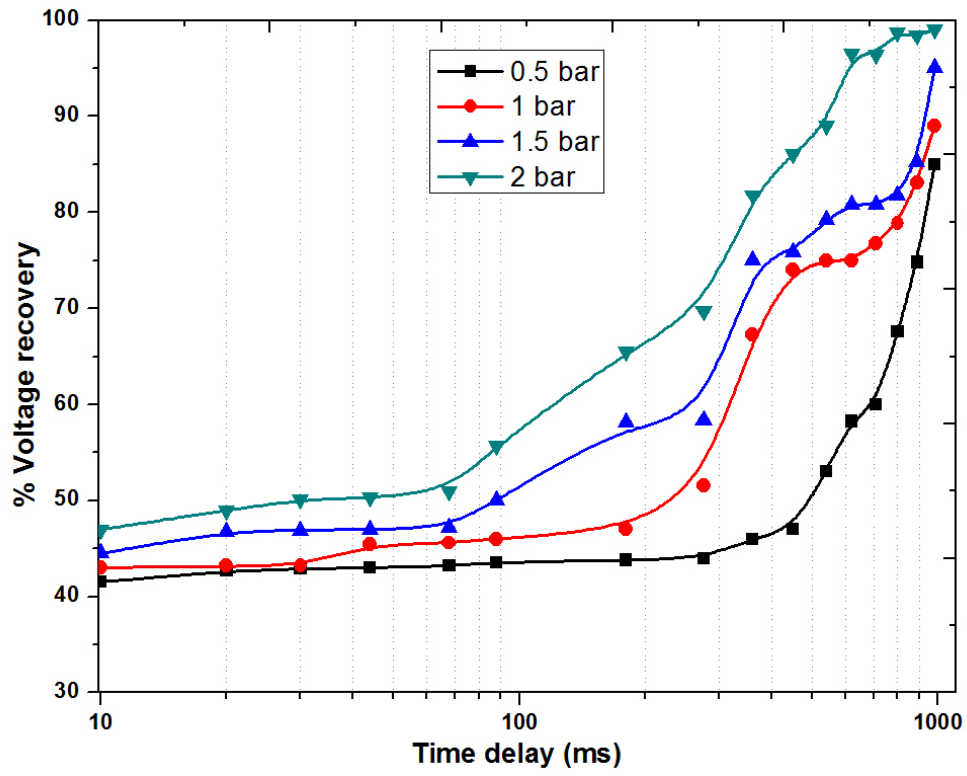
Figure. 4.7 Typical waveform of the voltage across the gap in the experiment with two-pulse method. (a) Time delay between two pulse for argon gas, 4 mm gap, 0 bar, and 360 ms delay. (b) Breakdown and recovery voltages argon, 4 mm gap, 2 bars, 300 ms delay.

In our experiments, two similar voltage pulses will be generated with a minimum inter pulse period of 1ms and used to pulse charge the spark gap. First pulse gives spark gap breakdown voltage (FPBDV). The second pulse breakdown voltage (SPBDV) gives the recovery voltage of the spark gap and corresponding time indicates the time of recovery.

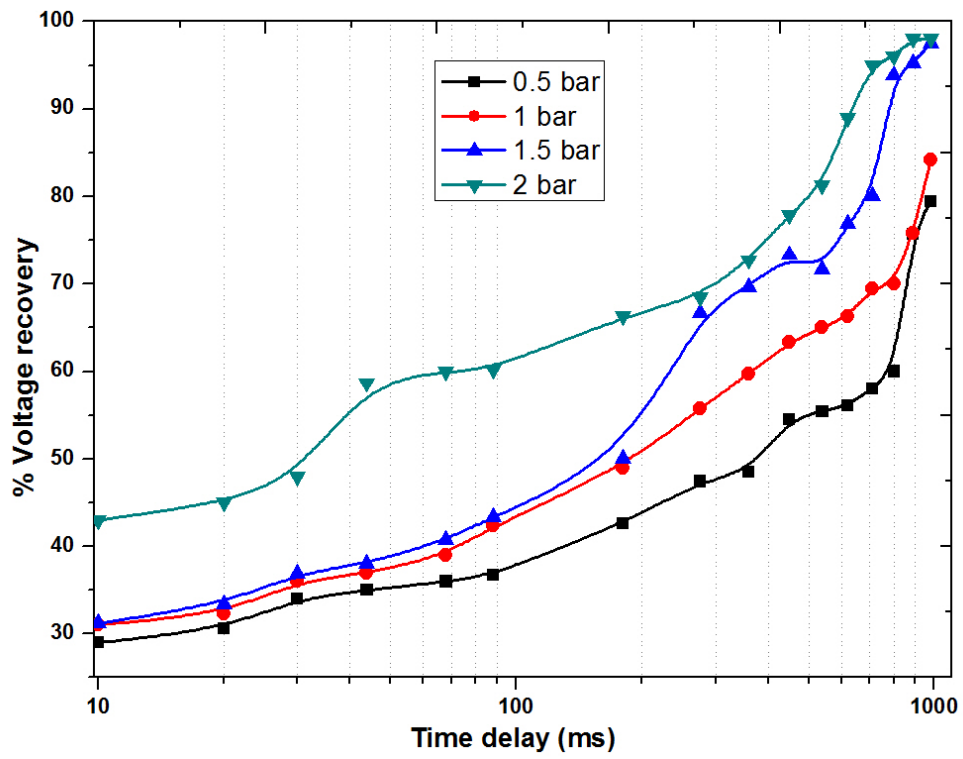
The parameters studied with the experiments were the effect of operating pressure and spark gap distance on the rate of rise of recovery voltage. Argon and nitrogen gases were used for 0-2 bar pressure range and a gap distance of 2-4 mm is used in the experiments. With this method we can accurately apply delay pulses to the spark gap to measure the recovery times. A sample of the two voltage pulse with a delay of 360ms is shown in Figure 4.7 (a). Since we are using pulse charging to the spark gap the second pulse shape at the time of breakdown varies in amplitude and pulse width depending on the delay between pulses. Figure 4.7 (b) shows the breakdown and recovery voltage pulses with 300 ms delay.

4.3 Effect of gas, gap distance and pressure variation on spark gap recovery

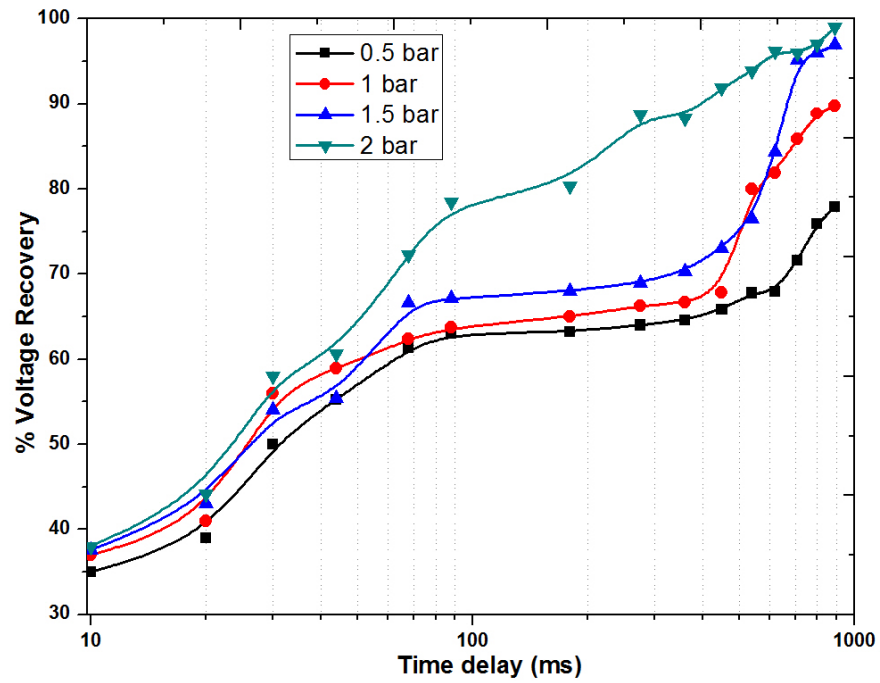
It is observed that pressure has a significant effect on the recovery time of the spark gap. The complete recovery of the spark gap (without gas flow technique) is observed around 1s. Figures 4.8 (a),(b), and (c) shows the percentage recovery as a function of the delay times for 2mm, 3mm and 4mm gap distances respectively for argon gas. Similar procedure was followed to find out the recovery curves for nitrogen gas. Figures 4.9 (a), (b), and (c) shows the percentage recovery as a function of the delay times for 1mm, 2mm and 3mm gap distances respectively for Nitrogen gas. Each data point marked in figure are the average of 10 shots with same experimental conditions. Before each shot, the electrode were cleaned and repeated the experiment to measure the breakdown voltage.



4.8 (a)

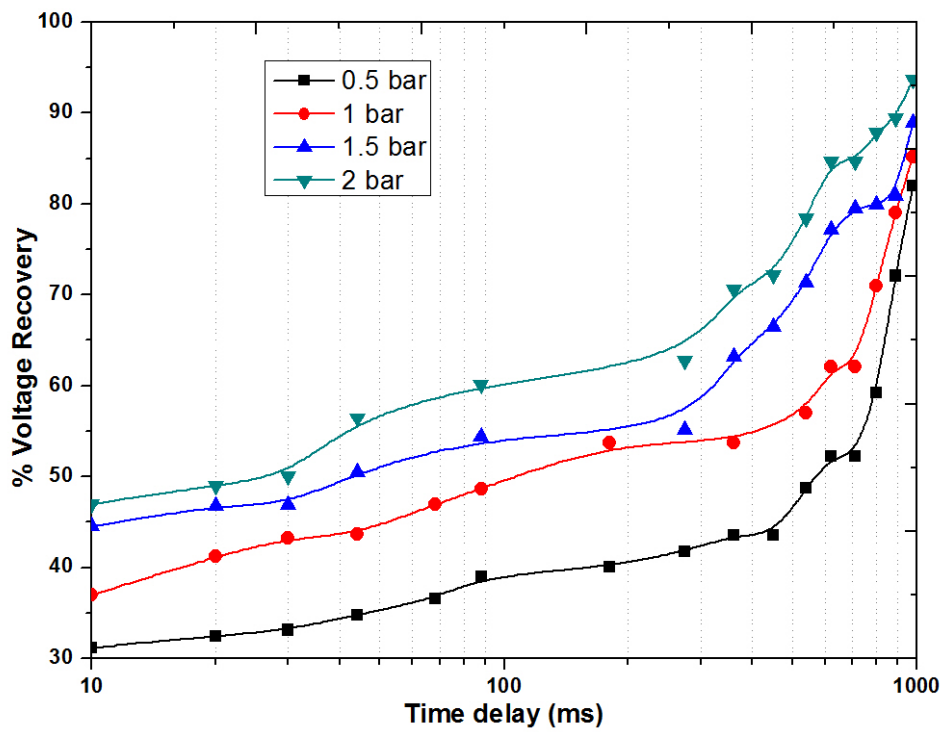


4.8 (b)

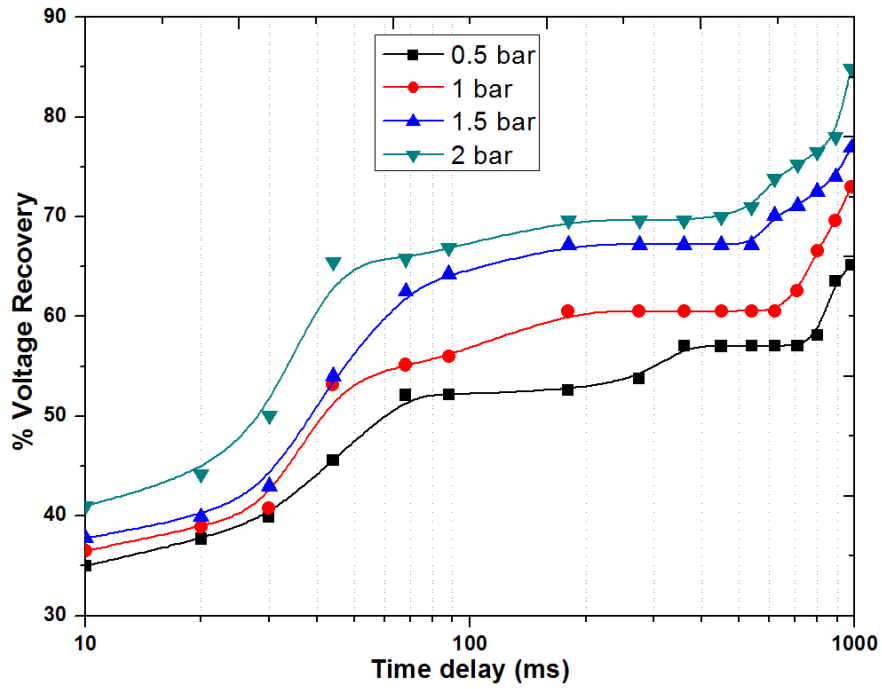


4.8 (c)

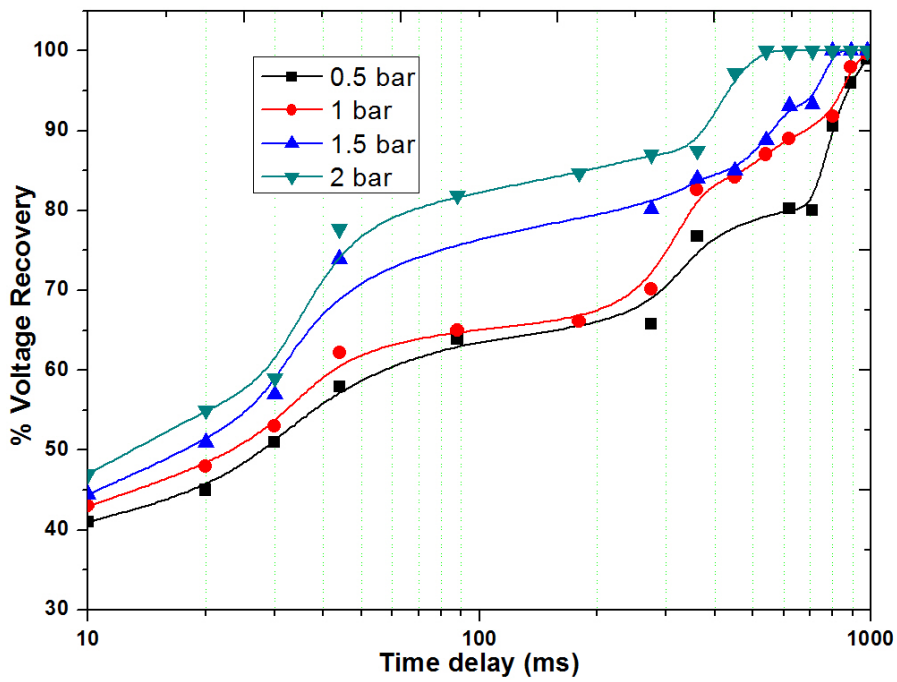
Figures 4.8 (a),(b), and (c) shows the percentage recovery as a function of the delay times for 2mm, 3mm and 4mm gap distances respectively for argon gas.



4.9 (a)



4.9 (b)



4.9 (c)

Figures 4.9 (a), (b), and (c) shows the percentage recovery as a function of the delay times for 1mm, 2mm and 3mm gap distances respectively for Nitrogen gas.

The secondary pulse breakdown voltages (SPBDV) plotted in the figures is expressed as a percentage of the first pulse breakdown voltage (FPBDV) for the purpose of result comparison.

- It is observed that a plateau in the rate of rise of recovery curves during which the degree of voltage recovery remains almost constant. This was observed by previous researchers in high pressure gasses [60, 84]. It may be caused by the residual long lived particles that can continuously produce sufficient amount of the electrons to quickly initiate the second breakdown.
- The increase in pressure causes an upward shift to this plateau. Also as the gap distance increases, this plateau is prominent. This may be caused by the large space between the electrodes that can have large no of particles to ionize the gap for second pulse.
- Recovery time decreases as pressure increases. This is due to increase in pressure cause more frequent collisions in the gap that leads to a fast removal of the deposited heat from the arc channel.
- The results also shows the short gaps recover faster than long gaps. Since the discharge currents are almost same, the deposited energy during the first pulse breakdown should be more or less the same. Furthermore, the recovery rate of a spark gap is independent of value of energy transferred through it [85]. Also, the simulations of [86] shows that the deposited heat is removed from the gap mainly due to axial heat flow through metallic electrodes. Hence in the shorter spark gap, the heat is quickly removed by the electrodes so that the cooling of the gap will be faster.
- For nitrogen gas, whose molecule is composed of two identical atoms, the recovery will be affected by the delay recombination of the residual nitrogen atoms.

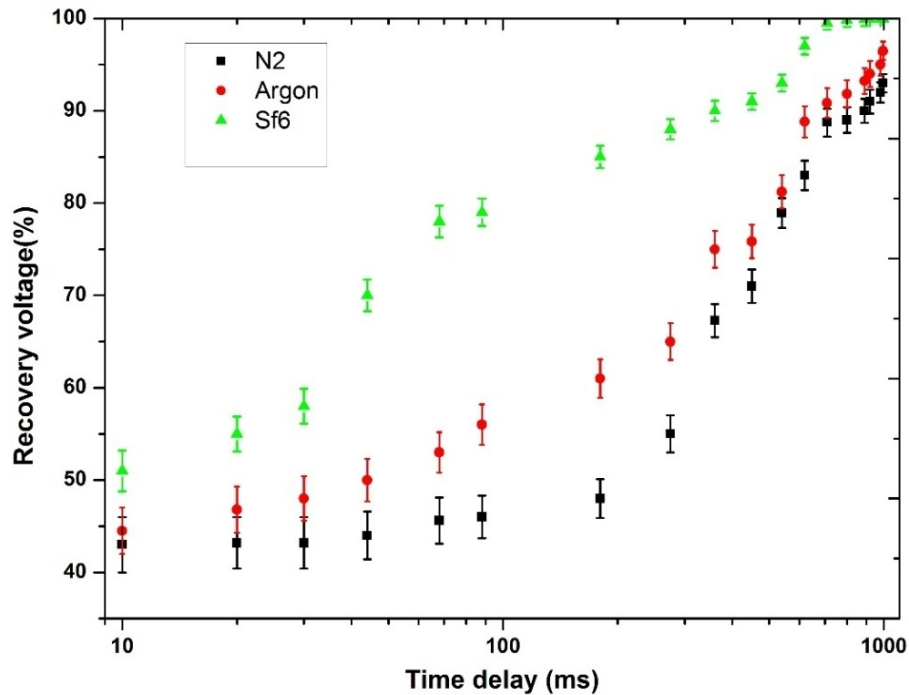


Figure 4.10. “% Voltage recovery” in 2mm spark gap at 2 bar pressure with Nitrogen, Argon and Sf₆ gas ambiances.

Also, a set of experiments were conducted with Nitrogen and Sf₆ gases to compare with the argon gas characteristics. Figure 4.10 shows the “% voltage recovery” data for N₂, Argon and Sf₆ with 2mm gap distance and at 2bar pressure. It can be observed that, Sf₆ has high percentage of voltage recovery than Argon followed by N₂. This may be due to the electro negative nature of Sf₆ that can de-ionize the spark channel faster compare to remaining two gas mediums. It seems to have a slightly faster recovery rate for Argon gas compared to nitrogen.

4.4 Experimental Investigations of Pulse Charged Spark Gap Recovery Times and Influencing Factors

The dielectric Recovery data of spark gap plays a basic role, but it has been inadequately studied for the repetitive pulse charge conditions. In the following sections, some of the factors which affect the recovery of spark gap switch for pulse charged operation are

described. Here also, a two pulse technique has been used in which first pulse is applied to the spark gap to over-volt the gap and initiates the breakdown and second pulse is used to determine the recovery voltage of the gap. The effect of electrode size, pulse rise time and conduction current on the spark gap recovery performance is presented. Experiments were performed by using a double-pulse generator capable of generating 40 kV pulses with a delay of 1ms-1s.

4.4.1 Effect of electrode shape and size on spark gap recovery

The electrode shape and size is an important factor which can influence the recovery time of the spark gap switch. Also, the selection of the electrodes based on material can play a major role in the recovery of spark gap switch. A recovery study by C S Reddy et.al [87] shows the electrode material effect on recovery time of the spark gap switch and found that the Stainless steel electrodes has faster recovery rate compare to copper electrodes. In this sub section, the effect of electrode geometry on the rate of rise of voltage recovery is discussed.

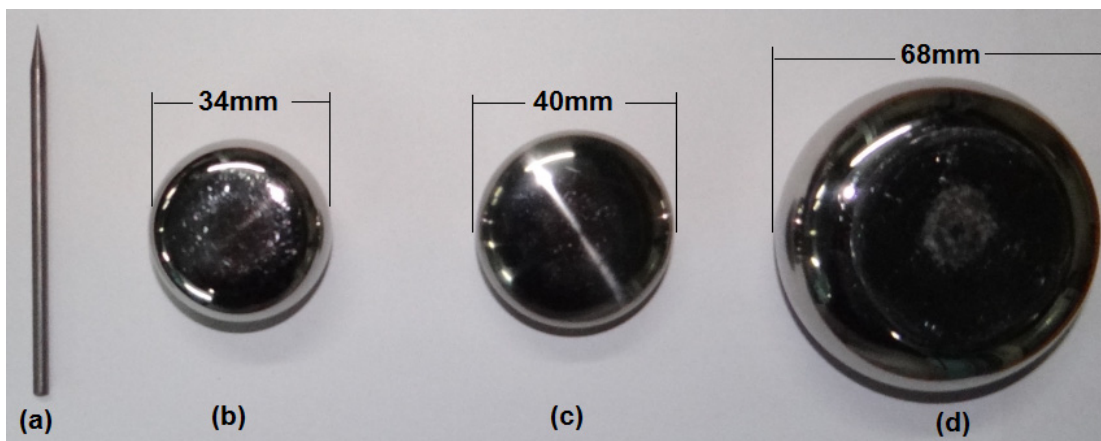


Figure.4.11. Different sized electrodes used for the spark gap recovery experiments. (a) Thin needle used for the point-plane spark gap configuration (b) 34mm diameter (c) 40mm diameter and (d) 68mm diameter electrodes used for parallel-plane spark gap configuration

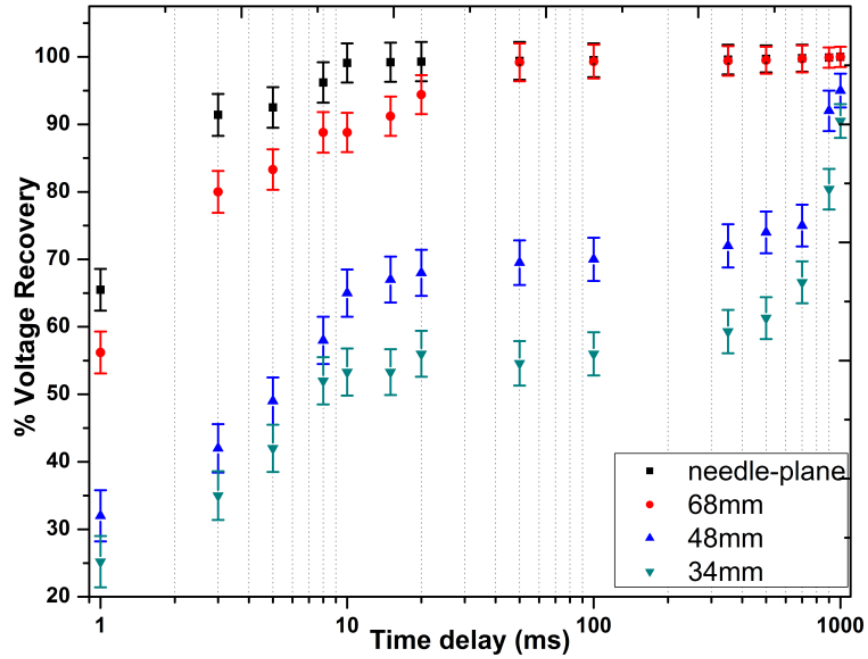


Figure.4.12. Rate of rise of voltage recovery for different electrode configuration with 2mm gap distance.

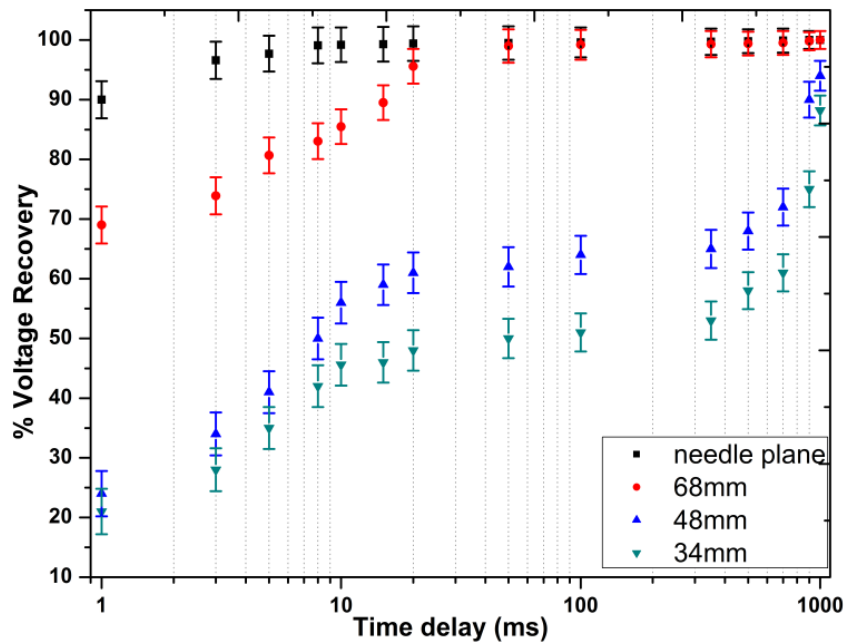


Figure.4.13. Rate of rise of voltage recovery for different electrode configuration with 3 mm gap distance.

A parallel-Rogowsky sparkgap configuration with 34mm, 40mm and 68mm diameter, made with stain less steel were investigated. A point-Rogowsky spark gap configuration also studied for 2 mm and 3 mm gap distances in open air, atmospheric conditions. Figure 4.11 shows the electrode of different diameters which are used in the experiment. All electrodes used in the experiment were polished and first cleaned with trichloroethylene and then with alcohol before spark gap experiments. Figure 4.12 and 4.13 shows the rate of rise of voltage recovery characteristics with different electrode sizes for 2 mm and 3 mm gap respectively. The figures indicate the point-Rogowsky configuration has the fast recovery rate compare to the parallel-Rogowsky spark gap configuration. And also the electrodes with 34 mm and 48 mm diameter has lowest recovery rate for both 2 mm and 3 mm gap distances. The spark gap with 68 mm diameter electrodes has better recovery compared to the lower diameter electrodes. This signifies that, the deposited heat is removed from the gap mainly due to the axial heat flow through metallic electrodes. Since the electrodes in a shorter gap tend to remove heat quickly and results in faster cooling of the spark gap [86]. This results in a faster recovery rate in short gap with longer diameter electrodes compared to long gaps. It can also be explained by following the temperature decay model proposed by Tsuruta et.al [69]. The recovery time of a spark gap is determined by total electrode heat flow axially and the heat dissipation in to the gap radially. Perkins et.al [88] have reported experimental recovery times of an 8 cm long air spark gap and shows that the recovery was solely governed by radial heat flow. From the experiments of Tsuruta et.al [44], the recovery time depends on both radial heat dissipation as well as axial heat flow through electrodes for an intermediate lengths. His results for 7 mm and 9 mm gap distance shows that the hot gap between electrodes is cooled by the axial and radial heat decay, but the axial heat decay through electrodes plays a dominant role. But for shorter gaps the thermal conduction of heat through the electrodes of the spark gap plays a significant role in the recovery of spark gap. Since for a gap between

electrodes whose diameters are much larger than the gap spacing, the heat flow to the ambient gas is limited only to a restricted space between electrodes.

In case of a point- Rogowsky profile electrode configuration, the heat in the gap can decay to a larger region because of the small diameter of the point electrode, and the hot gap loses its temperature faster than the parallel-Rogowsky configuration by a faster radial-gas heat flow. Due to this reason, our experimental results shows slightly faster recovery time for point-Rogowsky profile compared to parallel-Rogowsky configuration. This was observed even quicker in 3 mm gap compared to 2 mm gap distance.

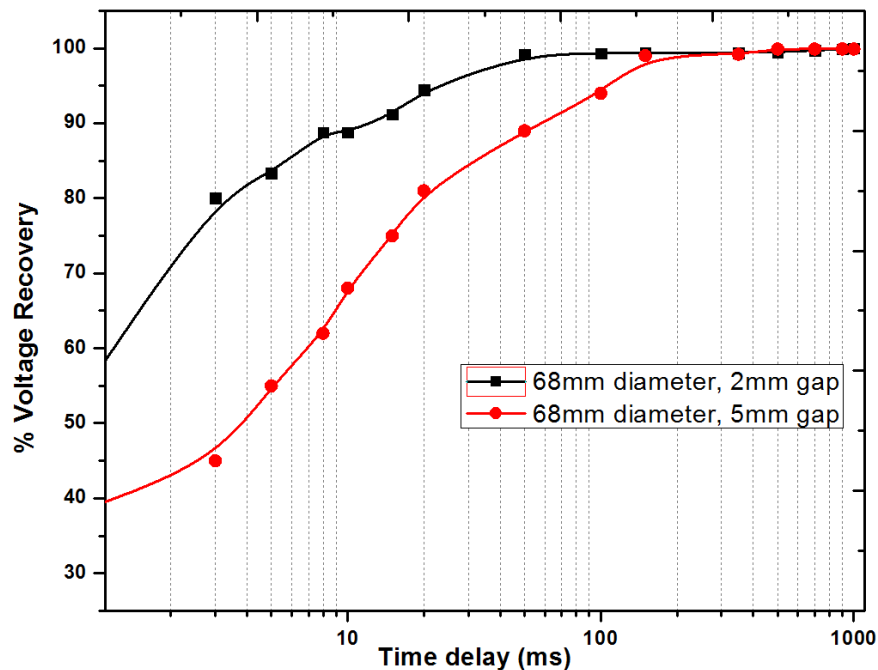


Figure.4.14. Voltage recovery variation for 2mm and 5 mm spark gap distance with 68 mm diameter Parallel-Rogowsky electrode configuration.

In our study to see the distance effect on the recovery time, a comparison has been shown in figure 4.14. This shows the experimental voltage recovery variation for 2mm and 5 mm spark gap distance with 68 mm diameter Parallel-Rogowsky electrode configuration. From the graph, the 2 mm gap fully recovers in 20ms, whereas for 5 mm gap it is around 150ms. this

signifies that the shorter gaps recover faster by dissipating heat through electrodes compared to the longer gap distances. So, the axial heat flow through the electrodes plays a dominant role in the recovery of shorter gaps [69].

4.4.2 Effect of pulse shape and size on spark gap recovery

The recovery time of a spark gap switch is also depends on the rate at which the pulse applied the spark gap. After the application of the pulse, the gap breakdown at a voltage level depends on the rise time of the pulse and tries to reach its pre-breakdown status by dissipating the heat to the surrounding electrodes and ambience. In general, the breakdown process in a spark gap can be considered as 4 stages: (1) Availability of seed electrons to start electron avalanches, (2) Generation of streamer by the growth of electron avalanches, (3) Bridging of the gap by conducting channel, (4) generation of an arc by heating the conducting channel.

Since the rate at which the pulse applied, effect all these stages, the breakdown voltage of a spark gap depends on rise time of the pulse as well as the amplitude. The slow rise of the applied voltage pulse results in a lower breakdown voltage. The lowest breakdown voltage is static breakdown voltage (DC). In our case, Pulse breakdown happens at a voltage higher than DC voltage and is called over-volted breakdown.

So, from the above explanation, the faster the pulse rise rate, the higher the breakdown voltage and consequently it takes more recovery time to attain its pre breakdown status.

The effect of pulse rise time on the voltage recovery time of spark gap was investigated in this sub section. The wave shape is one of the main parameter that could affect the final pulse repetition frequency of the system. The rise time of the output voltage pulse of the power modulator depends on the 'L' and 'C' of the circuit. In our experimental facility shown in figure.4.1, it is possible to vary the Capacitance that can change the shape of the voltage pulse.

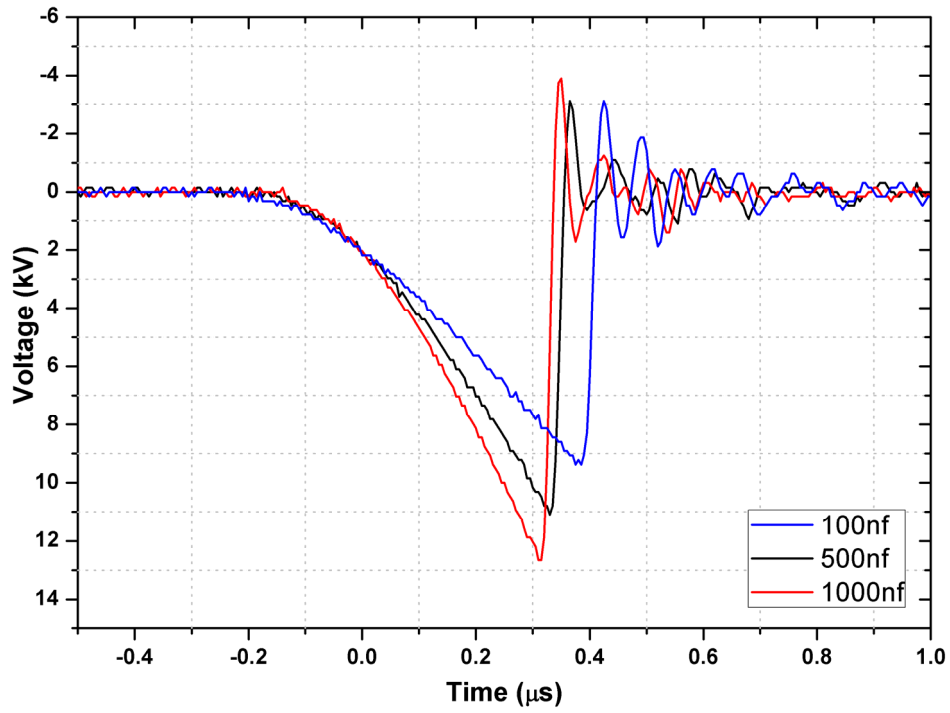


Figure.4.15. Voltage pulses with different rise times due to capacitor variation in the pulse modulator.

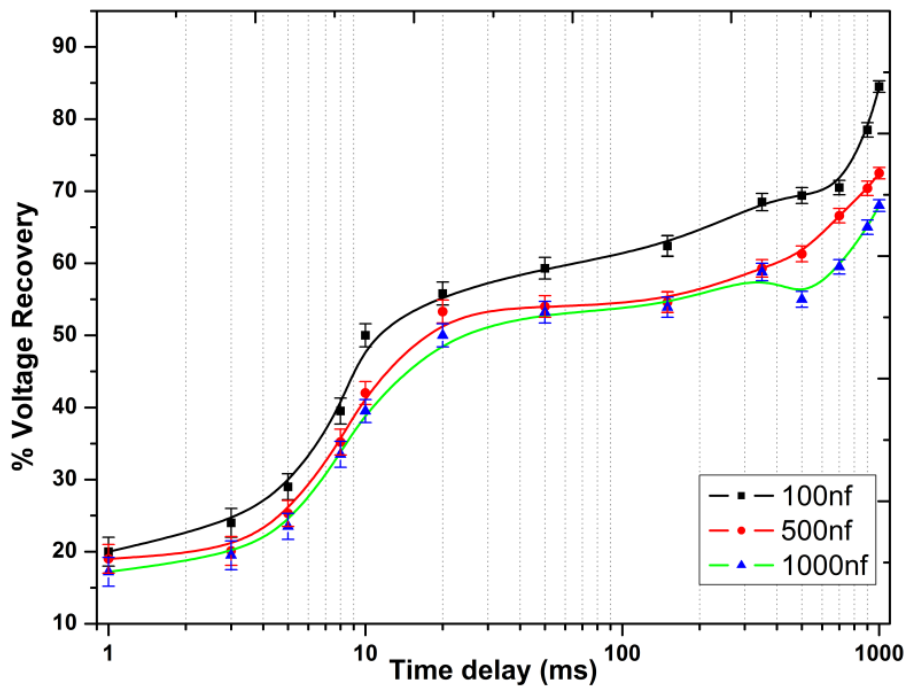


Figure.4.16. Effect of pulse rise time on the Rate of rise of voltage recovery with 2mm gap distance.

An attempt has been made to change the voltage pulse rise time by varying capacitor in the modulator setup. The output breakdown pulse waveforms for 100nf, 500nf and 1000nf capacitors were shown in figure 4.15. The rise times of 400 ns, 320 ns and 300 ns were observed for charging capacitors of 100 nf, 500 nf and 1000 nf respectively. The respective rate rise of voltage recovery characteristics for the different rise time was shown in figure 4.16. Although, there is no big variation observed in the characteristics, the pattern shows a diminished pulse repetition with increase in the pulse rise time. It also shows that the pulse rise time effects breakdown voltage more rather than the recovery time of the spark gap.

4.4.3 Effect of discharge current on spark gap recovery

The effect of peak value of conduction current on the percentage of voltage recovery of the spark gap was determined by adding an external resistance in series, between the pulse modulator and the spark gap switch. Due to the current heating in the arc column, density in the gap volume decreases during the discharge period. This density will be increased during the recovery period. The time taken for the density recovery will depend up on the current through the gap during the arcing period. In our experiments, the recovery measurements were made with two sets of gap distances 2 mm and 3 mm at open air conditions. The different values of resistance used are 500 Ω , 200 Ω , 100 Ω and 0 Ω (no external resistance). Figure 4.17 and 4.18 shows the effect of conduction current on the rate of rise of voltage recovery of spark gap with 2 mm and 3 mm gap distances respectively. It was observed the time taken for the voltage to reach its static (DC) breakdown voltage level is around 10ms. After this point an intermediate plateau is observed in the recovery characteristics. An increase in the output impedance resulted in a decrease in the time taken to reach the plateau voltage. However the reason for plateau was not clear and this was observed by previous researches. Once, this voltage level reached, only limited effect was observed for a further increase of resistance from 200 Ω to 500 Ω . This effect of discharge current on the recovery

rate of Sf_6 gas spark gap at 1 bar was also observed by Scott j. Macgregor et.al [89]. The time taken to reach the plateau voltage level in his experiments was reduced from 10ms to 2ms for an impedance addition of 800Ω from 400Ω .

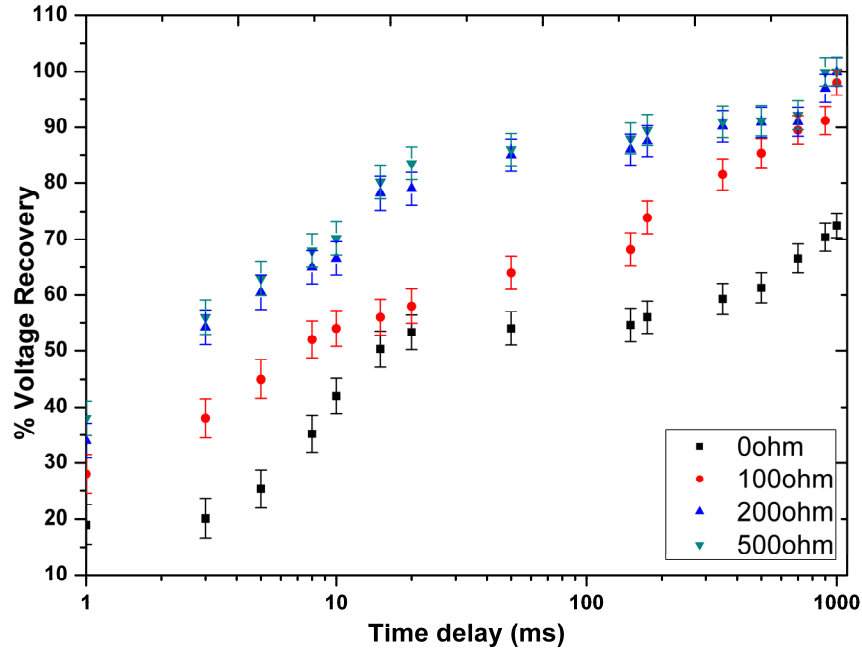


Figure.4.17. Rate of rise of voltage recovery for variation in conduction current with 2 mm gap distance.

The effect of pulse polarity on recovery of spark gap was also estimated for a point-plane electrode configuration. In point-plane geometries the polarities of the applied pulse has a major impact on the formation of arc. This polarity effect also tends to be enhanced for short and fast pulses. To see the polarity effect, experiments were conducted for 2 mm gap, point-rogowsky profile with positive and negative polarity voltage pulses. The figure 4.19 shows the recovery characteristics obtained for a delay time of 1ms to 1s. We can observe that the recovery time for both polarities was almost similar. In our experimental observations, where, recovery of the spark gap is considered rather than breakdown, this polarity effect is not notable. This may be due to the high density of ions and excited metastable particles present

in the gap after the breakdown, whose space charge weakens the polarity dependence in the point-Rogowsky profile [90].

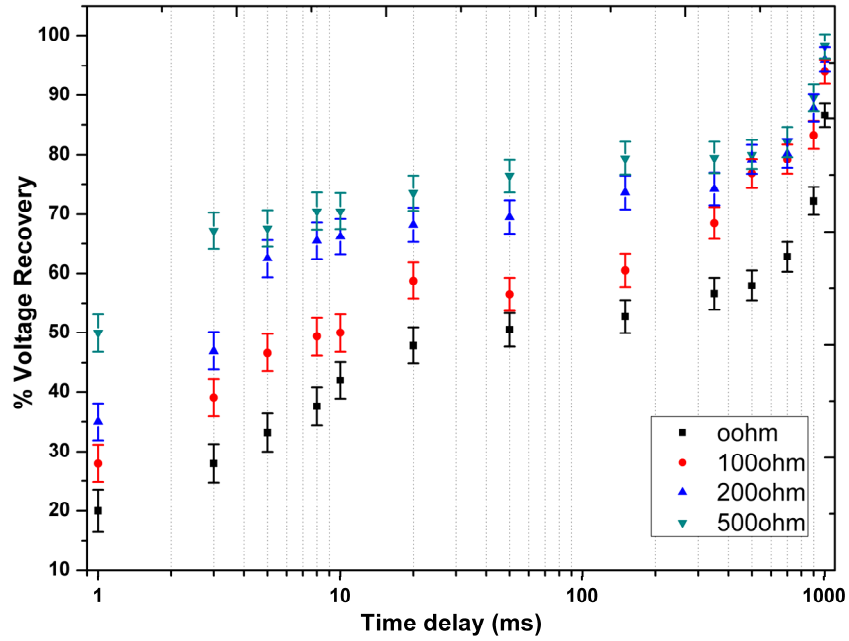


Figure.4.18. Rate of rise of voltage recovery for variation in conduction current with 3 mm gap distance.

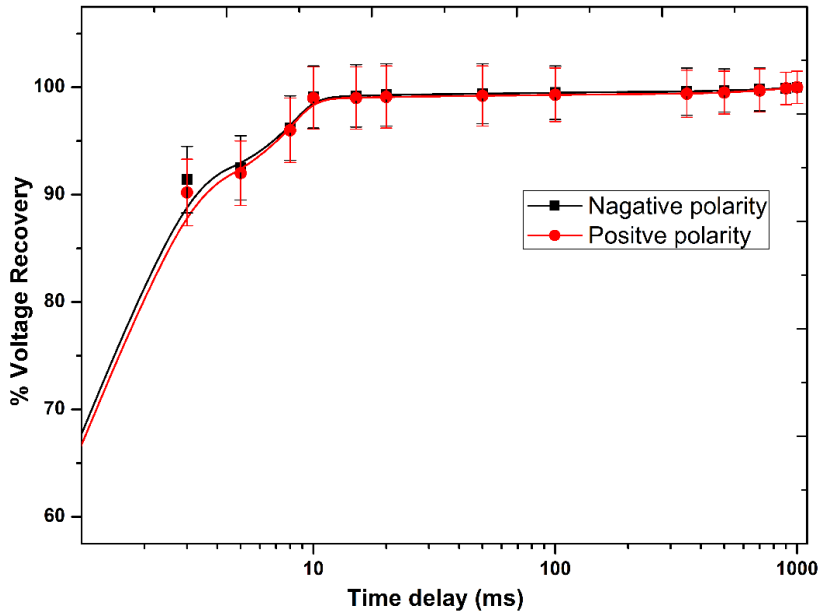


Figure 4.19: The recovery characteristics of point-Rogowsky profile with 2 mm gap for positive and negative polarity pulses.

4.5 Summery

The voltage recovery characteristics of a pulse charge spark gap switch have been studied for a varying switch operating conditions. The factors which influence the rate of rise of voltage recovery have been investigated by using a double-pulse technique. The factors studied were, the effect of electrode shape and size, gap distance, effect of pulse rise time, the conduction current and the pulse polarity in the spark gap. The results are summarized as follows:

- Recovery strongly depends on the geometry as well as gap distance. The point-Rogowsky gap recovers faster compared to parallel-Rogowsky configuration.
- Shorter gaps recover faster compared to longer gaps due to faster axial heat decay through the electrodes.
- A large diameter of rogowsky profile electrodes has fast recovery characteristics compared to low diameter electrode spark gap configuration.
- An improvement in the pulse rise time was resulted in a slow recovery rate of the spark gap. An intermediate plateau is always observed in the recovery characteristics of spark gap.
- The decrease in the discharge current by adding extra output impedance resulted in a faster recovery.
- The polarity of the applied voltage pulse seems to have less effect on the recovery times of point-rogowsky configuration spark gap.

CHAPTER 5

COMPUTATIONAL STUDY OF GAS DENSITY RECOVERY OF SPARK GAP

5.1 Introduction

The electrical breakdown and pre-breakdown characteristics of gases at atmospheric pressure and above, and at low pressures are widely investigated and there is reasonable agreement on the mechanism of growth of the current in the breakdown. But the recovery processes after the sparkgap breakdown are not studied extensively at high pressures. During the breakdown of a spark gap, the gas between the spark electrodes can be rapidly ionized by a suitable potential difference applied to the electrodes. Thus the gas is changed from a good insulator into a good electrical conductor, a process known as over-volted breakdown of the gas.

The gas is at first fully ionized and expands due to the high temperatures caused by the spark. At atmospheric pressure, electron-ion recombination produces a neutral gas between the spark gap electrodes within a few hundred microseconds after the passage of the discharge current. The pressure in the channel also rapidly returns to its original value because acoustic wave propagation quickly smooth out the pressure gradients produced by the spark. However, the temperature gradients in the inter electrode gas are not smoothed out so rapidly. Since the pressure is constant, the cooling of the gas increases its density from a low value just after the high current pulse ceases, up to its original value. Because it is easier to ionize the gas at its reduced density, the magnitude of the voltage needed to re-strike a spark in the post-discharge era will increase as a function of time. The gradual relaxation of the breakdown voltage to some steady value (close to its pre-breakdown value) after a spark gap breakdown is referred to as spark gap recovery [91–93]. The understanding of the recovery phenomenon is very important if spark gap switches are to be operated at high repetition rates.

The researchers are trying to understand the dynamics of breakdown process and its recovery inside spark gap switch [94, 95]. The two major factors that influence the dielectric characteristics of gas switch are the temperature and rate of change in the gas density. Following a breakdown, the spark gap contains hot decaying plasma in which the degree of ionization is rapidly decreasing. But the hot gas remains for a relatively long time and the cooling can be done by heat flow to the surrounding ambient gas. For the measurement of these parameters like velocity, temperature, and density of the gap needs very complex and costly experimental setups. In order to understand the characteristics of the arc, some papers [96 - 98] mainly depended on the experimental means to investigate the arc behavior although it is expensive and time consuming. Whereas it is still insufficient to obtain some internal parameters of the arc plasma, such as gas velocity, current density, and so on. With the continuous development of the computational techniques and capability, it is possible to obtain the spark gap information which cannot be obtained by the experimental method alone, and the simulation is becoming an effective approach to complement the experimental research on the recovery behavior of the spark gap.

In this study, a two-dimensional axisymmetric computational model of spark gap recovery is presented to provide a better understanding of the dynamics of the recovery process. Also, the gas density recovery time of the spark gap from the simulations is compared with the breakdown voltage recovery time obtained from the two-pulse experiment presented in chapter 4. Argon gas experiments and simulation results were used in this comparisons. Discussions and the possible repetition frequencies are tabled at the end of this chapter.

5.2 Simulation method

The spark gap is filled with hot decaying plasma following a current discharge between the two electrodes. This decay contains rapidly decreasing degree of ionization. But the neutral hot gas remains for a relatively long time and is cooled by the heat flow to the surrounding ambient gas and the electrodes. The decay of the gas temperature is a very complicated phenomenon and depends on many factors, such as

thermal conductivity, specific heat at constant pressure, gas density and so on [99]. But, the recovery characteristics are governed almost entirely by the gas temperature [100]. The temperature decay in the switch following the equations below:

$$\frac{\partial \rho}{\partial t} + \nabla \cdot (\rho u) = 0 \quad (5.1)$$

$$\frac{\partial}{\partial t} (\rho u) + \nabla \cdot (\rho u u^T) = -\nabla p + \nabla \cdot [\mu (\nabla u + (\nabla u)^T) + \rho g] \quad (5.2)$$

$$\frac{\partial}{\partial t} (\rho H) + \nabla \cdot (\rho u H) = \nabla \cdot (h_t \nabla H) \quad (5.3)$$

Where, ρ is gas density, u is gas velocity, μ is viscosity, g is gravity, H is the total enthalpy and h_t is the heat transfer coefficient. Here equation (5.1) is the continuity equation, (5.2) is the conservation of momentum equation taking the gravity into account, (5.3) is the energy conservation equation. The 2-D axisymmetric spark gap simulation model has been built to study the recovery characteristics after the breakdown of the gas.

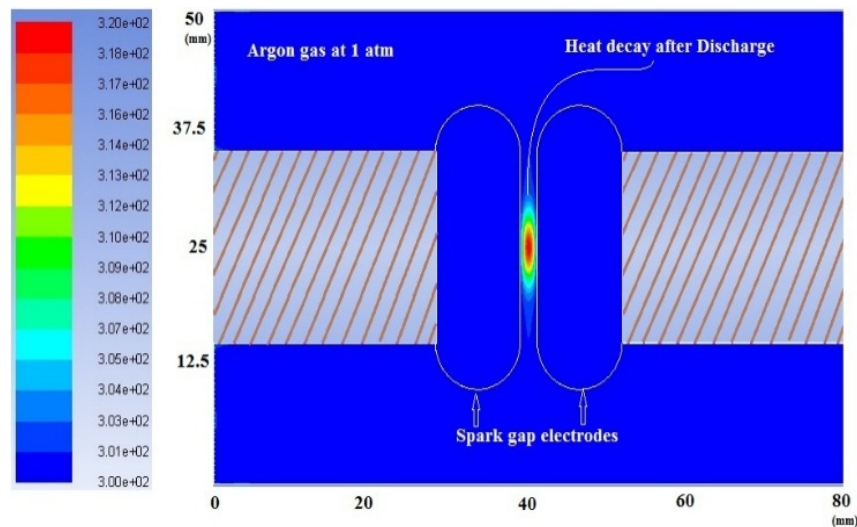


Figure 5.1. Simulated geometry of spark gap at 20ms, 2mm and 1atm argon gas

Figure 5.1 shows the simulated geometry of spark gap at 20ms, 2 mm and 1atm Argon gas. The solution domain ranges from 0 to 50 mm in r and 0 to 80 mm in the z directions. Because of the symmetry of the computational domain with respect to the $x-z$ plane, only half of the geometry is modelled to reduce the

calculation time. Refining the grid and decreasing the time-step did not cause any appreciable changes in the simulation results. The gap between the electrodes is taken equal to 2 mm, where the electrodes have rogowsky profile which is equivalent to our experimental electrode conditions.

In the computations, Equations (5.1), (5.2) and (5.3) are solved with the computational fluid dynamics code (ANSYS/Fluent) [111] which is a Control volume discretization technique. This computational domain also allows the user to write user-defined functions (UDFs) in the C language to customize the standard code to fit particular modelling needs. In this study, density, viscosity and thermal conductivity properties for high temperature argon gas are based on the data presented in [102] and used as UDFs in simulation. The UDF used in our simulations is given in Annexure – II.

The transient simulations presented in this study, use the experimental breakdown data for 2mm argon gas at 1atm pressure as initial conditions. The energy discharged into the spark gap is estimated from the experimental results. The data is averaged for 10 breakdown shots and used as the initial conditions for the simulation. The calculation of energy from the experimental data followed by the equation:

$$E_g = \frac{V.I}{\pi.r^2.h}.t \quad (5.4)$$

Where, V and I are breakdown voltage and current values measured, h is the gap distance (2mm) and r is the radius of the spark. The radius ‘r’ was taken [103] as 1mm for our numerical study. Since, the duration of the breakdown between the electrodes is in the order of sub micro seconds, the spark channel will expand and quickly extinguish from the initial channel radius ‘r’. So, keeping the deposited energy and duration of the spark unchanged, the small variation of radius ‘r’ seems to have less effect on the final results of the simulation. The estimated energy from equation (5.4) is the initial condition to the simulation model for a discharge time-period (‘t’). This time is the averaged pulse discharge time taken from the experiment. Also, the initial conditions for the simulation are, pressure, p = 1atm, temperature, t= 300k and the density of the gas, ρ for the argon calculated by the ideal gas equation. The simulation runs with a very small time step.

5.3 Results and Analysis

We used experimental discharged energy as an input to our simulation model. The decay time of density from the simulation is compared with the recovery time of the spark gap, estimated from the double pulse method. The experimental setup and procedure to estimate the recovery time of argon spark gap was explained in our previous work [104]. Both the simulation and experiments were conducted for a decay time of more than 1sec. The variation of temperature and density for the simulation time is shown in figure.5.2. The energy is simulated during the discharge period t , (242ns) taken from experimental breakdown pulse. Figure 6.3 shows the typical waveforms of voltage pulse and discharge current pulse of the spark gap. Each value of the V , I and t were taken from an average of 10 experimental shots. Before each set of shots, the electrodes were cleaned and repeated the experiment to measure the breakdown voltage.

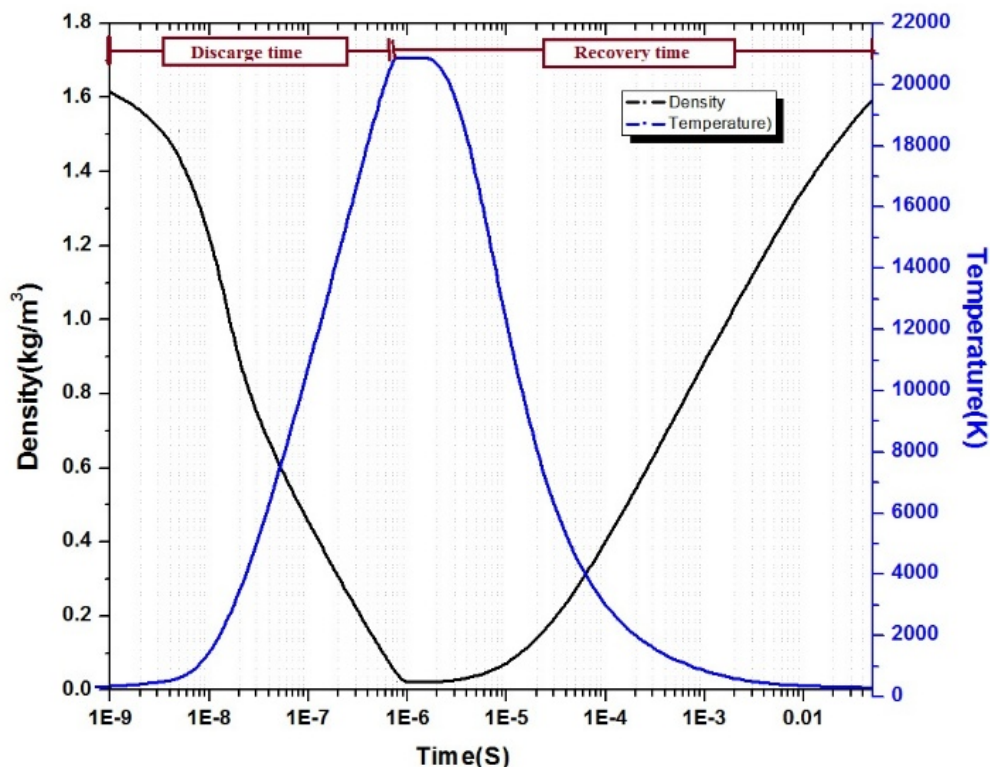


Figure 5.2. Density and temperature variation for the simulation time for 2mm argon spark gap at 1atm pressure.

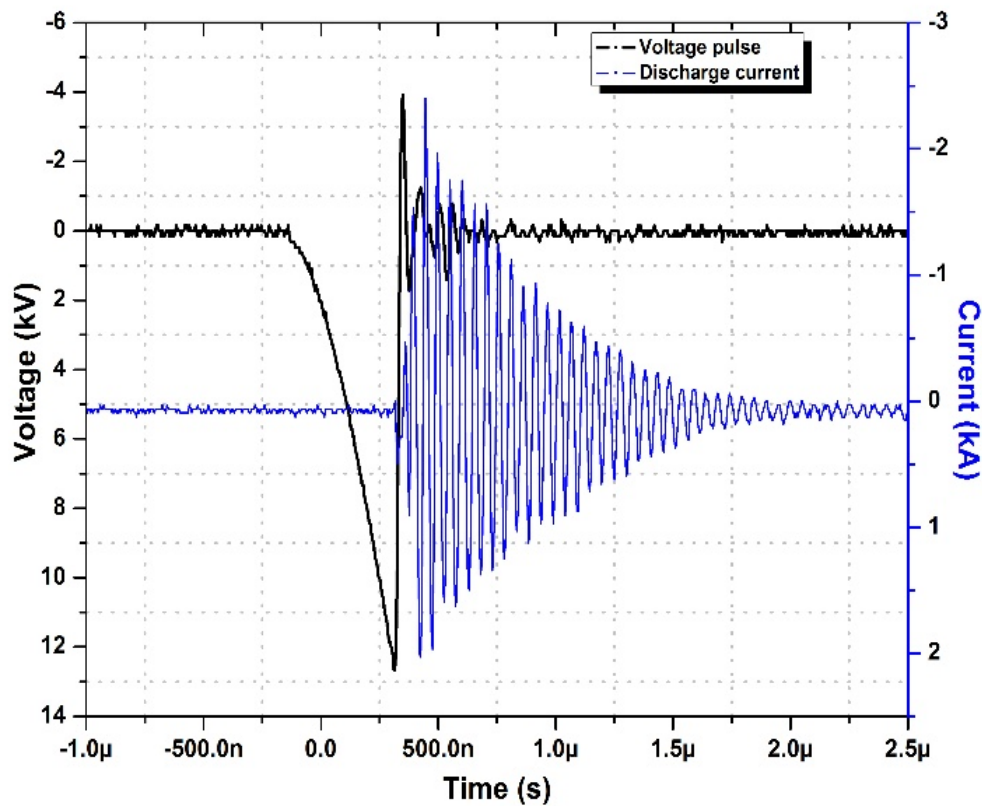


Figure 5.3. Typical waveforms of voltage pulse and discharge current

Immediately following the extinction of the pulse, the volume between two electrodes is filled with hot decaying plasma. Figure.5.2 shows that the density during the discharge period decreases due to the expansion as a result of the current heating, whereas the temperature of the gas increases. Once the discharge ceases, spark gap tries to come back to its pre breakdown status by dissipating the heat to the ambient gas and walls of the electrodes. Our simulation shows that the gap has recovered to its initial pre-discharge state in 58ms. Figure 5.4, shows the different time contours of the recovery process for gas density and temperature. It consists of 8 contours taken in the time sequence after the extinction of the spark energy. If the time reference $t=0$ was set at the beginning of the discharge, the contours were taken at $10\mu\text{s}$, $150\mu\text{s}$, 1ms and 50ms respectively. The electrodes are located at the sides of the contours where the profile of rogovsky shaped electrode can be seen.

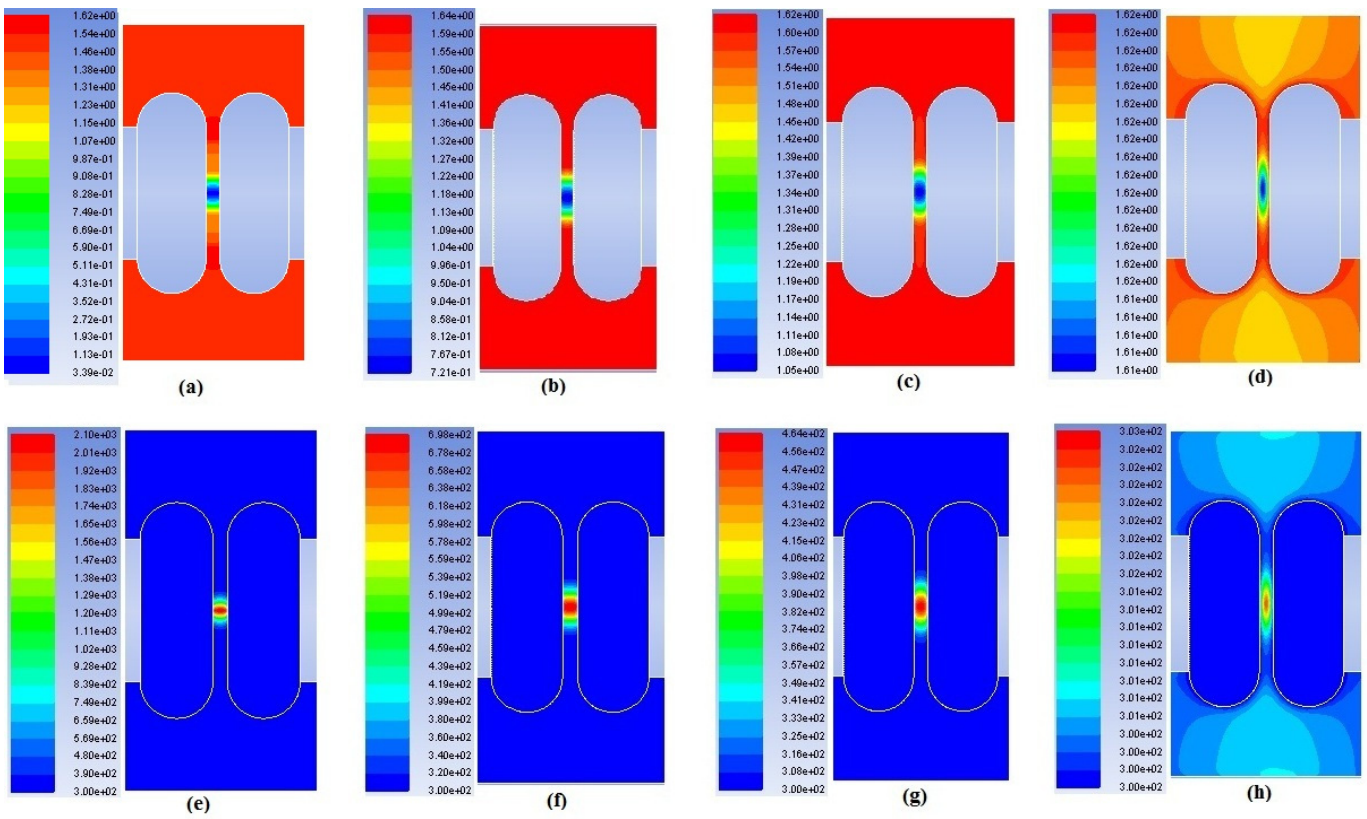


Figure 5.4. Simulation contours showing the recovery process of the gas density and temperature in a 2mm gap at 1atm pressure, (a) gas density at $t=10\mu\text{s}$, (b) gas density at $t=150\mu\text{s}$, (c) gas density at $t=1\text{ms}$, (d) gas density at $t=50\text{ms}$, (e) Temperature at $t=10\mu\text{s}$, (f) Temperature at $t=150\mu\text{s}$, (g) Temperature at $t=1\text{ms}$, (h) Temperature at $t=50\text{ms}$.

If we look carefully at the contours (a) to (d), we observe the density in the gap has recovered from 0.0339 kg/m^3 to 1.61 kg/m^3 , which is close to pre-breakdown density value of 1.62 kg/m^3 . The density profile in the gap tends to become circular as it recovers from the breakdown. It may be due to the reason that the deposited heat energy is removed from the gap mainly due to an axial heat flow through the metallic electrodes. The gas density profile along the spark channel length at different decay time is shown in figure 5.5. This shows the density is recovered at the walls of the electrodes quickly compare to the middle of the spark channel. This leads to a faster recovery of gas density for the shorter gaps compared to the long distance spark gaps. This supports the numerical results of Xinxin Wang [86].

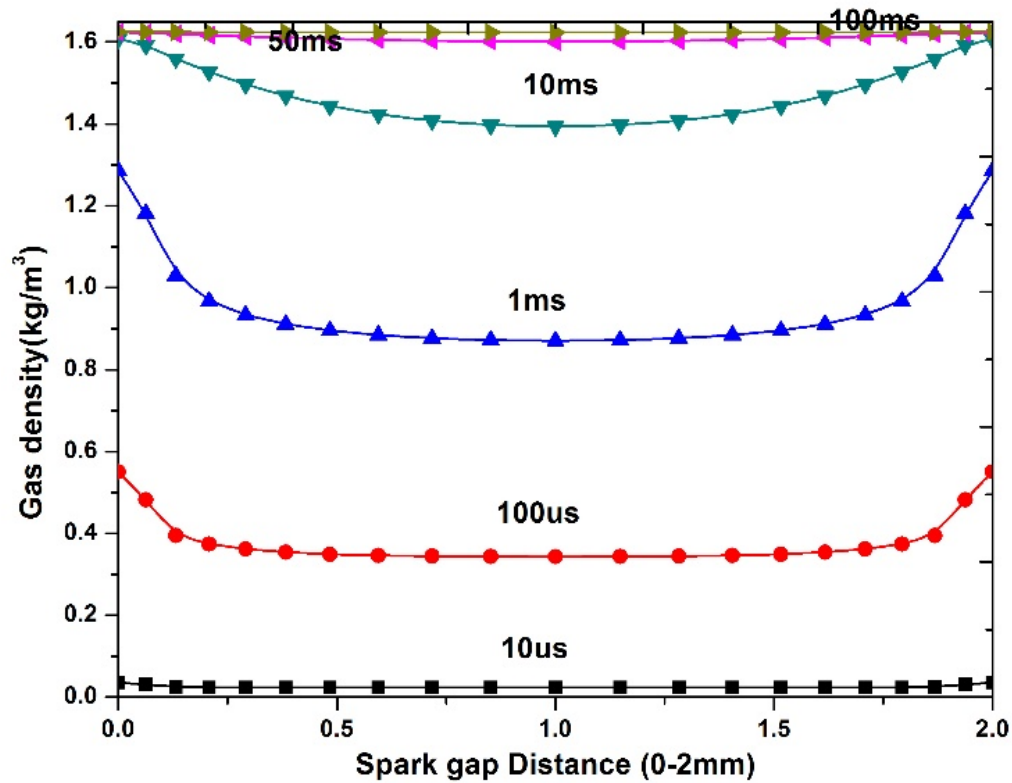


Figure 5.5. Variation of Argon gas density along the spark channel length for 10 μ s to 100ms.

It also shows, the rate of recovery is very quick immediately after the breakdown. We can also observe the gas density is completely recovered around 58ms in the gap. But the recovery voltage determined with double pulse experiment [105] is about 45% at 58ms.

It also shows, the rate of recovery is very quick immediately after the breakdown. We can also observe the gas density is completely recovered around 58ms in the gap. But the recovery voltage determined with double pulse experiment in chapter 4, is about 40% at 58ms.

This mechanism for delayed recovery of the ability to be over-volted was also observed by Xinjing Cai [60] for nitrogen gas. In his experiments, the nitrogen gas density recovery was investigate by using Mach-Zehnder interferometry and the hold off voltage of a spark gap after breakdown by two pulse method. The exact reason for this behaviour is not explained. It may be caused by some long-lived particles those can continuously produce sufficient amount of the electrons to initiate the second breakdown [106]. An attempt has been made to see the effect of gas pressure on the density recovery.

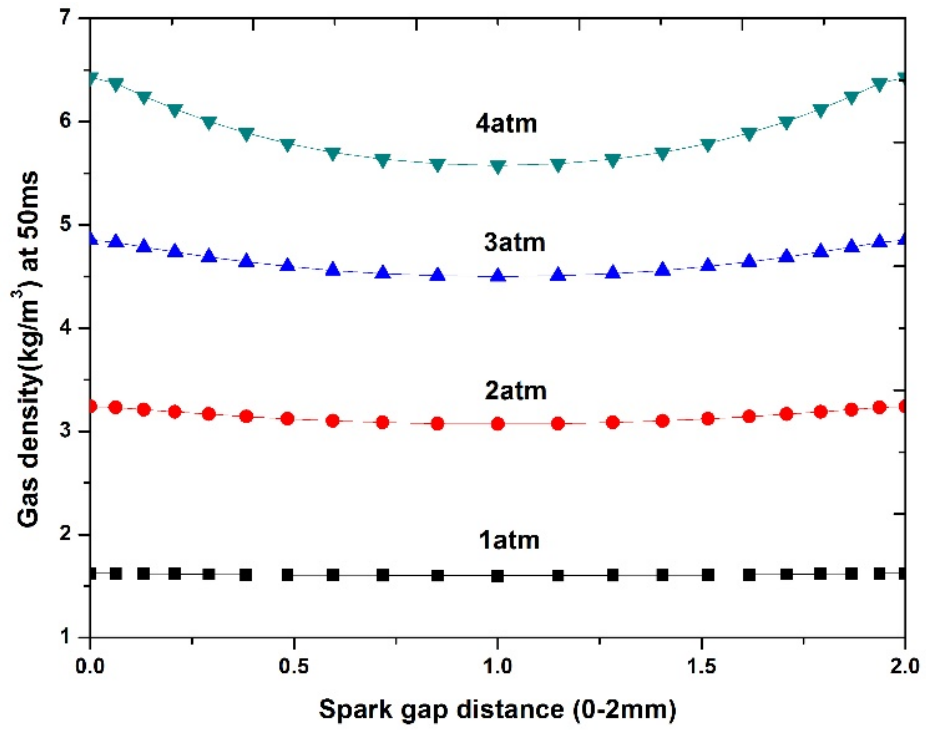


Figure 5.6. Variation of Argon gas density along the spark channel length for 1atm to 4atm pressure at 50ms simulation time

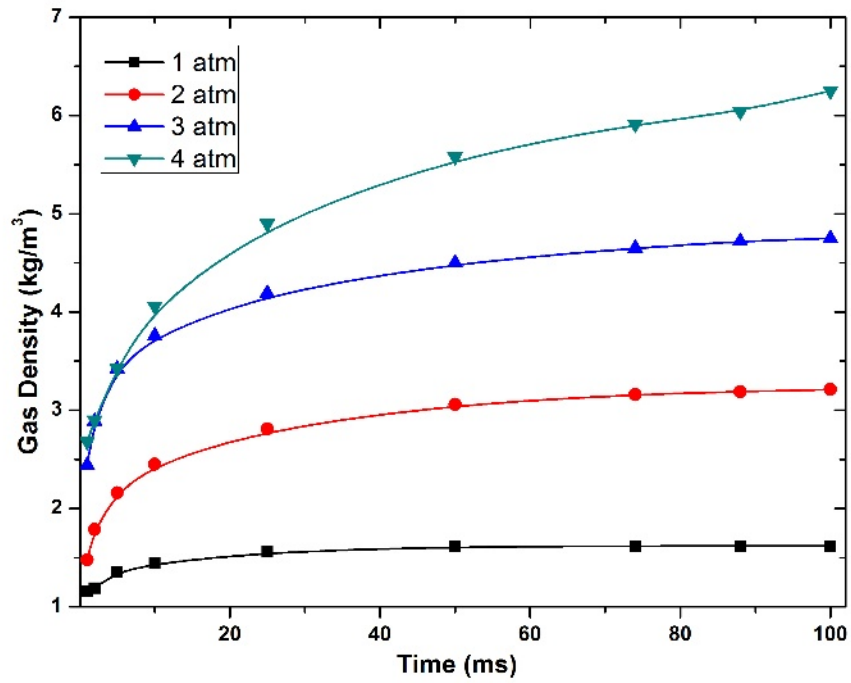


Figure 5.7. Variation of argon gas density with time for 1atm to 4 atm pressures at 1mm distance along the spark gap

Figure 5.6. Shows the variation of argon gas density along the spark channel length for 1atm to 4atm pressure at 50ms. This shows the rate of recovery of density has substantially improved with increase in pressure. This suggests that the high pressure spark gap will recover faster compared to low pressure spark gaps. Also, Figure 5.7 shows the gas density as a function of time for different Argon gas pressures along the spark gap. These results clearly indicate that the recovery of gas density is quicker in high pressure gas compared to low pressure.

5.4 Comparison of Neutral gas density recovery and Voltage Recovery

So, from the 2-D simulation model which was developed with same (2mm) gap, filled with argon gas, the recovery time of the gas density was obtained. The computations have been done by fluid code which uses a control volume discretization technique. The results show that the gas density of the gap has recovered in 58ms, where the over-voltage breakdown strength of the gap (measured by two-pulse technique) recovers to only 45% as shown in chapter 4. This may be due to some particles residing in the gap even after density recovery that can cause the second breakdown very quickly. The explanation as follows.

5.4.1 Explanation for faster gas density recovery time to voltage recovery time of spark gap

The neutral gas density R_N as a function of time was shown in Fig. 5.8. At the beginning, the gas density in the region centered on the spark channel was decreased to 29% of the initial pre discharge density (ρ_0) due to the expansion as a result of the current heating. As more and more heat is removed from the region, the gas density gradually recovers, approaching to its original value of density at $t=58$ ms. The experiment on the voltage recovery for the same gap was performed with two-pulse method and discussed in chapter 3 and 4. By varying delay time between pulses, the % voltage recovery ($\%R_{vb}$) was obtained for argon gas for comparison purpose is shown in Fig. 5.9. By comparing R_N and R_{vb} , the gap almost fully recovers its gas density at $t=58$ ms, it only recovers about 45% of its overvolted breakdown voltage.

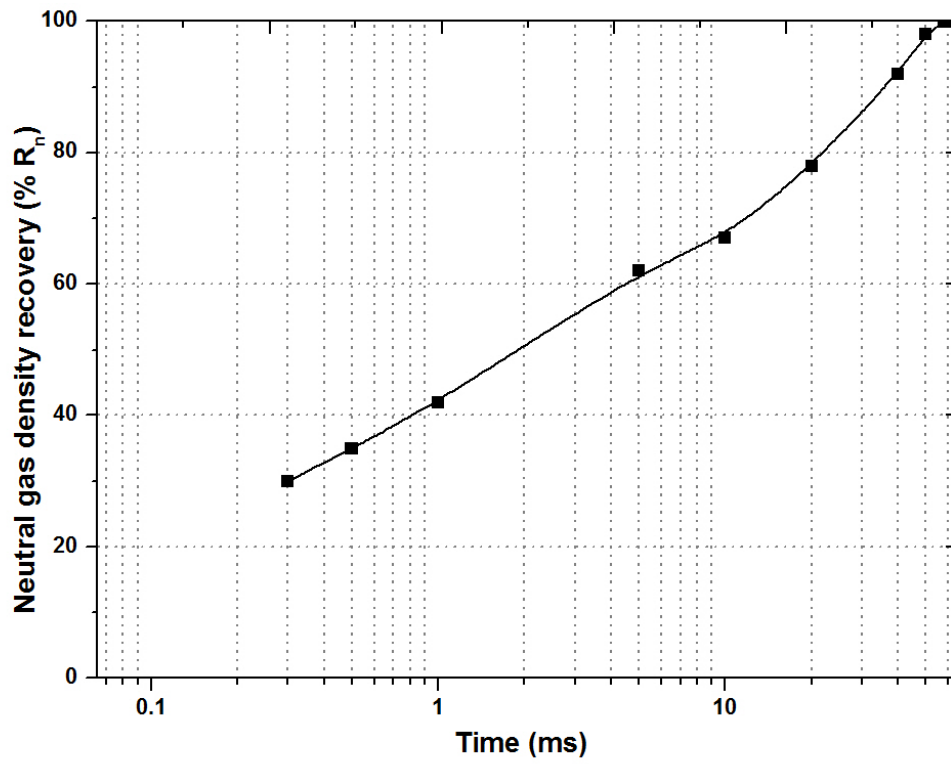


Figure 5.8 Neutral gas density recovery inside the gap

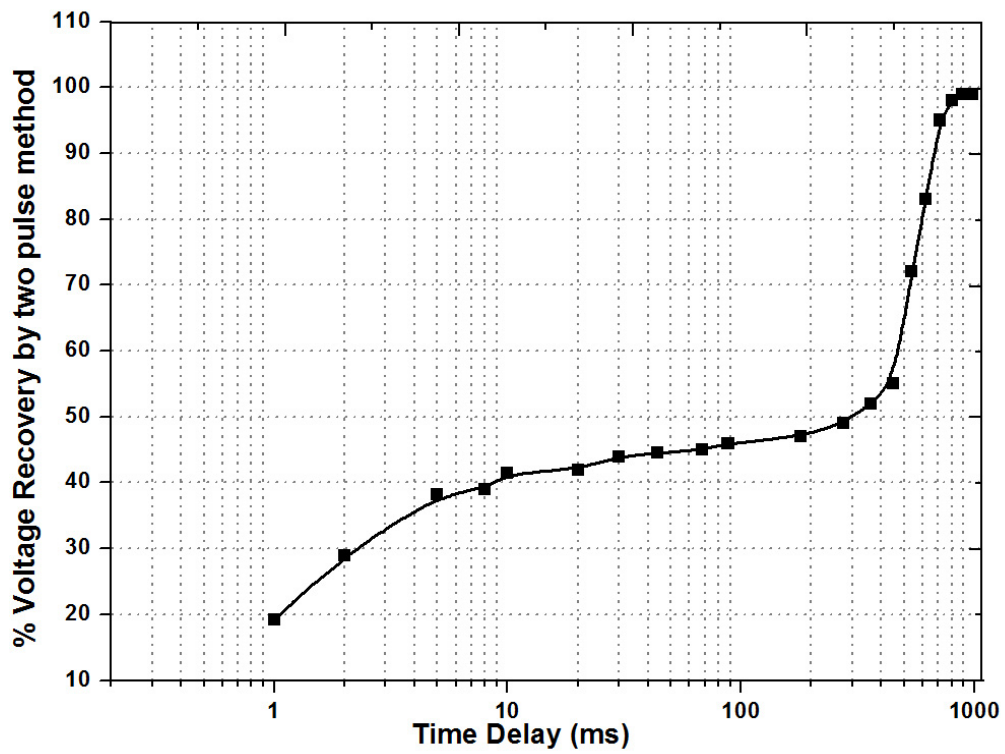


Figure 5.9 Voltage recovery of the gap

The processes governing the delay recovery of voltage was not fully clear, but we guess there may be long-lived particles that can continuously produce the electrons to quickly initiate the second breakdown. For Argon, the long-lived metastable atom is famous for producing electrons [107].

If we are right in our conjecture that the initial electrons are produced by the delayed recombination of the residual metastable atoms of Argon gas, the intermediate plateau, and the second rising edge on the R_{vb} curve can be explained as the following.

We know for breaking down of a gas gap, not only a sufficient high voltage (V_{b0}), but also sufficient long time t_d are needed.

$$V_b = V_{b0} + \frac{dV}{dt} \cdot t_d \quad (5.5)$$

Where, $t_d = t_s + t_f$

t_d is the total breakdown delay

t_s is statistic delay time

t_f is formative delay time

dV/dt is rise rate of applied voltage.

In the time duration of the intermediate plateau, Δt is relatively short from the first breakdown and more residual metastable atoms are survived. Therefore, at any moment there are always the electrons produced by penning effect of the metastable atoms for initiating the second breakdown. In this case, t_s can be considered close to 0. So, V_{b2} is expressed as:

$$V_b = V_{b0} + \frac{dV}{dt} \cdot t_f \quad \text{Since } t_s \approx 0. \quad (5.6)$$

For a given tested gap and a given applied voltage, t_f is almost constant, which makes V_{b2} a constant and a plateau on the R_{vb} curve. As the time elapses, the Δt becomes relatively longer in the time duration of the second rising edge. t_s is no longer considered close to zero, due to more and more residual atoms vanishing.

Longer and longer t_s are required for the second breakdown to happen, which leads to V_{b2} to rise again and the recovery of the over-volted breakdown voltage to begin.

5.4.2 Explanation of Voltage recovery curve pattern

Almost all of the voltage recovery curve shows an intermediate plateau. Figure 5.10 shows a typical % voltage recovery curve (R_{vb}) pattern. It has clearly 3 time phases. The explanation for different phases can be given as follows.

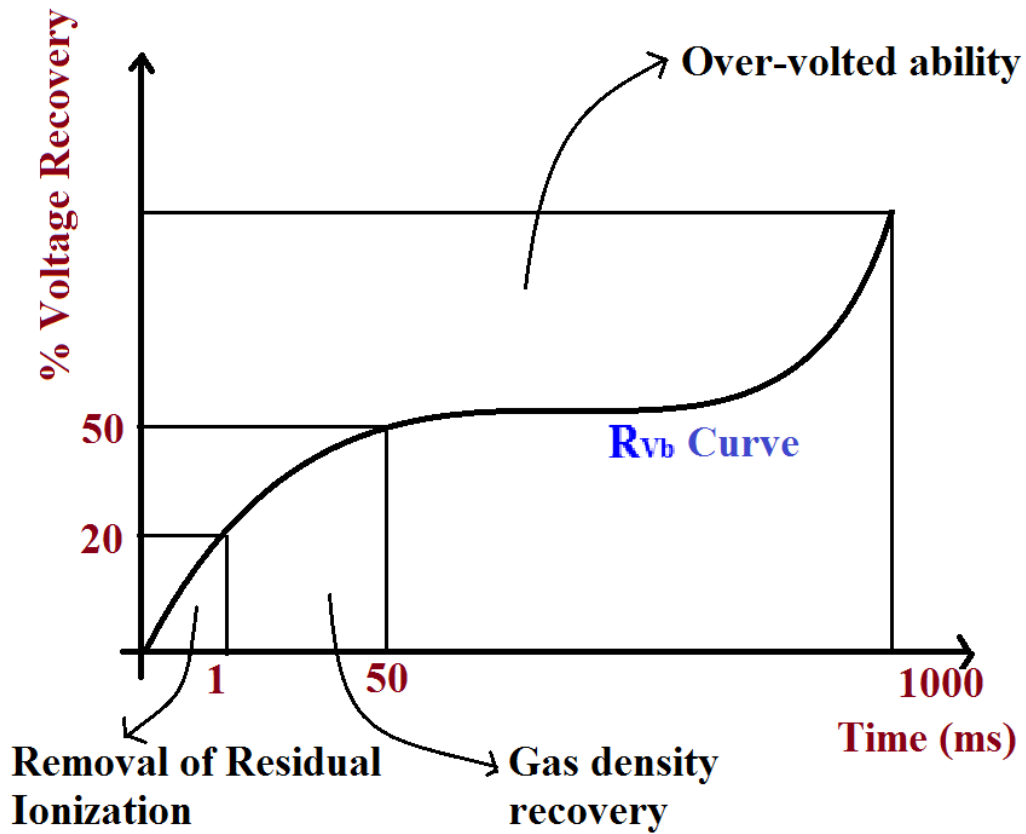


Figure. 5.10. Voltage recovery curve explanation

As we know, immediately after the extinction of an arc channel, the volume of the channel is filled with hot decaying plasma. Therefore, the gaseous recovery includes the recovery of the gas density and the electro-neutrality. The electro neutrality recovery is the removal from the gas any residual ionization by recombination, attachment, diffusion, and so on. So, the first phase is the de-ionization of the arc channel by recombination, attachment and diffusion etc. This takes for the gap less than 1ms and R_{vb} recovers

around 20%. The neutral gas density recovery is the removal from the gas the arc deposited energy in the form of heat by thermal conduction, convection, and radiation and it takes around 58ms. At this point the voltage recovers around 50% only. Later recovery attributes to over voltage capability of the spark gap. This 3rd recovery phase causes the long delay for the spark gap to recover to its full self-break down voltage level. Increasing the pressure also reduce the time required for 1 and 2 phases. We can improve the repetition rate by operating spark gap at reduced self-breakdown voltage by triggering at lower break down voltage. (We can reduce the time required for the plateau.). Table 5.1 above shows the possible operating frequencies that can be obtained by operating the spark gap at below self-break down voltage level.

Table: 5.1 possible operating frequency of spark gap switch

2 mm gap	Argon gas			Nitrogen gas		
	Pressure (atm)	Recovery time (ms)	Repetition rate (Hz)	Pressure (atm)	Recovery time (ms)	Repetition rate (Hz)
75% of the self-breakdown voltage	1	380	2.6	1	220	4.5
	2	200	5	2	150	6.6
	3	135	7.4	3	100	10
	4	90	11	4	88	11.3
50% of the self-breakdown voltage	1	180	5.5	1	90	11
	2	92	10.8	2	72	14
	3	45	22	3	30	34
	4	4	250	4	1.6	625
25% of the self-breakdown voltage	1	1.5	667	1	1.5	667
	2	1.5	667	2	1.4	715
	3	1.5	835	3	1.2	835
	4	1.2	835	4	1.1	900

5.5 Summery:

From all these computational study and comparison with the experimental data in chapter 4, a qualitatively consistent picture of the free recovery of spark gaps emerges. Typically gas density recovery to 100% occurs in 50ms whereas pulse breakdown voltage level of the spark gap reaches to 50% within 50ms. Recovery results from the gas density (temperature) returning to the ambient level. This pulse break down strength recovery delay may be caused by some long-lived particles (which are resulted from the initial discharge in the gap) those can continuously produce sufficient amount of the electrons to initiate the second breakdown. For the electro-negative gases, such as Sf_6 and air, the prolonged recovery of the latter phases was attributed to the residual negative ions that have relatively long-life times and can play an active role in the production of seed electrons for the second breakdown through the process of the collisional detachment. As for nitrogen that is not electronegative, we may suggest that the process governing the latter phases is related to the delayed recombination of the residual nitrogen atoms. The metastable molecules and the atoms of nitrogen are known for their ability to store energy over extended periods of time. The explanation based on the nitrogen atoms remaining from the previous discharge and recombining on the cathode to produce the initial electrons for the succeeding discharge was shown to be fully consistent with all the experimental data obtained in the afterglow experiments [108]. For Argon gas, the long-lived metastable atom is famous for producing electrons.

CHAPTER 6

RECOVERY ANALYSIS OF SPARK GAP BY ANODE TEMPERATURE DECAY METHOD

6.1 Introduction

The electrical breakdown and pre-breakdown characteristics of gases at atmospheric pressure and above, and at low pressures are widely investigated and there is reasonable agreement on the mechanism of growth of the current in the breakdown. But the recovery processes after the sparkgap breakdown are not studied extensively with short duration pulses. These are due to the present experimental voltage & current pulses having short durations which do not allow sufficient time for the metal surface to melt. The breakdown in the gap is initiated by breakdown of micro-projections on the cathode. The plasma produced acts as a source of electrons and results in breakdown of the gap due to gaseous discharge. There are two most common modes of discharges based on discharge current. In low current discharge, the anode is basically passive and acts as a collector of positive ions. In high current discharges, a fully developed anode spot is formed. The developments of anode spots have been studied extensively and the corresponding peak anode spot temperatures are listed in a Table 6-1[34, 49, 109 -115]. This anode spot has a temperature near atmospheric boiling temperature of anode material and is a source of metal vapors and ions. The formation of anode spot is preceded by anode foot-point, which is luminous but cooler than anode spot. The transition current value increases with increase in discharge frequency. The mechanism controlling the transition of vacuum diffuse arc into the anode spot depends upon the electrode geometry, the electrode material, current waveform and frequency / pulse width. The experimental conditions like magnetic constriction in the gap plasma, or anode material melting / evaporation can trigger the transition.

Table 6.1. Temperature of Anode spot/foot points.

SOURCE	METHOD	ANODE SPOT/ FOOTPOINT	MATERIAL/ WAVEFORM	TEMPERATURE
Nagesh et al [34,49]	Anode Temperature Decay Calculation	Anode Foot Point	SS/100ns pulse SS/100ns pulse SS/100ns pulse	2773K (H ₂ gas) 1570k (Ar gas) 1400k (D ₂ gas)
Frind et. Al [109]	Anode Temp. Decay/ Fast Photography	Anode Foot point Anode spot Anode spot Anode spot	Cu / 300μs pulse Cu / 300μs pulse Cu / 4500μs pulse Cu / 4500μs pulse	1797K (3*10 ⁵ W/cm ²) 3178K (1*10 ⁶ W/cm ²) 2888K (3*10 ⁵ W/cm ²) 3273K (1*10 ⁶ W/cm ²)
Gundersen [110]	High speed colour Photography	Anode Foot Point	Cu / DC	1370K
Mitchell [111]	Erosion Data Optical Comparision	Anode spot Anode spot	Cu/50Hz	<3230-3350K >2730-2800K
Klapas/Holmes [112]	1.5μm detector	Anode Foot point	Cu / DC	1360K(dull) 1570K(sharp)
Cobine and Burger [113]	Theoretical Erosion data	Anode spot Anode spot Anode spot	Al / 60Hz Cu / 60Hz Ni / 60Hz	2640K-3320K 2490-3040K 3040K-3650K
Grissom/Newton [114]	1.8-5.5μm detector	Anode spot Anode spot	Al/ μs pulse Cu/ μs pulse	2270-2700K 2900-3700K
Lyubinov et.al [115]	Optical Spectra	Anode spot	Al/ μs pulse	>2800K

The critical current required for anode spot formation varies from several hundred amperes at 100ms duration [116], to 740A, 30ms [109] to 1260A, 4ms [111]. The peak power densities on anode reported by Mesyats et.al. [117] are (i) 8×10^{11} W/m² for 1mm gap, 40 kV and 7.5×10^{12} W/m², 2mm gap, 30kV with current densities varying from 2.8×10^7 A/m², 36ns duration to 3.5×10^6 A/m², 72ns duration (copper electrodes). The plastic deformation (flow of metal under cold conditions) starts at power densities of 0.8 to 2.5×10^{11} W/m², for 5 to 80ns durations and 0.4 to 2mm gaps. The craters can be formed on anode at power densities of 1.2 to 4.0×10^{11}

W/m^2 resulting in anode temperatures of 1300K. The critical power densities at which melt zones could be observed is about $6 \times 10^{11} \text{ W/m}^2$ (20ns duration, 0.8mm gap) with an anode temperatures of 1800K at the end of the pulse. The specific energy introduced to the anode can be in excess of specific sublimation energy. This results in evaporation of electrode surface without melting in short duration pulses.

The experimental arc discharge times of Frind et.al [109] are $300\mu\text{s}$ and $4500\mu\text{s}$ and currents in the range of 250A to 12kA. Since the discharges are in vacuum having longer pulse durations with higher currents, the anode spot has been observed in this case. Hence the discharge is expected to consist mainly of metal vapors. The ionization potential (7.5V) is assumed to be equal to the anode drop. Rich & Farrall [118] has assumed that recovery pressure is equal to twice the gap spacing as mean free path in the recovery of circuit breakers. There is good agreement in some cases and large difference in others. Tsuruta & Ebara [69] has calculated the recovery of air gaps based on gas temperature decay with the assumption as the gas temperature reduces to 300K at full recovery from peak discharge temperatures of 2000-5000K. There is good agreement at gap spacing of 3mm but the calculated recovery time is lower for 1mm and higher for 7mm than the experimental value.

In the present case, the discharge in the gap rises the temperature of the electrode. Depending upon the pulse duration & energy of the applied pulse, the pressure and temperature will rise. When the peak power is low or higher duration pulses are applied, the discharge between electrodes produces arcs. This rises the temperature in the discharge column and pressure increases due to formation of plasma. This rise in temperature and pressure are governed by Clausius-Clapeyron equation. Here the electrode first melts and then vaporizes depending upon the energy dissipated in the arc. When the temperature is increased, the pressure will also rise to keep the working constant volume in equilibrium in steps. Generally anode spot is

formed in these cases with the anode drop of 7.5V. This type of behavior is expected in case of circuit breakers. But when the discharge in the gap is due to short duration pulses of high peak power discharges, the electrode does not melt at the discharge initiation point/ surface. The discharge initiating point / surface of electrode will vaporize and gets ionized. Generally anode foot points are formed in these cases with the anode drop in the range of 10-60V depending upon the operating pressure. In our calculations, it is assumed that anode foot-points can be formed as per [109], [110]. These have low temperatures compared to anode spots. Electrode surface evaporates due to discharge current in the gap depending upon the energy transferred to anode. The recovery process depends upon the metal vapor ejected from the electrode due to temperature rise of anode. The metal vapor decreases the pressure in the gap that reduces the breakdown voltage of the gap.

Presently there are no methods ideally suitable for calculation of recovery times of sparkgaps. However an attempt has been made to analyze the recovery times of sparkgaps by anode temperature rise and decay method. This chapter discusses two methods by which the surface temperature of anode can be measured for the estimation of recovery time during pulse period and after pulse extinction. The first method presents a theoretical model in which, a transient heat flow equation is solved to calculate the surface temperature based on the input flux density. The heat flux is calculated for a 10 μ s pulse width, 30 kA pulse and is applied to the copper and stainless steel anodes. The second part presents a computational model developed in FEM based software to compute the temperature decay. Simulations have been carried out for different materials including Cu and SS.

6.2. Theoretical Analysis

The temperature is an important factor in the recovery process of the spark gap switch. The anode surface temperature is calculated based on the input heat-flux density to the anode

surface and heat-decay mechanisms for different anode materials. To see the anode temperature rise and decay, a transient heat flow equation has been sought out for a semi-infinite solid. The differential equation for the temperature distribution $t(x, \tau)$, for the surface temperature of a semi-infinite solid lowered from t_i to t_0 , is

$$\frac{\partial^2 t(x, \tau)}{\partial x^2} = \frac{1}{\alpha} \frac{\partial t(x, \tau)}{\partial \tau} \quad (6.1)$$

Where, t = temperature (K)

τ = time (s)

α = thermal diffusivity (cm^2/s).

By applying Laplace transformation, the above differential equation becomes,

$$sT(x, s) - f(x) = \alpha \frac{d^2 T(x, s)}{dx^2} \quad (6.2)$$

Where, $L [t(x, \tau)] = \int_0^{\infty} t(x, \tau) e^{-s\tau} d\tau = T(x, s)$

Thus, differential partial equation (6.1) for the inverted transform of the function $t(x, \tau)$ turns into an ordinary differential equation for the transform $T(x, s)$, since $T(x, s)$ does not depend on τ .

Now introducing the special condition that the temperature of the body before cooling is the same everywhere and equal to t_i , (i.e., $f(x) = t_i = \text{constant}$).

$$\frac{d^2 T(x, s)}{dx^2} - \frac{s}{\alpha} [T(x, s) + (\frac{t_i}{\alpha})] = 0 \quad (6.3)$$

A general solution of this differential equation may be written as,

$$T(x, s) - \frac{t_i}{s} = A_1 \exp[\sqrt{\frac{s}{\alpha}} x] + B_1 \exp[-\sqrt{\frac{s}{\alpha}} x] \quad (6.4)$$

Where, A_1 and B_1 are constants to be determined by the boundary conditions. Using the Laplace transformation for the boundary conditions,

$$L [t(0, \tau)] = 0, \quad T(0, s) = 0 \quad (6.5)$$

$$L \left[\frac{\partial t(\infty, \tau)}{\partial x} \right] = 0, \quad \frac{dT}{dx}(\infty, s) = 0 \quad (6.6)$$

From final condition, it follows that $A_1 = 0$ and $B_1 = -\frac{t_i}{s}$, and solution written as

$$\frac{t_i}{s} - T(x, s) = \frac{t_i}{s} \exp \left[-\sqrt{\frac{s}{\alpha}} x \right] \quad (6.7)$$

By using the inverse transforms,

$$L^{-1} \left[\left(\frac{1}{s} \right) \exp[-k\sqrt{s}] \right] = 1 - \operatorname{erf} \left(\frac{k}{2\sqrt{\tau}} \right) \quad (6.8)$$

In our problem $k = \frac{x}{\sqrt{\alpha}}$, and if the initial temperature is uniformly distributed over the anode

length, then the equation becomes,

$$\frac{t(x, \tau) - t_0}{t_i - t_0} = \operatorname{erf} \left(\frac{x}{2\sqrt{\alpha\tau}} \right) \quad (6.9)$$

Where $\operatorname{erf}(x/(2\sqrt{\alpha\tau}))$ is a Gauss error function and is defined as,

$$\operatorname{erf} \left(\frac{x}{2\sqrt{\alpha\tau}} \right) = \frac{2}{\sqrt{\pi}} \cdot \int_0^{\frac{x}{2\sqrt{\alpha\tau}}} e^{-\eta^2} d\eta \quad (6.10)$$

Performing the partial differentiation, gives,

$$\frac{\partial t}{\partial x} = \frac{t_i - t_0}{\sqrt{\alpha\tau\pi}} \cdot e^{-\left(\frac{x^2}{4\alpha\tau}\right)} \quad (6.11)$$

For a short, instantaneous pulse having specific heat flux S applied to a body, which is having zero initial temperature, then the resulting temperature rise is,

$$T_r = \frac{0.239 S \Delta \tau}{\rho c \sqrt{\pi \alpha \tau}} \cdot e^{-\left(\frac{x^2}{4\alpha\tau}\right)} \quad (6.12)$$

Where, T_r = Rise in temperature.

S = specific heat flux from the arc to the surface.

$\Delta \tau$ = pulse time interval in sec.

ρ = density.

c = specific heat.

α = thermal diffusivity.

τ = time since heat pulse is applied.

x = depth in the solid body.

(The factor 0.239 allows specific heat flux to be in watts)

The specific heat flux can be calculated by the formula of Burger and Cobine (113).

$$P_a = Ja (V_a + \phi + V_T) + P_n + P_r] \text{ watts /m}^2 \dots\dots\dots (6.13)$$

Where, P_a = Specific heat flux in watts /m²

P_n = Neutral atom energy = 0.13x 10⁸ watts /m² for temperatures <6273K

= for temperatures of \approx 15273K it can be neglected (completely ionized).

P_r = Radiant energy density = 0.75x10⁸ watts /m² (for temperatures of <6273K)

= 3x10⁹ watts /m² (for temperatures of >15273K)

J_a = Anode current density A/m²

V_T = Electron thermal energy = 1eV for 6000K and 2eV for 15000K

ϕ = Work function of the electrode, \approx 4.5 volts for most metals.

V_a = anode drop.

The anode voltage drops are calculated based on Ref. (119). In the present work, the metal surface has been assumed to vaporize within the pulse duration due to high peak power density. Hence the discharge is assumed to be predominately gas discharge and for calculation of anode temperature rise, anode drop is assumed to be gas discharge anode drop. The anode drop depends upon the gap pressures. The general trend is it increases with reduction in pressure. The anode drop data are not available for all the present experimental pressures. The range of anode drops for various discharges varies from 10V to 60V, depending upon the

conditions of the discharge. The recovery times are calculated based on the reported data of anode drops.

For finding the current density (J_a), Two new set of spark gaps were taken and thoroughly polished and cleaned. Then they are conditioned in situ by discharging micro ampere current through electrodes till it reaches the current reduces to minimum for that voltage. Then without touching the electrode surface, checked for the surface of electrode by microscope for the pitting. Noted down the largest size of pitting. This is usually very small in microns. Then we have taken only one shot in our experimental setup with maximum current for that gas or electrodes. For other electrodes the procedure was repeated and measured the arc spot diameter. Using this area, the current density has been calculated from the references (120, 118). So, corresponding to the spot diameter and anode voltage drop, the heat flux applied to the anode electrode works out to be $5.82 \times 10^{11} \text{w/m}^2$.

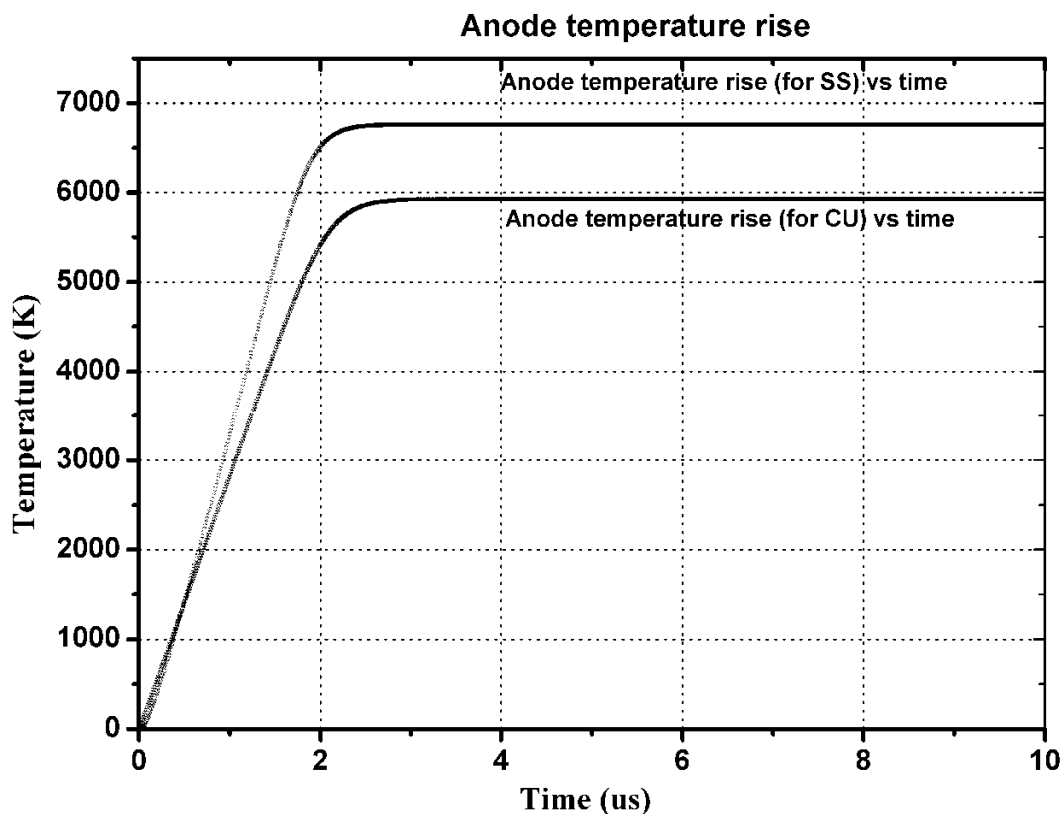


Figure .6.1 Anode temperature rise for copper and stainless steel materials

So, by using the above formulae and values, the anode temperature rise for copper and stainless steel materials for a heat flux of 5.82×10^{11} w/m² were calculated and shown in Figure 6.1. Anode temperature will reach equilibrium value which is determined by the temperature at which, energy losses due to vaporization from the anode surface become equal to the energy input to the anode. This value of equilibrium temperature is less for Cu anodes compare to Stainless steel anodes for applied heat flux. The parameters for Copper and Stainless steel at atmospheric condition are shown in Table 6.2 [122]-[123].

Table 6.2. Thermal data for Cu and Stainless Steel materials

Parameters	Copper	Stainless Steel
Specific heat flux in W/cm ²	5.82×10^7	5.82×10^7
Density in gram/cm ³	8.92	7.85
Specific heat in Cal/gram-K	0.0923	0.38
Thermal diffusivity in cm ² sec	1.12	0.042

The temperature of the anode reduces to pre-breakdown temperature as the applied pulse ceases. This decay is due to vaporization of electrode during the initial period as well as cooling of the electrode. This temperature decay at the surface and at specific points within the contact material can be calculated using the equation of [109]

$$T_d = \frac{0.239 (S - WE(T)) \Delta \tau}{\rho c \sqrt{\pi \alpha \tau}} \cdot e^{-\left(\frac{x^2}{4\alpha \tau}\right)} \quad (6.14)$$

Where, WE (T) is an empirical relation for anode temperature decay flux of the vaporization in time $\Delta \tau$ and the values are taken from [124] and modified for atmospheric pressure conditions as follows.

$$\begin{aligned} WE(T) &= 16200 [T / 2595]^{9.91} \text{ for copper electrodes} \\ &= 19970 [T / 2960]^{10.5} \text{ for stainless steel electrodes} \end{aligned}$$

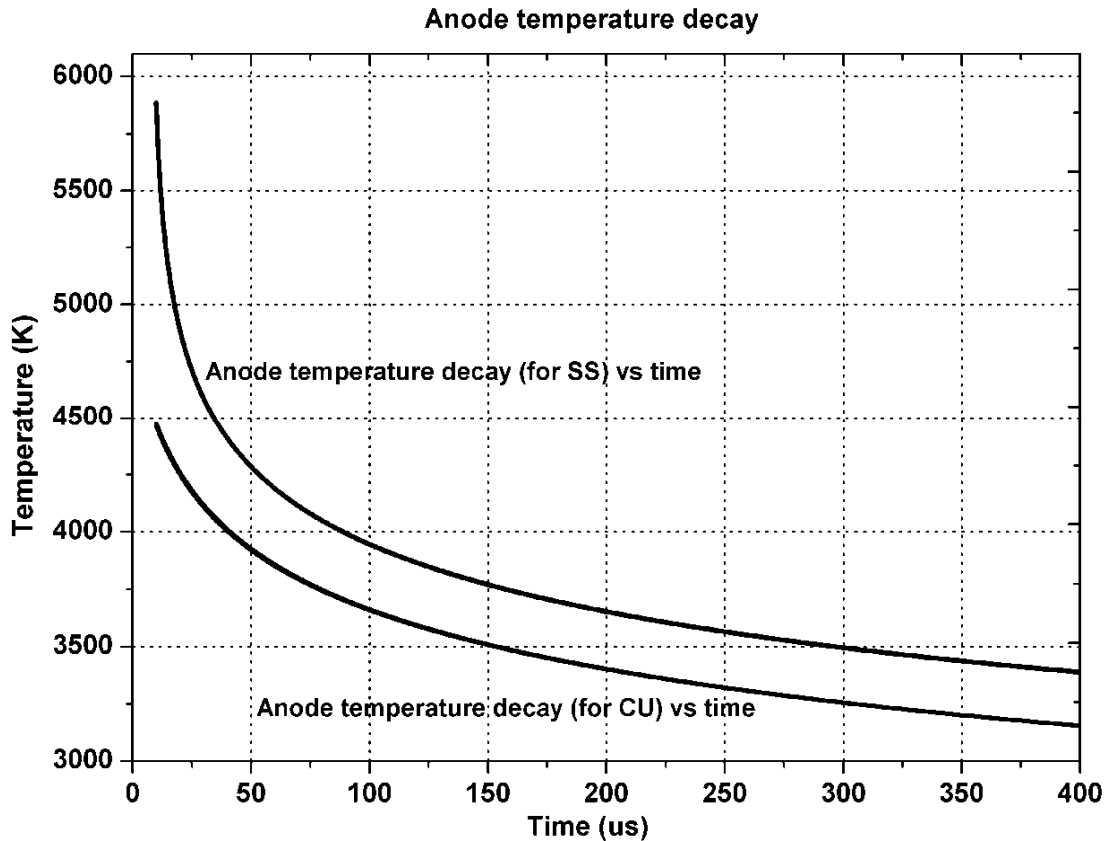


Figure.6.2 Anode temperature Decay for copper and stainless steel materials

Once the anode temperature decayed to their respective vaporization temperature, the spark gap has assumed to be recovered. The vaporization temperature for copper and stainless steel at atmospheric conditions are 2868K and 3233K respectively. Figure.6.2 shows the anode temperature decay for copper and stainless steel materials. The temperature decay is exponential for temperatures greater than 3273K for Cu and 3773K for SS. This changes from exponential to linear and become invariant for temperatures less than 3273K for Cu and 3773K for SS. The initial exponential decay is due to metal vaporization and after this decay is due to only cooling of anode. The decay time to vaporization temperature is around 300 μ s and is closely matching with the experimental results of G. Frind. In his measurements, recovery time increases slowly and reaches 40 μ s at 4 kA. Then the curve attains a value of 630 μ s for 12 kA current.

6.3. Spark gap temperature decay Model by FEM based simulations

A heat transient simulation model is developed using FEM based software (COMSOL Multiphysics) to study the temperature decay in copper, stainless steel, silver, tungsten and graphite materials. COMSOL Multiphysics is a finite element analysis, solver and Simulation software for various physics and engineering applications, especially coupled phenomena, or Multiphysics. In addition to conventional physics-based user interfaces, COMSOL Multiphysics also allows for entering coupled systems of partial differential equations (PDEs). The approach starts with first principles like transport phenomena, electromagnetic field theory, and solid mechanics as the basic fibers of the software. Then, in an elegant and flexible user interface, these fibers can be weaved together in a self-consistent way to solve particular simulation needs. With COMSOL Multiphysics conventional models for one type of physics can be extended into Multiphysics models that solve coupled physics phenomena—and do so simultaneously. It is a flexible platform that allows users to model all relevant physical aspects of their designs. For instance in nature electricity is always accompanied by some thermal effect; the two are fully compatible. Enforcing compatibility guarantees consistent Multiphysics models and the knowledge that we never have to worry about creating a disconnected model again. If we find ourselves in need of including another physical effect, we can just add it. If one of the inputs to our model requires a formula, we can just enter it. Using tools like parameterized geometry, interactive meshing and custom solver sequences, we can quickly adapt to the ebbs and flows of our requirements. Using these physics interfaces, we can perform various types of studies including: –Stationary and time-dependent (transient) studies –Linear and nonlinear studies –Eigen frequency, modal, and frequency response studies when solving the models, COMSOL Multiphysics uses the proven finite element method (FEM). The software runs the finite element analysis together with adaptive meshing (if selected) and error control using a variety of numerical solvers.

COMSOL Multiphysics creates sequences to record all steps that create the geometry, mesh, studies and solver settings, and visualization and results presentation. Partial differential equations (PDEs) form the basis for the laws of science and provide the foundation for modeling a wide range of scientific and engineering phenomena.

An attempt has been made to develop a temperature decay model in three dimensions. This model gives the feasibility of estimating the decay time of deferent materials which are provided in the library. The total recovery time is not possible to estimate by the anode temperature decay method for temperatures less than vaporization temperature. The temperature decay model of the switch following the equations below:

$$\rho C_p \frac{\partial T}{\partial t} + \rho C_p \mathbf{u}_{trans} \cdot \nabla T = \nabla \cdot (K \nabla T) + Q \quad (6.15)$$

$$-n \cdot (-K \nabla T) = h \cdot (T_{ext} - T) \quad (6.16)$$

$$-n \cdot (-K \nabla T) = \varepsilon \sigma (T_{amb}^4 - T^4) \quad (6.17)$$

Where, K = Thermal conductivity (W/m-K)

P = Density (kg/m³)

C_p= Heat capacity at constant pressure (J/kg-K)

h = Heat transfer co-efficient (W/m²-K)

T_{ext}= External temperature (K)

ε = Surface emissivity

T_{amb}= Ambient temperature (K).

Equation (6.15) is Heat transfer equation in solids; (6.16) is convective cooling equation; (6.17) is surface to ambient radiation equation. Physics controlled and very fine meshing is used in the simulation. The simulated geometry is shown in Figure 6.3. The spark gap chamber dimensions used in the simulations are length-160 mm, hight-80 mm and depth-80 mm. The electrode materials used are copper, stainless steel, silver, graphite and tungsten.

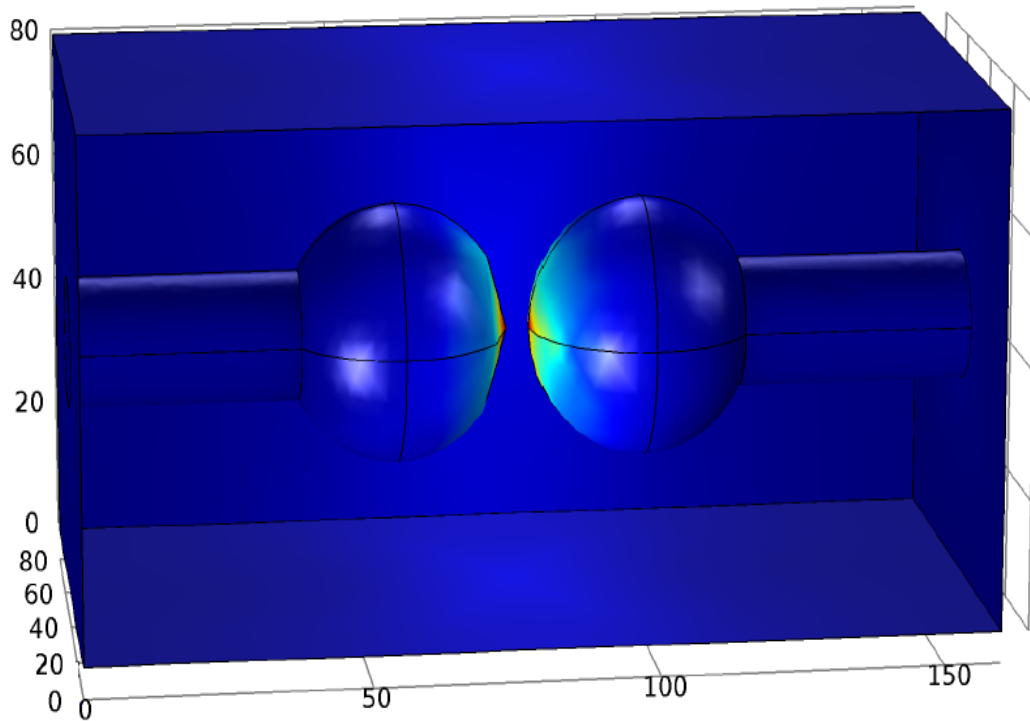


Figure .6.3. Simulated geometry of spark gap.

In this work, we used the software to see the temperature decay time of the electrodes after spark gap breakdown. The heat input to the electrodes was given as specific heat flux to the corresponding current pulses of 5 kA, 10 kA, 15 kA, 20 kA, 25 kA and 30 kA are calculated by the equation 6.13 and applied to the surface of the anode. These specific heat fluxes was calculated based on the current and spot diameters taken from the reference (120, 118). The time to decay the electrode temperature to room temperature is estimated for different materials and compared with the literature.

The specific heat flux data for different current ranges are listed in Table.6.3. The simulation decay curve is linear compared to the theoretical model curve, because the simulation does not consider the initial temperature decay due to metal vaporization. Since actual spark gap recovery involves electrodes as well as gas temperature recovery, the obtained recovery time may differ with the experimental values which consist of both the electrode and the gas temperature recovery.

Table 6.3. Specific heat flux data for different current range

Current in kA	Specific heat flux in W/cm ²
5	0.9776*10 ⁷
10	1.9463*10 ⁷
15	2.91*10 ⁷
20	3.88*10 ⁷
25	4.8525*10 ⁷
30	5.82*10 ⁷

6.4. Simulation Results and analysis

The decay time is an important parameter of the spark gap switches used in repetitive pulse power systems. The time taken for the spark gap to recover to its original pre-breakdown status before application of next pulse is called the full decay (100%) time. In our case, the time taken by the spark gap electrodes to reduce its temperature to initial value (300K) is taken as full decay or recovery time of spark gap. Analyzing the temperature decay of copper, stainless steel, tungsten, silver and graphite, it is observed that faster decay in temperature occurs in tungsten followed by stainless steel. However, graphite seems to have a slower fall of temperature because of the higher heat capacity at constant pressure (C_p) compared to all other materials. This effects the life time in case of repetitive operations. Copper and silver show a similar variation in temperature decay characteristics, because of their thermal conductivity values are very close to each other. (Copper-400 W/m-K and silver-429 W/m-K). Temperature decay curves for copper, stainless steel, silver, tungsten and graphite for 30 kA pulse are shown in Figure 6.4. For copper the decay time is more for 30 kA as compared to other values of current. This may be due to higher temperature rise during the breakdown compared to the other lesser value current pulses.

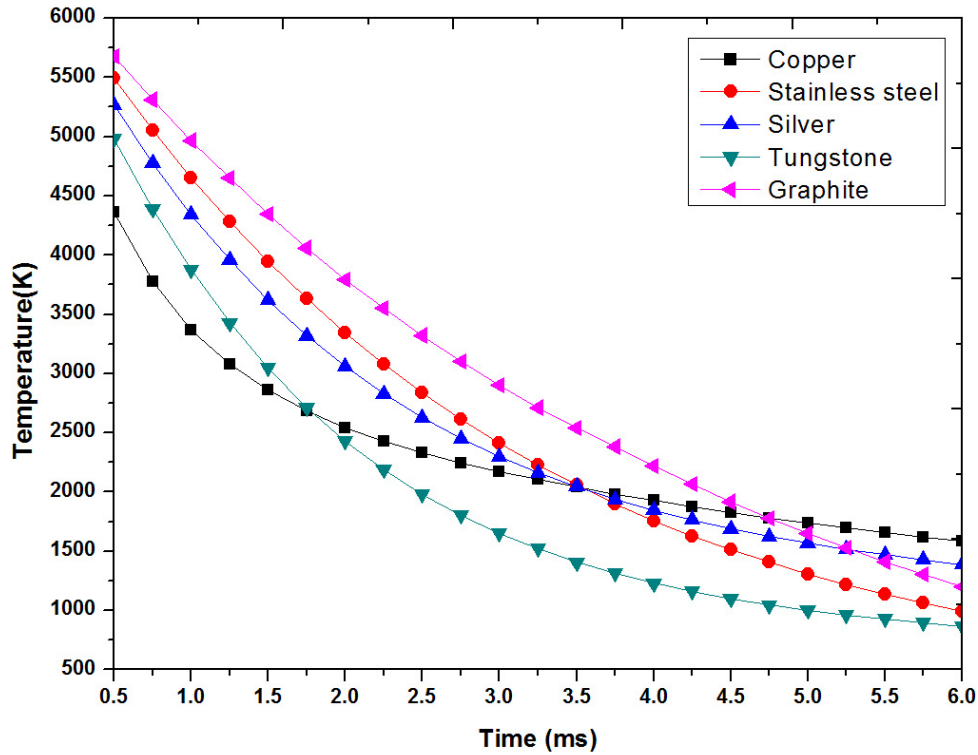


Figure. 6.4 Temperature decay curves for copper stainless steel, silver, tungsten and Graphite for 30 kA pulse.

This high temperature requires more time to recover to its initial state. A higher value of specific heat flux causes increase in temperature difference of the material for repetitive operation. This enhancement in temperature difference leads to reduction in switching frequency and hence unsuitable for high frequency operation. Temperature decay curves of copper for 5 kA, 10 kA, 15 kA, 20 kA, 25 kA and 30 kA current pulses are shown in Figure 6.5. This surface temperature decay measurement of anode is also essential for understanding the recovery of dielectric strength in vacuum interrupts. Edgar Dullini [56] has measured the decay of anode temperature after interruption of high current arcs. In his experiments, the anode temperature decays to 1600 K in 4ms for a current pulse of 7 kA. This decay time is around 4.15ms in our simulation results.

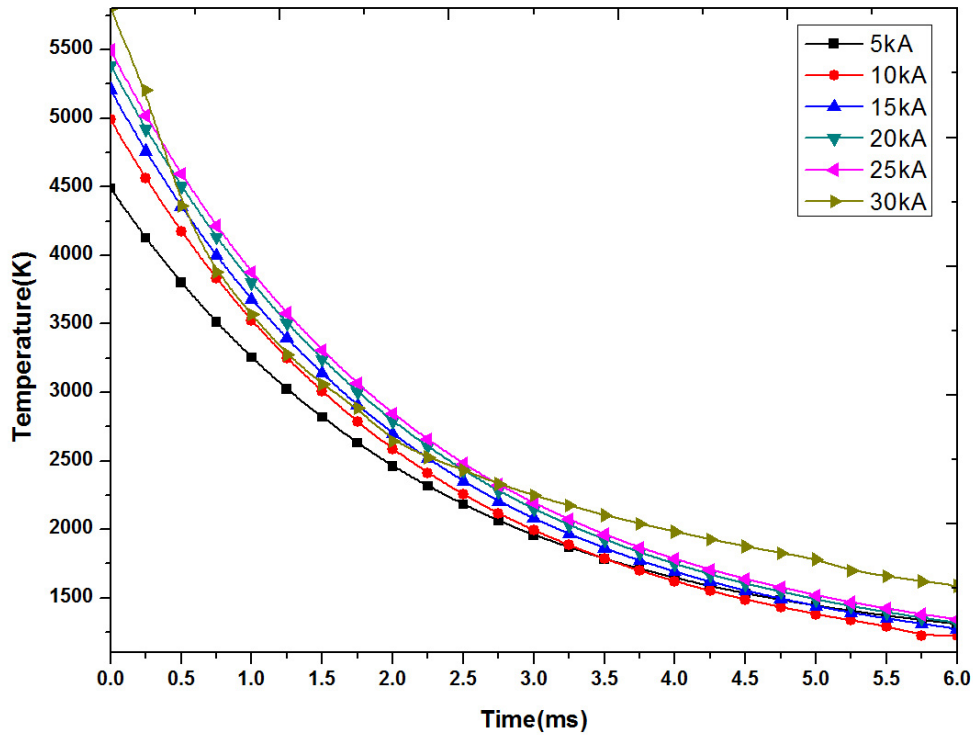


Figure 6.5 Temperature decay curves of copper for different current pulses.

The decay rate of stainless steel is more compared to copper except for 30 kA, where an anomalous behavior is observed in case of copper. The heat flux corresponds to the 30 kA discharge current, transfers a great amount of thermal energy into the electrodes. This may be reason this behavior. Our simulation shows a significant variation in the recovery time of the copper and stainless steel electrodes. SS has a decay of 6500 K to 1000K in 6ms and copper having 5500 K to 1000 K in 6ms. Also, we observe very high difference in the decay rate for a simulation time corresponds to 300 K temperature. The variation of decay temperature with time is independent of current in case of stainless steel, making it useful for high current operation, without the need of additional cooling arrangement. Temperature decay curves of stainless steel for 5 kA, 10 kA, 15 kA, 20 kA, 25 kA and 30 kA current pulses are shown in Figure 6.6.

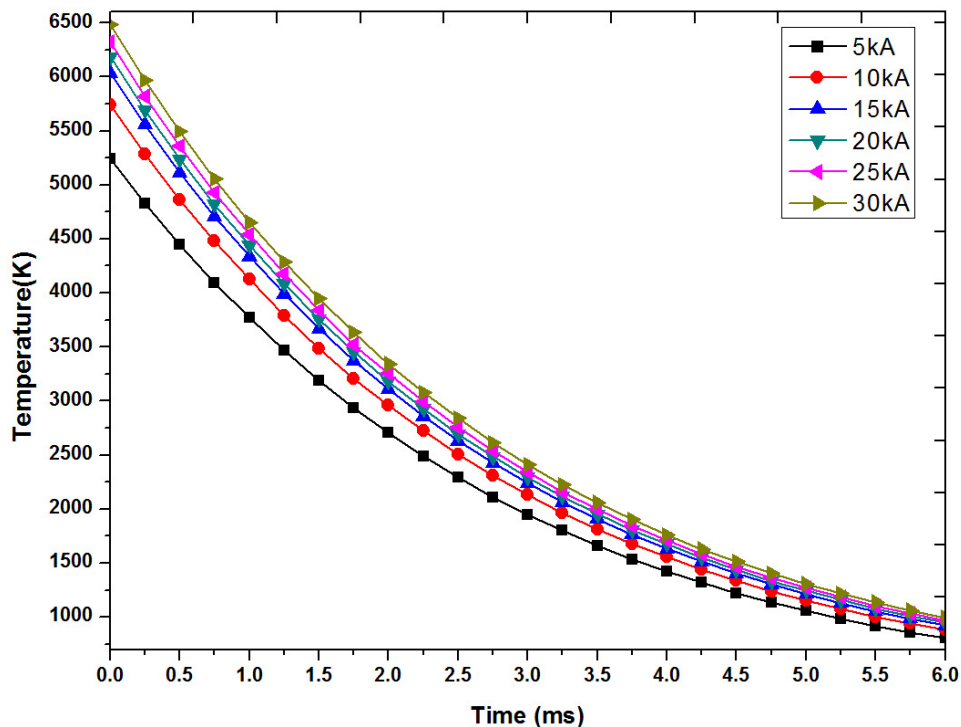


Figure 6.6 Temperature decay curves of stainless steel for different current pulses.

The spark gap switches used in repetitive pulse power systems, decides the operating frequency of the total system. Faster recovery switches increases the repetition rate of the systems. One of the key parameter that affects the recovery is the temperature decay of the spark gap electrodes. This simulation mainly concentrates on the time taken by different electrodes materials to decay their heat to its initial temperature value (i.e., value before applying the current pulse). This decay time corresponds to the recovery time of the spark gap. Also, to explain the total temperature recovery time, Figure 6.7 was drawn for stainless steel electrode materials with different discharge currents. For a 30kA current pulse the complete recovery time of S.S spark gap is around 19ms. Also, the simulations show a faster recovery in tungsten followed by SS. Copper and silver shows a similar decay profile, whereas graphite spark gaps have lowest repetitive rate compared to all materials used in the simulations. All these results presented in this chapter was presented and published (87, 125).

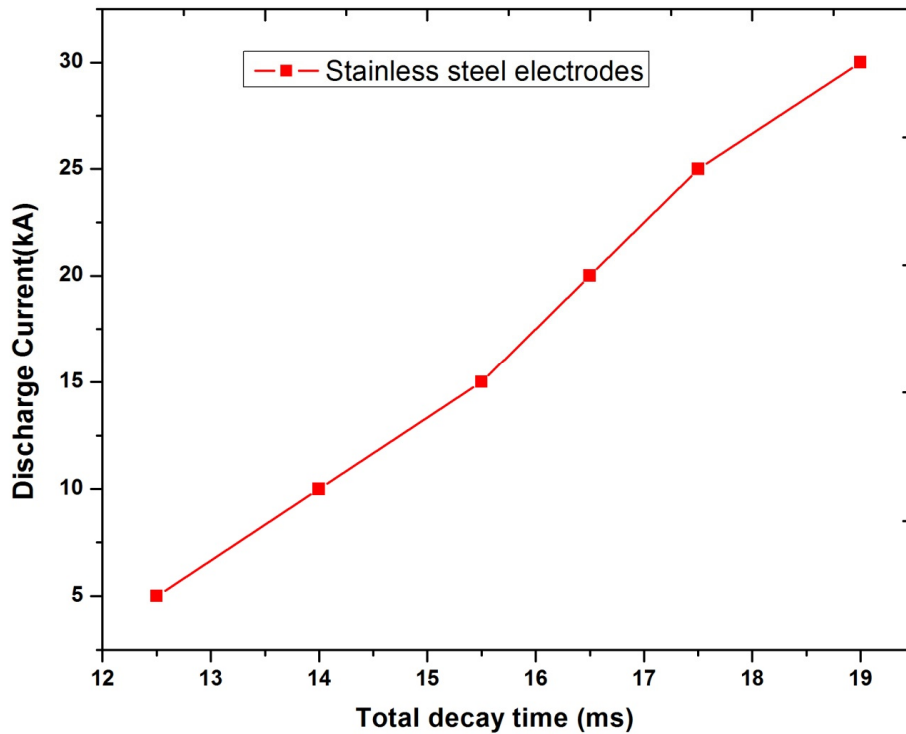


Figure 6.7 Total temperature decay time curves of stainless steel for different discharge current pulses.

6.5 Summery:

A theoretical method is presented to estimate the recovery time of spark gap by estimating the anode surface temperature. The time required for electrode to reach the ambient temperature was estimated with this method to analyze the recovery of the spark gap. The calculation shows stainless steel spark gaps having higher temperature rise compared to copper for 30 kA current pulse. The decay time is around $300\mu\text{s}$ and is closely matching with the experimental results. A 3 dimensional computational model was also developed to see the effect of anode temperature decay on the recovery of spark gap. Different electrode materials are also tried in the simulations other than the copper and stainless steel. Simulations shows a faster recovery in tungsten followed by SS. Copper and silver shows a similar decay profile. However graphite spark gaps have lowest repetitive rate.

CHAPTER 7

SUMMARY AND FUTURE PERSPECTIVE

The fundamental study is on the recovery characteristics high pressure gas spark gap which directly determines the pulse repetitive frequency of the pulse power system. The following conclusions were made on the above studies:

1. A pulse transformer based double pulse generator capable of generating 40 kV peak pulses with rise time of 300ns and 1.5 μ s FWHM and with a delay of 1ms -1s was developed. A matrix transformer topology is used to get fast rise times by reducing $LiCa$ product in the circuit. A sparkgap chamber of which electrodes are of Rogowsky profile type, made up of Stainless steel material and thickness of 15mm are used in the recovery study. The voltage recovery study was carried out by employing double-pulse method without employing any gas flow technique.
2. The recovery time and voltage studies are conducted in the pressure range of 0-4 bar pressure range for argon and nitrogen gases, with the help of a high pressure sparkgap. Pressure has significant effect on the recovery of the spark gap. Recovery time decreases with increase in pressure and Shorter gaps in length are recovering faster than longer gaps. It was observed that time taken for complete recovery without gas flow techniques is more than 1s. An intermediate plateau was observed in the spark gap recovery curves. This is due to long-lived particles that can continuously produce the electrons to quickly initiate the second breakdown. The recovery time estimated for Argon and Nitrogen gases and a comparison have been made with the Sf_6 gas recovery

time. Due to its electronegative nature Sf_6 has high percentage of voltage recovery than Argon followed by N_2 . Also the factors which affect the recovery of spark gap switch for pulse charged operation like electrode size, pulse rise time and conduction current have been studied. An increase in the output impedance resulted in a decrease in the time taken for recovery of spark gap. Also, the switch recovery appears to be largely dependent of electrode shape and size compare to the pulse rise time.

3. A two-dimensional axisymmetric computational model of spark gap recovery is presented to provide a better understanding of the dynamics of the recovery process. In this model, we investigate the internal changing parameters through the computational method, while the voltage recovery of spark gap was measured by two-pulse experiment. It was shown that the gas density in a 2 mm spark gap filled with argon gas recovers to 100% in 58ms, but the hold-off voltage of the spark gap after breakdown recovers about 45% of its original overvolted breakdown voltage. This shows the voltage recovery of a spark gap is significantly slower compared to the gas density recovery. This delayed voltage recovery compared to gas density recovery was observed in all types (monoatomic, diatomic and electronegative) of gases used in the experiment. This phenomenon in monoatomic gas like Argon is due to penning ionization which produce the long lived metastable Argon atoms. For the gases whose molecule is composed of two identical atoms, such as nitrogen, the process governing the delayed recovery may be related to the delayed recombination of the residual nitrogen atoms. The atoms of nitrogen are known for their ability to store energy over extended periods of time and may recombine on the cathode to produce the initial

electrons for the second breakdown. For the electronegative gases such as Sf_6 , the prolonged recovery was attributed to the residual negative ions that have relatively long lifetimes and play an active role in the production of seed electrons for the second breakdown through the collisional detachment. Based on the above observations the possible operating frequencies that can be obtained by triggering the spark gap at below self-break down voltage level was also suggested.

4. An attempt has been made to analyze the recovery times of high pressure sparkgaps based on anode temperature rise and decay. A theoretical method has been proposed to estimate the behavior of copper and stainless steel materials for a range of specific heat flux densities corresponding to different current pulses. During the pulse period of $10\mu\text{s}$, the temperature rise for SS is higher than Copper. After current zero, the anode temperature decays to the vaporization temperature of the material and determines the recovery time of the spark gap. The solid phase recovery times from anode temperature rise and decay method are generally in good agreement with the experimental recovery times. This temperature decay is also verified by a heat transient computational model developed in FEM based software. Simulations have been carried out for different materials including Cu and SS.

Further research is open for studying and analyzing different gas mixtures at higher pressure levels for understanding and minimizing the problem of recovery problems of spark gap. Finally some suggested future work is outlined

- I. The recovery study in gas mixture can be studied in future and also data on D₂O gas recovery can be useful for achieving faster repetitive pulse power systems.
- II. The use of streak camera to study the recovery phenomenon inside the spark gap with gas mixtures.

Present work has contributed to a better understanding of recovery in a spark gap used as a switch in high voltage pulse power systems. The study carried out in this thesis is useful in the development of reliable, efficient and high rep-rate spark gap switch for pulse power systems.

REFERENCES

- [1] Mankowski, J., M. Kristiansen, "A Review of Short Pulse Generator Technology," IEEE Transactions on Plasma Science, vol.28, no.1, pp.102-108, February 2000.
- [2] Liu, J. B., Wang, F., Li, G., Kuthi, A., Gutmark, E. J., Ronney, P. D., and Gundersen, M. A., "Transient Plasma Ignition," IEEE Trans. Plasma Sci., Vol. 33, No. 2, pp. 326-327, April 2005.
- [3] Wang, F., Liu, J. B., Sinibaldi, J., Brophy, C., Kuthi, A., Jiang, C., Ronney, P., and Gundersen, M. A., "Transient Plasma Ignition of Quiescent and Flowing Air/Fuel Mixtures," IEEE Trans. on Plasma Sci., Vol. 33, No. 2, pp. 844-849, April 2005.
- [4] Smulders, E. H. W. M., van Heesch, B. E. J. M., and van Paasen, S. S. V. B., "Pulsed Power Corona Discharges for Air Pollution Control," IEEE Trans. Plasma Sci., Vol. 26, No. 5, pp. 1476-1484, Oct., 1998.
- [5] D'Agostino, R., Favia, P., Kawai, Y., Ikegami, H., Sato, N., and Arefi-Khonsari, F., Advanced Plasma Technology, Wiley-Vch, 2008.
- [6] Galindo, F. G., Vernier, P. T., Dejmek, P., Vicente, A., and Gundersen, M. A., "Pulsed electric field reduces the permeability of potato cell wall," Bio-electromagnetics, Vol. 29, No. 4, pp. 296-301, May, 2008.
- [7] Garon, E. B., Sawcer, D., Vernier, P. T., Tang, T., Sun, Y., Marcu, L., Gundersen, M. A., and Koeffler, H. P., "In vitro and in vivo evaluation and a case report of intense nanosecond pulsed electric field as a local therapy for human malignancies," Int. J. Cancer 121, pp. 675-682, 2007.
- [8] Schoenbach, K. H., Peterkin, F. E., Alden, R. W., Beebe, S. J., "The Effect of Pulsed Electric Fields on Biological Cells: Experiments and Applications," IEEE Trans. Plasma Sci., vol. 25, No.2, pp. 284-292, April, 1997.
- [9] Martin, T. H., Guenther, A. H. and Kristiansen, M., "Gas Discharge Closing Switches", New York: Plenum Press, 1990.

- [10] Simek, M., M. Clupek, V. Babicky', and P. Sunka, "Production of reactive species by atmospheric pressure streamers in N₂-O₂ mixtures," *Pure Appl. Chem.*, Vol. 78, No. 6, pp. 1213-1225, 2006.
- [11] Schamiloglu, E. et al, "Modern Pulsed Power: Charlie Martin and Beyond", *Proceeding of the IEEE*, Vol 92(7) 1014, July 2004.
- [12] T. R. Burkes, "General Switching Considerations," in *Gas Discharge Closing Switches*. vol. 2, G. Schaefer, M. Kristiansen, and A. Guenther, Eds. New York: Plenum Press, 1990, pp. 1-13.
- [13] G. Schaefer, M. Kristiansen, and A. Guenter, „Gas Discharge Closing Switches“ vol. 2. New York: Plenum Press, 1990.
- [14] M. A. Gundersen, "Gas-phase pulsed power switches," *Plasma Science, IEEE Transactions on*, vol. 19, pp. 1123-1131, 1991.
- [15] Burkes, T. R., J. P. Craig, M. O. Hagler, M. Kristiansen, W. M. Portnoy, "A review of high-power switch technology," *IEEE Transactions on Electron Devices*, Vol 26, Issue 10, Oct 1979 Page(s):1401 – 1411.
- [16] W. C. Nunnally and A. L. Donaldson, "Self Breakdown Gaps," in *Gas Discharge Closing Switches*. vol. 2, G. Schaefer, M. Kristiansen, and A. Guenther, Eds. New York: Plenum Press, 1990, pp. 47-61.
- [17] M. Gundersen, "Thyratrons," in *Gas Discharge Closing Switches*. vol. 2, A. Guenter and M. Kristiansen, Eds. New York: Plenum, 1990, pp. 375-378.
- [18] C. A. Pirrie and H. Menown, "The evolution of the hydrogen thyatron," 2000, pp. 9-16.
- [19] J. Creedon, "Design Principles and Operation Characteristics of Hydrogen Thyratrons," in *Gas Discharge Closing Switches*.
- [20] Alstom FS2000 pseudospark switch datasheet.
- [21] Hartmann, W., and M. A. Gundersen, "Origin of anomalous emission in superdense glow discharge," *Phys. Rev. Lett.*, vol. 60, pp. 2371-2374, 1988.
- [22] J. Christiansen, "The Pseudospark Switch," in *Gas Discharge Closing Switches*. vol. 2 New York: Plenum Press, 1990.

- [23] S. Linder. "Power semiconductors". EPFL Press, Lausanne, 2006.
- [24] F. J. Zutavern, G. M. Loubriel, M. W. O'Malley, L. P. Shanwald, W. D. Helgeson, D. L. McLaughlin, and B. B. McKenzie, "Photoconductive semiconductor switch experiments for pulsed power applications," *IEEE Trans. Electron Devices*, vol. 37, pp. 2472-2477, 1990.
- [25] M. D. Pocha and R. L. Druce, "35-kV GaAs subnanosecond photoconductive switches," *Electron Devices, IEEE Transactions on*, Volume 37, Issue 12, Part 2, pp. 2486 - 2492, 1990.
- [26] H. Schoenbach, V. K. Lakdawala, D. C. Stout, T. F. Smith, and R. P. Brinkmann, "Electron-beam-controlled high-power semiconductor switches," *IEEE Trans. Electron Devices*, vol. 36, pp. 1793-1802, 1989.
- [27] P. Hadizad, J. H. Hur, H. Zhao, K. Kaviani, M. A. Gundersen, and H. R. Fetterman, "A high voltage GaAs static induction transistor," *Power Modulator Symposium, 1992. Conference Record of the 1992 Twentieth*, 23-25 Jun 1992.
- [28] M. Gundersen, J. Dickens, and W. Nunnally, "Compact, Portable Pulsed Power: Physics and Applications," *Proc. of IEEE 15th International Pulsed Power Conference*, 2003.
- [29] I. A. Khan, J. A. Cooper, Jr., M. A. Capano, T. Isaacs-Smith, and J. R. Williams, "High-Voltage UMOSFETs in 4H SiC," *Power Semiconductor Devices and IC's, 2002 . Proceedings of the 14th International Symposium on*, June 2002, pp. 157-160.
- [30] J. Tan, J. A. Cooper, Jr., and M. R. Melloch, "High-voltage accumulation-layer MOSFET's in 4H-SiC," *IEEE Electron Device Lett.*, vol. 19, pp. 487-489, 1998.
- [31] Simek, M., M. Clupek, V. Babicky', and P. Sunka, "Production of reactive species by atmospheric pressure streamers in N₂-O₂ mixtures," *Pure Appl. Chem.*, Vol. 78, No. 6, pp. 1213-1225, 2006.
- [32] G. J. J. Winands, Z. Liu, A. J. M. Pemen, E. J. M. van Heesch, and K. Yan, "Long lifetime, triggered, spark-gap switch for repetitive pulsed power applications", *Review of Scientific Instruments* 76, 085107, 2005.

- [33] J. Deng, R. H. Stark, and K. H. Schoenbach, "A compact, nanosecond pulse generator with water as dielectric and as switch medium," Pulsed Power Plasma Science, Digest of Technical Papers, pp. 1587-1590, 2001.
- [34] S. Xiao, J. Kolb, S. Katsuki, R. P. Joshi, M. Laroussi, and K. H. Schoenbach, "High power, high recovery rate water switch," Pulsed Power Conference, Digest of Technical Papers, 14th IEEE International, pp.649-652, 2003.
- [35] S. Xiao, J. Kolb, S. Kono, S. Katsuki, R. P. Joshi, M. Laroussi, and K. H. Schoenbach, "High power water switches: postbreakdown phenomena and dielectric recovery," IEEE Transactions on Dielectrics and Electrical Insulation Vol.11, No. 4, 2004.
- [36] K. V. Nagesh, "A study of recovery times of low pressure sparkgaps," Ph.D. dissertation, Indian Institute of Science, Bangalore, July 1997.
- [37] Electron Beam / Particle Beam Fusion progress reports. SAND-77-1414, SAN-78-0080, SAN-79-0002, SAN-79-1011, SAND-79-1944, SAND-79-0974.
- [38] Allen Ramrus, "Development of a 100kV, multi megawatt repetition rate gas switch," IEEE Trans. on Electron Devices, Vol. 26, No.10, Oct. 1979, pp.1417.
- [39] A. Ramrus and J. Shannon, "Testing of a 100 kV, 100Hz Rep-Rate gas switch," IEEE Trans. on Plasma Science, Vol.PS-8, No.3, 1980, pp.160-162.
- [40] M.F. Rose and M.T. Glancy, "High repetition rate miniature triggered spark switch," IEEE Trans. on Plasma Science, Vol.PS-8, No.3, 1980, pp.139-142
- [41] Hirishi Arita, "Switching Characteristics of the Triggered Vacuum Gap for a high repetition rate Pulse Power Source," IEEE Trans. on Plasma science, Vol.PS-20, No.2, April, 1992, pp 76-79.
- [42] C.H. Yeh, M. Hagler and M. Kristiansen, "Voltage recovery measurements in a high energy sparkgap," I.P.P.C.-83, pp.159-162.
- [43] S.E. Sampayan, S.H. Gurbaxian and M.T. Buttram, "Recovery properties of vacuum sparkgaps," IEEE Trans. on Plasma Science, Vol.PS-17, No.6, 1989, pp.889-896.

- [44] Koichi Tsuruta et al., "Experimental study of the voltage recovery of small air gaps", IEEE Trans. on Plasma Science, Vol. PS-17, No. 3, June, 1989, pp. 560-564.
- [45] F.M. Bieniosek, J. Honig and E.A. Theby, MEDIA-II. Two Pulse Generator Development, Rev. Sci. Instru. Vol. 61(6), June, 1990, pp. 1713-15.
- [46] S.L. Moran and L.F. Rinhart, "Voltage recovery time of small spark gaps", IEEE Trans. on Plasma Science, Vol. PS-10, No. 4, Dec. 1982, pp. 277.
- [47] Plasma Diagnostics, Ed. W. Lochte-Holtgreven, North Holland Publishing Co., Amsterdam, (1968), Chap. 8 on Microwave Diagnostics Techniques, by H. Hermansdorfer, pp. 478.
- [48] Plasma Diagnostics, Ed. W. Lochte - Holtgreven, North Holland Publishing Co., Amsterdam, (1968), Chap. 5 on Quantitative Spectroscopy and Spectral Photometry by W. Lochte - Holtgreven, pp. 250.
- [49] K.V. Nagesh, P.H. Ron, G.R. Nagabushana, & R.S. Nema, "Over Recovery in Low Pressure Sparkgaps", IEEE Trans. On Plasma science, Vol. 27, No. 1, Feb. 1999, p. 199-210.
- [50] K.V. Nagesh, P.H. Ron, G.R. Nagabushana, & R.S. Nema, "Over Recovery in Low Pressure Sparkgaps-conformation of pressure reduction in over recovery", IEEE Trans. On Plasma science, Vol. 27, No. 6, Dec. 1999, p. 1559-1565.
- [51] A. Larsson, "Gas-discharge closing switches and their time jitter," IEEE Trans. Plasma Sci., vol. 40, no. 10, pp. 2431-2442, Oct. 2012.
- [52] A. Larsson, D. Yap, and J. Au, "Operating conditions and switching delay time of a corona stabilized switch during repetitive operation," IEEE Trans. Plasma Sci., vol. 41, no. 10, pp. 2605-2608, Oct. 2013.
- [53] A. Larsson, D. Yap, and Y. W. Lim, "Time jitter study of a corona-stabilized closing switch," IEEE Trans. Plasma Sci., vol. 40, no. 10, pp. 2646-2652, Oct. 2012.
- [54] L.G. Christophorou, D.L. McCorkle, S.R. Hunter, "Gas Mixtures for Spark Gap Closing Switches with Emphasis on Efficiency of Operation", Gaseous Dielectrics, Vol. 5, pp. 381-388, 1987.

- [55] G. Schaefer, M. Kritiansen, A. Guenther, "Gas Discharge Closing Switches", Volume 2, New York, Plenum Press, 1990.
- [56] L.G. Christophorou, L.A. Pinnaduwege, "Basic physics of Gaseous Dielectrics", IEEE Trans. on Elec. Ins., Vol. 25, pp. 55–74, 1990.
- [57] S.L.Moran and L.W.Hardsty, "High Repetition rate Hydrogen Sparkgap", IEEE Trans. on Electron Devices, Vol.38, No.4, 1991, pp.726.
- [58] S.L.Moran, M.G.Grothaus and L.W.Hardsty, Hydrogen Spark Switches for REP-Rated Accelerators, Proc. Inter. Conf. on High Power Particle Beams, Part.III, May 25-29, 1992, pp.726.
- [59] XinjingCai, XiaobingZou, Xinxin Wang, Liming Wang, ZhichengGuan and Weihua Jiang, "Over-Voltaged breakdown and recovery of short nitrogen spark gaps", Laser and Particle Beams (2010), 28, 443–450.
- [60] XinjingCai, XiaobingZou, Xinxin Wang, Liming Wang, ZhichengGuan and Weihua Jiang, "Recovery of gas density in a nitrogen gap after breakdown", Applied physics letters, 97, 101501, 2010.
- [61] E.A.Abramyan, "Transformer type Accelerators for Intense Electron Beams", IEEE Trans. on Nuclear Science, Vol. NS-18, No.3, June 1971, pp.447.
- [62] Yin.Yi, liujinliang, ZhongHuihuang and Feng Jiahuai, "Experimental study of the Recovery Times of Spark gap Switch with Different Gases", Plasma science and Technology, vol.10, No.3, 2008.
- [63] J.L. Liu, Y. Yin, T.W. Zhan, J.H Feng , H.H Zhong, "Application of a self-breakdown hydrogen spark gap switch on high power pulse modulator", 16th IEEE International Pulsed Power Conference, pp: 455 - 458 17-22 June 2007.
- [64] M. O. Hagler and M. Kristiansen, Workshop on Repetitive Spark Gap Operation, Tamarron, CO, Jan. 17-19, 1983.
- [65] S. J. MacGregor, F. A. Tuema, S. M. Turnbull, and O. Farish, "The operation of repetitive high pressure spark gap switches," J. Appl. Phys., vol. 26, p. 954-958, 1993.

- [66] J. M. Meek and J. D. Craggs, *Electrical Breakdown of Gases*, New York: Wiley, 1978, ch. 8.
- [67] S. M. Turnbull, "A quantitative schlieren method for measurement of neutral gas density in highpressure gas switches," *Meas. Scr. Technol.*, vol. 4, pp. 1154-1 159, 1993.
- [68] E.Fiorentino et.al., High Repetition Rate Electron Beam with Resonant Transformer. *IL. NUOVO CIMENTO Vol.71B, No.2, 11, Ottobre 1982, pp.205.*
- [69] K.Tsuruta and H.Ebara, "Modelling of a Gas Temperature decay after arc discharge in small air gaps", *IEEE Trans. on Electrical Insulation Vol.EI-27, No.3, June 1992, pp.451.*
- [70] Electron Beam / Particle Beam Fusion progress reports. SAND-77-1414, SAN-78-0080, SAN-79-0002, SAN-79-1011, SAND-79-1944, SAND-79-0974.
- [71] M.T.Glancy and M.F.Rose, Surface Ageing in high repetition rate spark switches with aluminum and brass electrodes, *IEEE Trans. on Plasma Science, Vol.PS-8, No.3, Sep. 1980, pp. 143-148.*
- [72] Harold Watson, "Long life high repetition rate sparkgap", *IEEE Trans. on Plasma Science, Vol.PS-8, No.3, 1980, pp.154.*
- [73] Harold Watson, "High voltage pulser development", *IEEE Trans. on Electron Devices, Vol.ED-26, No.10, Oct. 1979, pp.1518.*
- [74] M.Dufour et.al. "Novel short recovery time high voltage switch", *Rev. Sci. Instru. Vol.47(12), Dec. 1976, pp.1552-53.*
- [75] E.H.J.Lauer, D.L.Birx, J.A.Masamitsu, R.E.Melendez, I.G.Smith and S.S.Yu, Low, "Pressure Switch Progress report: UCID-18848", Nov., 1980. Lawrence Livermore Laboratory.
- [76] E.J.Lauer et.al., "Breakdown and Recovery of a 250kV Low Pressure Sparkgap". *IEEE Trans. on Plasma Science, PS-10, Octo. 1982, pp.294.*
- [77] E.J.lauer, S.S.Yu and D.M.Cox, Onset of self breakdown in a low pressure sparkgap. *Physical Review A, vol.23, No.5, May 1981, pp.2250-2259.*

- [78] Cladius Kozlik et.al.,“Triggered low-pressure pseudospark-based high power switch“, IEEE Trans. on Plasma Science, Vol.PS-17, No.5, Octo, 1989, pp758-760.
- [79] R.J.Harvey,“Operating characteristics of the crossed field closing switch“, IEEE Trans. on Electron Devices, Vol.ED-26, No.10, Oct. 1979, pp.1472-1482.
- [80] R.A.Dougal, Gibson Morris.Jr. and G.D.Volakakis,“Low loss high repetition rate vacuum switching“, IEEE Trans. on Plasma Science, Vol.PS-198, No.5, Oct. 1991, pp.976-988.
- [81] G. N. Glasoe and J. V. Lebacqz, "Pulse Generators", MIT Radiation Laboratory Series, vol. 5, McGraw-Hill Book Company, New York, (1948).
- [82] C.S.Reddy, A.Patel, P.Naresh, Archanasharma and K.C.Mittal, “Experimental investigations of argon spark gap recovery times by developing a high voltage double pulse generator”, Review of scientific instruments, Vol.85, 064703, 2014.
- [83] D. Bortis,G. Ortiz, J. W. Kolar and J. Biela “Design procedure for compact pulse transformers with rectangular pulse shape and fast rise times”, IEEE Transactions on Dielectrics and Electrical Insulation, Vol.18, No.4, 2011.
- [84] Scott J. Macgregor,Steven M. Turnbull, Fadhil A. Tuema, and Owen Farish,“Factors Affecting and Methods of Improving the pulse rep. freq .of pulse charged &DC charged high pressure gas switches”, IEEE Trans. Plasma. Sci., Vol.25, no.2, 1997.
- [85] D. J. Biswas,J. P. Nilaya and U. K. Chatterjee, “On the recovery of a spark gap in a fast discharge circuit’, Review of scientific Instruments, Volume 69, Number12, (1998).
- [86] Xinxin Wang, HaiyunLuo and Yuan Hu “Numerical simulation of gas discharge in a gas peaking switch”, IEEE transactions on plasma science, 35, 702-708, (2007).
- [87] C.S.Reddy, Archanasharma and K.C.Mittal, “Recovery analysis of spark gap by anode temperature decay method for different materials” International journal of applied electromagnetics and mechanics, Vol. 47, pp. 643-651, 2015.
- [88] J. F. Perkins and A. B. Parker, “Mechanism of dielectric recovery in uniform and non-uniform field gaps after high-current high-pressure spark discharges,” Proc. of IEEE,vol. 117, no. 7. pp. 1460-1466. 1970.

- [89] Scott j. Macgregor, M. Turnbull, F. A. Tuema and O. Farish, “ Factors affecting and methods of improving the pulse repetition frequency of pulse charged and DC-Charged high pressure gas switches”, IEEE Trans. Plasma Sci, vol. 25, pp. 110-117, April 1997.
- [90] Tao Shao, Guangsheng sun, Ping yan and Shichang Zhang, “Repetitive Nanosecond-Pulse breakdown in Tip-Plane Gaps of Air”, IEEE Trans. Plasma Sci, vol. 34, pp. 1620-1625, October 2006.
- [91] J.D.Cobine, Gaseous Conductors, Dover Publications, Chapter II, pp.29, chapter.4.9, pp.102, Newyork, 1958.
- [92] Edels, H., and Crawford, F.W. C. I. G.R. E. Paris Paper No. 102, 1956.
- [93] Edels, H., and Crawford, F.W., Proc. Instn. Elect. Engrs. , 1074, 202, 1960.
- [94] Tao Shao, Guangsheng sun, Ping yan and Shichang Zhang, “Breakdown phenomena in nitrogen due to repetitive nanosecond-pulses”, IEEE Trans. Dielectr. Electr. Insul. Vol. 14, pp. 813-819, 2007.
- [95] Yin.Yi, liujinliang, Zhong Huihuang and Feng Jiahuai, “Experimental study of the Recovery Times of Spark gap Switch with Different Gases”, Plasma science and Technology, vol.10, No.3, 2008.
- [96] McBride J W, Pechrach K and Weaver P M, “Arc Root Commutation from Moving Contacts in low voltage devices”, IEEE Trans.Compon. Packag. Manuf. Technol. 24 331–6, 2001.
- [97] Peter R Z and Werner F R, “Arc structure, arc motion, and gas pressure between laterally enclosed arc runners”, IEEE Trans. Compon. Packag. Manuf. Technol. 24 337–41, 2001.
- [98] Rodriguez P, Didier J, Bernard G and Rowe S, “Arc-contact-insulating wall interactions in low voltage circuit-breakers”, IEEE Trans. Power Deliv. 13 480–8, 1998.
- [99] X. S. Deng, S. Chen, D.J Li, “Recovery of gas insulation after breakdown under $(1-\cos \omega t)$ nanosecond pulses,” high voltage engineering, 1993, 14(4),7-12.
- [100] K.Tsurutha, H. Ebara, “ A model of gas temperature decay after arc extinction of small air gaps” proceedings of the 3rd international conference on properties and applications of dielectric materials, 1991:377-380.

- [101] 5-11 Ansys Fluent Theory guide.
- [102] Maher I. Boulos, Pierre Fanchais and Emil Pfender, "Thermal plasmas, fundamentals and applications", Volume 1.
- [103] K. K. Trusov, "Spark cross size in a sliding sub microsecond discharge of opposite polarities in rare gases: experiment and application of ionization wave front propagation theory to analysis", *J. Phys. D: Appl. Phys.* 43, 10pp, 2010.
- [104] C.S.Reddy, A.Patel, P.Naresh, Archanasharma and K.C.Mittal, "Experimental investigations of argon spark gap recovery times by developing a high voltage double pulse generator", *Review of scientific instruments*, Vol.85, 064703, 2014.
- [105] C.S.Reddy, A.Patel, P.Naresh, Archanasharma and K.C.Mittal, "Voltage Recovery Characteristics of Spark gap using Repetitive Pulse Power System", presented at IPMHVC, Santa Fe-NM, USA, and June 1-5, 2014.
- [106] A. Bogaerts and R. Gijbels, "Modelling of metastable argon atoms in a direct-current glow discharge" *Physical Review A*, Vol.52, No.5, Nov 1995.
- [107] M. M. Pejovic and G. S. Ristic, "Memory effects in argon, nitrogen, and hydrogen," *IEEE Trans. Plasma Sci.*, vol. 30, no. 3, pp. 1315–1319, Jun. 2002.
- [108] PETROVIC', et. al., "Memory effects in the afterglow: Open questions on long-lived species and the role of surface processes". *J. Phys.D: Appl. Phys.* 34, 1756–1768. . (2001).
- [109] G.Frind, J.J.Carroll and E.J.Tuohy, Recovery times of Vacuum Interrupters which have stationary Anode spots, *IEEE Trans. on Power Apparatus and systems*, Vol.PAS-10 1, No.4, April 1982, pp775-781.
- [110] G.Gundersen, "Anode Spot formation in vacuum Arcs", Thesis, Norweg, Inst. Tech. Trondheim, Norway, 1971.
- [111] G.R.Mitchell, et.al, High Current Vacuum Arcs, Part I and II , *Proc. IEE*, Vol. 1 17, No.12, pp.2315-2332,1970.
- [112] D.Klapas and R.Holmes, "Anode Spot Temperature in vacuum Arcs", Presented at XI Conf. Phen. Ion. Gases, 82, (Prague, Czechoslovakia) 1973.

- [113] E.E.Burger and ID.Cobine, Analysis of electrode Phenomena in the high current Arcs, Journal of Applied Physics, Vo1.26, No.7, July, 1955. Pp 895-900.
- [114] J.T.Grissom and IC.Newton, Anode Surface radiance from micro second vacuum Arcs, J Appl. Phys. Vo1.45, 1974., pp-2885-94.
- [115] G.A.Lyubimov et.al., "A Study of Parameters of Anode Spot on Aluminum", J. Phys.D.Vol 3, 1980., pp-1655-64.
- [116] C.W.Kimblin, "Anode Voltage Drop and Anode Spot Temperature in dc Vacuum Arcs", J. Appl. Phys. Vo1.40, 1969., pp-1744-52.
- [117] G.A.Mesyats and D.IProskurovsky, Pulsed Electrical Discharges in Vacuum, Springer-Verlag, July 1988, Chap.4.53,
- [118] JA.Rich and G.A.Farrall, "Vacuum arc Recovery Phenomena", Proceedings of the IEEE, Vol. 52, Nov. 1964, pp.1293-1301.
- [119] David.R.Lide, Handbook of Chemistry and Physics, 76th Edition, 1995-1996, CRC Press.
- [120] Somerville et. al, "Electrode Phenomena in Transient Arcs", Proc. Phys. society (London), B65, 963 (1952).
- [121] V.Casalegno, P. Vavassori, M. Valle, M.Ferraris, M.Salvo, G.Pinstsuk, "Measurement of thermal properties of a ceramic/metal joint by laser flash method", Journal of Nuclear Materials, 407, 2010, pp83-87.
- [122] The physics Hypertextbook, Available: <http://www.physics.info>.
- [123] K.V.Nagesh, "Theoretical analysis of the recovery times in low pressure sparkgaps-anode temperature decay method," APAC, India, 2007.
- [124] C.S.Reddy, et. al, "Effect of anode temperature rise and decay on recovery times of sparkgaps" IEEE 4th Euro-Asian Pulsed Power Conference (EAPPC/BEAMS 2012) Karlsruhe, Germany, October-2012.

ANNEXURE-I

Embedded program to generate time delay optical signals fed to IC MIC4452

[Example: Two optical pulses with 10 ms delay]

```
#include <stdio.h>
#include <intrins.h>
#include <P89V51Rx2.H>
#include <4bitlcd.h>

Code unsigned char msg1 [16] = {" Select Mode "};
Code unsigned char msg2 [16] = {" Pulse Counter "};
Code unsigned char msg3 [16] = {"Trigger Generator"};
Code unsigned char msg4 [16] = {"Electrical Pulse"};
Code unsigned char msg5 [16] = {" Optical Pulse "};
Code unsigned char msg6 [16] = {"  RESET  "};
Code unsigned char msg7 [16] = {"  FIBER1  "};
Code unsigned char msg8 [16] = {"  FIBER2  "};
Code unsigned char msg9 [16] = {" Triggering  "};
Code unsigned char msg10 [16] = {" Triggered  "};
Code unsigned char msg11 [16] = {"Select Input "};
Code unsigned char msg12 [16] = {" Select Output "};
Code unsigned char msg13 [16] = {" Press Menu "};
Code unsigned char msg14 [16] = {"Press Select "};
Code unsigned char msg15 [16] = {"Press RST to sel"};

Sbit  mode   =   P2^5;
Sbit  select =   P2^6;
Sbit  reset  =   P2^7;
Sbit  fibre1 =   P2^3;
sbit  fibre2 =   P2^2;
sbit  epulse =   P3^2;
sbit  opulse =   P3^3;
```

```

Unsigned int cnt,cnt2,pulsetime = 0x0000,pt1,pt2,pt3,pt4,pt5,pt6,interruptcnt,hexdata,ecnt, ocnt, msec;
Unsigned char temp, k, outcnt, intent, set;
Unsigned char rc v[10], fcmd[4], scmd[4];
Unsigned char pulse no = 0x00,pno,shots = 0x00;
Unsigned char asc_1, asc_2,asc_3,asc_4,asc_5,asc_6,asc_7,asc_8;
data bit diff, stop, tog = 0;
data bit flag = 0;
data bit exit, menu out, mntog, btn select = 0;
//void firing ();
//void delay ms(unsigned char k);
//char ascii_cnvt(char k1);
void delay ms(unsigned char k);
void timer0 (void) interrupt 1 using 2
{
  if(++interrupt cnt == 4 )
  {
    flag = 0;
    interrupt cnt = 0;
    if(++msec == 10)
      {
        diff = 1;
        msec = 0;
        TR0 = 0;
      } } TF0 = 0;
} main()
{
  mode = 1;
  select = 1;
  reset = 1;
  epulse = 1;
  opulse = 1;
  fibre1 = 0;
  fibre2 = 0;
  ecnt = 0x0000;

```

```

ocnt = 0x0000;
set = 0x00;
SP = 0x80;           // Initialize stack
IEN0 = 0x82;        // 0x92 for serial + timer 1 interrupt & IP = 0x01 for interrupt priority
TMOD = 0X22;        // Set Timer for 8-bit auto-reload mode
TH1 = 0XFD;         // Set Baud rate 9600
PCON = PCON & 0x7F; // To determine Baud Rate
RI = 0;
TI = 0;
SCON = 0x50;        //Set UART Mode 1 and enable Serial Reception
TR1 = 1;             //Start Timer 1 for RS232
TH0 = 0x05;
pt5 = 0x0000;
pulsetime = 0x50;
flag = 1;
init_lcd();
line1();
dptr = msg1;
Disp_LCD_message();
line2();
dptr = msg13;
Disp_LCD_message();
menuout = 0;
diff = 0;
msec = 0;
TR0 = 0;
while (1)
{
    if (!mode) // 50msec / 10 SHOTS
    {
        while(!menuout)
        {
            line1();
            dptr = msg14;
            Disp_LCD_message();
            line2();
        }
    }
}

```

```

dptr = msg15;
Disp_LCD_message();
if (!mode)
{
    btnselect = 1;
    Delay ms(10);
    Delay ms(10);
    Delay ms(10);
    mntog = !mntog;
}
while (btnselect == 1)
{
    if (mntog == 0)
    {
        delayms(10);
        set = 0x01;
        line2();
        dptr = msg2;
        Disp_LCD_message();
    }
    if (mntog == 1)
    {
        delayms(10);
        set = 0x02;
        line2();
        dptr = msg3;
        Disp_LCD_message();
    }
}
if (!mode)
{
    delay ms(10);
    Delay ms(10);
    Delay ms(10);
    mntog = !mntog;
}
if (!select)
{
    Delay ms(10);
    Delay ms(10);
    Delay ms(10);
    Menu out = 1;
}

```

```

        Btn select = 0;
    }    }    }    }

Menu out = 0;
while(set==0x01)
{
    line1 ();
    dptr = msg2;
    Disp_LCD_message();
    line2 ();
    dptr = msg11;
    Disp_LCD_message();
    ecnt = 0x0000;
    ocnt = 0x0000;
    if (!select)
    {
        Delay ms(10);
        Delay ms(10);
        Delay ms(10);
        tog = !tog;
    }
    While ((tog == 0) && (set == 0x01))
    {
        exit = 0;
        ecnt = 0x0000;
        line1 ();
        dptr = msg4;
        Disp_LCD_message();
        while (!exit)
        {
            if (epulse == 0)
            {
                ecnt++;
                Hex data = ecnt;
                asc_1 = (hex data % 0x0a) + 0x30;
                hex data = ecnt;
                hexdata = hexdata / 0x0a;
                asc_2 = (hexdata % 0x0a) + 0x30;
                hex data = ecnt;
            }
        }
    }
}

```

```
hexdata = hexdata / 0x0a;
hexdata = hexdata / 0x0a;
asc_3  = (hexdata % 0x0a) + 0x30;
hexdata = ecnt;
hexdata = hexdata / 0x0a;
hexdata = hexdata / 0x0a;
hexdata = hexdata / 0x0a;
asc_4  = (hexdata % 0x0a) + 0x30;
hexdata = ecnt;
hexdata = hexdata / 0x0a;
asc_5  = (hexdata % 0x0a) + 0x30;
line2());
LCD_Data = 'P';
Display();
LCD_Data = 'u';
Display();
LCD_Data = 'l';
Display();
LCD_Data = 's';
Display();
LCD_Data = 'e';
Display();
LCD_Data = 's';
Display();
LCD_Data = '=';
Display();
LCD_Data = ' ';
Display();
LCD_Data = asc_5;
Display();
LCD_Data = asc_4;
```

```

Display();
LCD_Data = asc_3;
Display();
LCD_Data = asc_2;
Display();
LCD_Data = asc_1;
Display();
LCD_Data = '';
Display();
LCD_Data = '';
Display();
LCD_Data = '';
Display();
if (!reset)
{
    ecnt = 0x0000;
    delayms(10);
    delayms(10);
    delayms(10);
}
}

if (!mode)
{
    exit = 1;
    tog = !tog;
    set = 0x00;
    delayms(10);
    delayms(10);
    delayms(10);
}

if (!select)
{
    exit = 1;
    tog = !tog;
    delayms(10);
    delayms(10);
    delayms(10);
}

```

```

        }
    }
}

while((tog == 1) && (set == 0x01))
{
    exit = 0;
    ocnt = 0x0000;
    line1 ();
    dptr = msg5;
    Disp_LCD_message();
    while (!exit)
    {
        if (opulse == 0)
        {
            ocnt++;
            hexdata = ocnt;
            asc_1 = (hexdata % 0x0a) + 0x30;

            hexdata = ocnt;
            hexdata = hexdata / 0x0a;
            asc_2 = (hexdata % 0x0a) + 0x30;
            hexdata = ocnt;
            hexdata = hexdata / 0x0a;
            hexdata = hexdata / 0x0a;
            asc_3 = (hexdata % 0x0a) + 0x30;
            hexdata = ocnt;
            hexdata = hexdata / 0x0a;
            hexdata = hexdata / 0x0a;
            hexdata = hexdata / 0x0a;
            asc_4 = (hexdata % 0x0a) + 0x30;
            hexdata = ocnt;
            hexdata = hexdata / 0x0a;
            asc_5 = (hexdata % 0x0a) + 0x30;
            line2();
            LCD_Data = 'P';
        }
    }
}

```

```
Display();
LCD_Data = 'u';
Display();
LCD_Data = 'l';
Display();
LCD_Data = 's';
Display();
LCD_Data = 'e';
Display();
LCD_Data = 's';
Display();
LCD_Data = '=';
Display();
LCD_Data = ' ';
Display();
LCD_Data = asc_5;
Display();
LCD_Data = asc_4;
Display();
LCD_Data = asc_3;
Display();
LCD_Data = asc_2;
Display();
LCD_Data = asc_1;
Display();
LCD_Data = ' ';
Display();
LCD_Data = ' ';
Display();
LCD_Data = ' ';
Display();
if (!reset)
{
    ocnt = 0x0000;
```

```

                                delayms(10);
                                }    }
if (!mode)
{    exit = 1;
    tog = !tog;
    set = 0x00;
    delayms(10);
    delayms(10);
    delayms(10);
}
if (!select)
{    exit = 1;
    tog = !tog;
    delayms(10);
    delayms(10);
    delayms(10);
}    }    }    }
while (set == 0x02)
{
    line1 ();
    dptr = msg3;
    Disp_LCD_message();
    line2 ();
    dptr = msg12;
    Disp_LCD_message();
    if (!select)
    {    delayms(10);
        delayms(10);
        delayms(10);
        tog = !tog;
    }
    while((tog == 0) && (set == 0x02))
    {    exit = 0;

```

```

line1 ();
dptr = msg7;
Disp_LCD_message();
while (!exit)
{
    if (reset == 0)
    {
        delayms(10);
        delayms(10);
        delayms(10);
        line2 ();
        dptr = msg9;
        Disp_LCD_message();
        fibre1 = 1;
        _nop_();
        fibre1 = 0;
        line2 ();
        dptr = msg10;
        Disp_LCD_message();
        delayms(10);
    }
}

```

```

        delayms(10);
        delayms(10);
        delayms(10);
    }
    if (!mode)
    {
        exit = 1;
        tog = !tog;
        set = 0x00;
        delayms(10);
        delayms(10);
        delayms(10);
    }
    if (!select)
    {
        exit = 1;
        tog = !tog;
        delayms(10);
        delayms(10);
        delayms(10);
    } } }
While ((tog == 1) && (set == 0x02))
{
    exit = 0;
    line1 ();
    dptr = msg8;
    Disp_LCD_message();
    while (!exit)
    {
        if (reset == 0)
        {
            delayms(10);
            delayms(10);
            delayms(10);
            line2 ();
            dptr = msg9;

```

```

Disp_LCD_message();
fibre2 = 1;
_nop_();
_nop_();
_nop_();
_nop_();
fibre2 = 0;
TR0 = 1;
while (diff == 0);
diff = 0;
TR0 = 0;
fibre2 = 1;
_nop_();
_nop_();
_nop_();
_nop_();
fibre2 = 0;
delayms(10);
line2 ();
dptr = msg10;
Disp_LCD_message();
delayms(10);
delayms(10);
//    delayms(10);
}
if (!mode)
{
    exit = 1;
    tog = !tog;
    set = 0x02;
    delayms(10);
    delayms(10);
    delayms(10);
}

```

```

        if (!select)
        {
            exit = 1;
            tog = !tog;
            delayms(10);
            delayms(10);
            delayms(10);
        }
    }
}

void delay ms(unsigned char k)
{
    temp = k;
    for (k = 0x00;k < temp; k++)
    {
        for (outcnt = 0x00; outcnt < 0x04;outcnt++)
        {
            for (intcnt = 0x00; intcnt < 0xff;intcnt++);
        }
    }
}

//char ascii_cnvrt(char k1)
//{
//if ('0' <= k1 && k1 <= '9')
//    {
//        k1 = k1 - 0x30;
//    }
//else
//    {
//        k1 = k1 - 0x37;
//    }
//return (k1);

```

ANNEXURE-II

The external code used in the simulations of gas density recovery by ANSYS/Fluent software.

//Gas Density of argon gas

```
For (temperature>23500)    dens=9.5e-3+ (9.1e-3)*(temperature-23500) / (24000-23500);
For (temperature<23500)    dens=1.0e-4+ (9.5e-3)*(temperature-21800) / (23500-21800);
For (temperature<21800)    dens=1.5e-2+ (1.0e-2)*(temperature-17300) / (21800-17300);
For temperature<17300)    dens=2.0e-2+ (1.5e-2)*(temperature-15000) / (17300-15000);
For (temperature<15000)    dens=5.0e-2+ (2.0e-2)*(temperature-9500) / (15000-9500);
For (temperature<9500)     dens=8.1e-2+ (5.0e-2)*(temperature-6000) / (9500-6000);
For (temperature<6000)     dens=1.0e-1+ (8.1e-2)*(temperature-4800) / (6000-4800);
For (temperature<4800)     dens=1.6e-1+ (1.0e-1)*(temperature-3000) / (4800-3000);
For (temperature<3000)     dens=5.0e-1+ (1.6e-1)*(temperature-1000) / (3000-1000);
For (temperature<1000)     dens=5.0e-1;
```

//Viscosity of argon gas

```
For (temperature>22500)    visc=5.0e-5 + (3.8e-5)*(temperature-22500) / (24000-22500);
For (temperature<22500)    visc=7.0e-5 + (5.0e-5)*(temperature-16000) / (22500-16000);
For (temperature<16000)    visc=1.0e-4 + (7.0e-5)*(temperature-15000) / (16000-15000);
For (temperature<15000)    visc=1.5e-4 + (1.0e-4)*(temperature-14000) / (15000-14000);
For (temperature<14000)    visc=2.0e-4 + (1.5e-4)*(temperature-13000) / (14000-13000);
For (temperature<13000)    visc=2.7e-4 + (2.0e-4)*(temperature-11500) / (13000-11500);
For (temperature<11500)    visc=2.5e-4 + (2.7e-4)*(temperature-9000) / (11500-9000);
For (temperature<9000)     visc=2.0e-4 + (2.5e-4)*(temperature-6500) / (9000-6500);
For (temperature<6500)     visc=1.5e-4 + (2.0e-4)*(temperature-4100) / (6500-4100);
For (temperature<4100)     visc=9.9e-5 + (1.5e-4)*(temperature-2300) / (4100-2300);
For (temperature<2300)     visc=5.7e-5 + (9.9e-5)*(temperature-1000) / (2300-1000);
For (temperature<1000)     visc=5.7e-5;
```

//Thermal conductivity of argon gas

For (tt>25000) th_con=2.39 + (4.03-2.39)*(25000-17000) / (24000-17000);

For (tt<25000) th_con=2.39 + (4.03-2.39)*(tt-17000) / (24000-17000);

For (tt<17000) th_con=0.266 + (2.39-0.266)*(tt-8000) / (17000-8000);

For (tt<8000) th_con=0.0267 + (.266-.0267)*(tt-500) / (8000-500);

For (tt<500) th_con=0.02;